UNIVERSITY OF CANTERBURY
Department of Physics and Astronomy
CHRISTCHURCH NEW ZEALAND

An Investigation into EPID Flood Fields Independent from the Linear Accelerator Beam

A thesis submitted in partial fulfilment of the requirements for the Degree of Master of Science in Medical Physics in the University Of Canterbury, New Zealand

Philip Satory

An Investigation into EPID Flood Fields Independent from the Linear Accelerator Beam

By

Philip Satory

Year 2006-2008

MSc Supervisors: Assoc. Prof. Lou Reinisch, Dr Juergen Meyer & Allan Stewart

Abstract

The EPID (electronic portal imaging device) was designed for in vivo imaging of patients during radiotherapy treatment. The ability of EPIDs to promptly acquire two dimensional data, lends them to be considered for use in quality assurance of the linac. This thesis set out to investigate the possibility of using a radionuclide, technetium 99 m (Tc99m), to produce a flood field for the calibration of an EPID, because using a beam calibrated EPID to measure the beam is self-referential.

The difference in relative response between the energy spectrum of a 6MV beam and the Tc99m was investigated using EGSNRC DoseXYZ Monte Carlo Modelling. The relative output ratio was calculated to be less than 1.6%. The dose response of the EPID with respect to dose rate was checked using different activities of Tc99m and found to be linear.

The flatness from a phantom was calculated, with a model in MATLAB, for a range of heights, overlaps, thickness, and deformations, to find the optimum balances between signal strength and flatness. This model was checked for accuracy using diagnostic radiographic film.

The culmination of the energy response, linearity and the calculated flatness is a flood field taken with a flood phantom on the EPID with low signal strength. To get a signal to noise ratio of 3% the mean of over 2000 flood field images were used. This accuracy was not adequate for clinical use but the averaging of pixels it is accurate enough for QA.

Acknowledgments

The idealist in me says money is not as important as the nourishing cultural system that sustains academic research, but the Realist in me says that funding is a vital part of the environment needed. So I would like to thank the clinical training authority (ministry of health) and the ADHB for providing funding for me whilst undertaking this thesis. In no particular order I'd like to thank a lot of people: the VHEMT; my riding buddies, CJ, Graham, Paul, Anne, Aaron and Chris; the local Varian engineer Sean Gum. Dave Lawson in the clinical engineering workshop at ACH; Allan Stewart my local supervisor; Assoc Prof. Lou Reinisch and Dr Juergen Meyer, my university supervisors; Isla Nixon and all the physics staff at the Auckland city hospital; my sister Rewa; Jane Kent; Steve Smart; Jared Steal; Sivanathan Sarasanandarajah; Bryn Currie and Roger Li; and the ACPSEM

Table of contents

Figures

Tables

Glossary of terms

ACH	Auckland City Hospital
ACPSEM	Australasian College of Physical Scientists and Engineers in medicine.
ADHB	Auckland district health board
aSi	Amorphous Silicon
CMM	Coordinate Measuring Machine
Cu	Copper
DTI	Dial Test Indicator
EPID	Electronic Portal Imaging Device
FWHM	Full Width Half Maximum
Gd	Gadolinium
Gd2O2S	Gadolinium Oxysulphide
IAS2	Image acquisition system
IAS2	Image Acquisition System 2
ISL	Inverse Square Law
Linac	Clinical linear accelerator.
MLC	Multi Leaf Collimator
NIST	National Institute of Standards and Technology
OD	Optical Density
PCM	Point Contribution Matrix
POI's	Points of Interest
PVE	Phantom Volume Element
QA	Quality Assurance
RCM	Relative Contribution Matrix
RT	Radiotherapists
TFT	Thin Film Transistor
tif	Tagged Image File Format

Glossary of equipment manufacturers used

Varian refers to Varian Medical Systems, Inc.; 3100 Hansen Way; Palo Alto, CA 94304-1038.

Vidar Scanner; Vidar Systems Corporation; 365 Herndon Parkway, Herndon, VA 20170.

MATLAB; The MathWorks, Inc.; 3 Apple Hill Drive; Natick, MA 01760-2098; UNITED STATES.

Maple; Mapelsoft; 615 Kumpf Drive; Ontario; Canada.

Introduction

"In 2003, there were 18,586 new registrations for cancer and 8027 recorded deaths from cancer, in New Zealand" [1]. The most common methods of treating cancer are surgery chemo therapy, and radio therapy, or some combination of these. 45 to 55 percent of these patients in New Zealand will have radiotherapy included as part of their treatment[2]. At Auckland City hospital, approximately 55% of these patients are treated in a curative manner, and approximately 45% receive palliative treatment.

Radiation therapy is the medical use of ionizing radiation to treat cancer, and is used to treat cancer that is localised as it can be targeted spatially. Ionizing radiation is deadly to all cells both cancerous and normal tissue, so it is prescribed in a manner to maximise the damage to the cancerous cells; and maximise the recovery of the normal tissue, and minimise the cancers recovery. The difference between normal tissue recovery and the lethal dose to the cancer is referred to as the therapeutic window. To treat deep seated tumours with external beam radiotherapy it is necessary to use high energy radiotherapy (greater than 1MV mean energy). In the delivery of high energy radiotherapy in NZ, the oncologist prescribes a treatment dose to be delivered, and marks the area to be treated on either a CT (computed tomography) or radiographic film. The radiotherapists (RT) plan how to deliver that dose via a computerised treatment planning system. A linac (clinical linear accelerator) is used to deliver the planned treatment to the patient, by the RTs. It is the medical physicists' task to ensure that the planned treatment is what will be delivered to the patient by the linac, and this requires extensive Quality Assurance (QA) of the linac, both mechanically and dosimetrically. Ensuring that the scales, that measure the geometry between the beam and patient, are accurate is an example of mechanical QA. Other regular QA tests that are done are an indirect measure of dosimetric properties of the linac, like the measuring of off access point doses is a gauge of whether beam energy has changed and the beam is in alignment. Off access point doses, and other QA test, could be made more efficiently, than by current methods, using an electronic portal imaging device (EPID)[3].

1.1 Portal Imaging

Portal imaging is an image taken of the exit radiation from the patient, immediately before or during treatment. While treating patients with radiotherapy it is necessary to use portal imaging to ensure that they are in the right position as compared with the patient's position in the planning CT (planning stage), deviation between the positions greater than the planning tolerances will compromise the outcome of the treatment. Regular portal imaging has been shown to produce better setup accuracy [4, 5]. This is done with a radiosensitive device in the exit beam from the patient (see Figure 1.1 and Figure 1.2). The portal imager can either be attached to the counter weight of the linac (Figure 1.2) or on a separate stand. Originally portal imaging was done with radiographic film; but the inconvenience of having to process the film between imaging and treating the patient and the inability to visualise the films to their full potential without computer enhancement [4] lead to the development of electronic portal imaging. The digitisation of images with analogue to digital converters (ADC) allows for digital manipulations, which improve the image clarity. Older EPIDs are either liquid filled Ion chamber based, which lack the resolution to replace film, or camera based systems which lack the detector quantum efficiency (DQE), due to losses in the optical coupling between the camera and the scintillator [4]. The more modern amorphous silicon (aSi) EPIDs have adequate resolution and improved contrast [6]. Due to the processes involved in manufacturing the EPIDs and their read out electronics they need to be calibrated to ensure each pixel has the same response characteristics. Because higher resolution electronic portal imaging devices (EPIDs) have become available film has been phased out. Because departments have moved to filmless environments, much research has gone into the use of EPIDs as a QA tool [7], and for dosimetry both pre-treatment [4, 8, 9] and transit [10] in-vivo dosimetry.

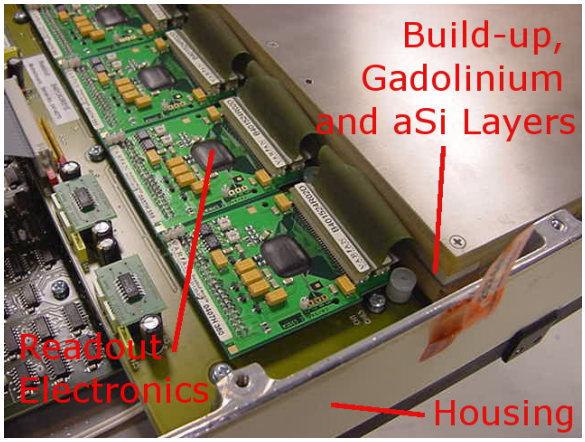

Figure 1.1 Internals of Varian aSi500 EPID showing the imaging cassette, electronics and housing

Figure 1.2 Varian linac with aSi EPID with the beam position illustrated

When using the EPID quantitatively as a QA tool the calibration becomes more critical than when the EPID is used qualitatively for visual comparison of portal images to planning images. The standard method of calibrating EPIDs is to use the linac beam to give an even dose to the entire EPID; this is called a flood field. The manufacturer's specification of beam profile flatness is ±3%, whilst the uneven profile does not have a drastic effect on image quality for patient setup purpose, as it has no discontinuities, it does become significant when the EPID is being used for QA. Another failing with using the beam is that it dose not have a constant energy spectrum across it, with softening of the beam towards the edge, which leads to an increased signal at the edge.

1.2 Aims of Research

It is the aim of this research to investigate the possibility of using a Tc99m (Technetium 99 m) filled flood phantom, to produce flood fields on a Varian aS500 EPID independent of the linac beam. The manufacturer's recommended method of removing the beam profile from the beam calibration is to measure the beam profile with an ion chamber and subtract it from the flood field [11]. Greer et al has proposed using a shifting the EPID under a smaller beam and overlapping the shifts so that the flatness of the beam is averaged out, Figure 1.3 [12]

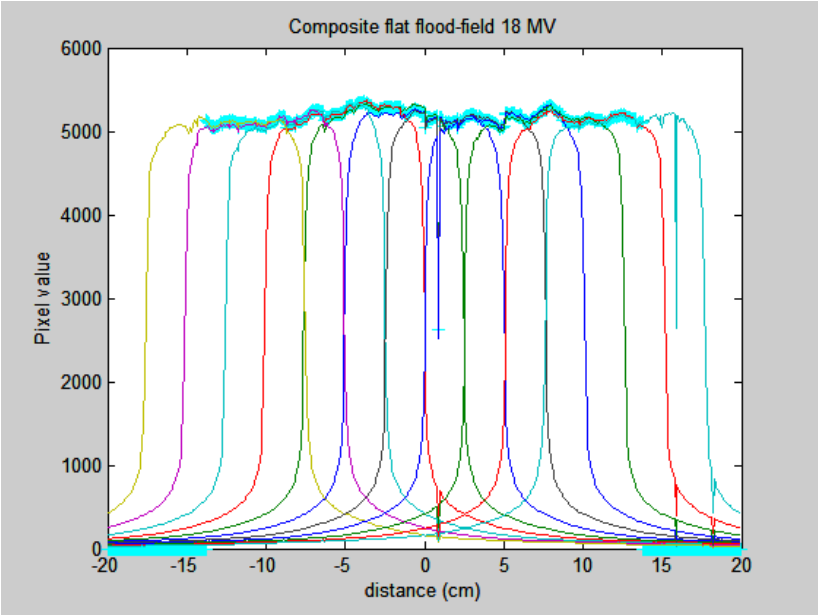

Figure 1.3. Composite flat flood field from 11 10x30cm beams by Greer et al[12].

Both of these methods still rely on the linac beam. To be fully independent of the linac beam an alternative source of radiation is needed to produce the flood field. In nuclear medicine it is common to use a tank filled with liquid radionuclide, called a flood phantom, to do QA on the gamma-cameras. This is due to the flood phantom having an even distribution of dose in the central area covered.

1.3 Outline of thesis

In Chapter 2 the ground work is to investigate whether it is feasible to achieve a meaningful flood field with a flood phantom. A detailed description of the Varian AS500 portal imaging system used for the experiments is presented. This is followed by Monte Carlo calculations, to investigate dose deposited in the EPID, with differing thicknesses of both gadolinium and copper build up, and for both a 6MV beam spectrum and a 141 KeV beam. Linearity of the EPID at dose rates achieved by the linac beam has been well established [13], but the dose rates achievable from Tc99m are well below these dose rates. The linearity was verified by using differing activities of Tc99m to spot check that the response is linear. The final part of chapter deals with the extrinsic issue of ghosting as a cause of background drift is investigated.

In Chapter 3 the process of the experimental methods used is described. This chapter is divided into three parts: the building of the computational model, in MATLAB®, to predict the field shape from the flood phantom; the comparison of the computational model with film work; flood fields, on the EPID, with the flood phantom;

The result of the MATLAB® model allows the investigation of the interdependence of the geometric properties and the tolerances of construction of the flood phantom and signal to noise ratio. This is followed by a description of techniques to compare a MATLAB® Model to a dose distribution in film, achieved by exposing diagnostic radiographic film with the flood phantom. And finally the process of acquiring flood field, on the EPID, with the flood phantom is delineated.

The results analysis and discussion of methods in Chapter 3 are presented in chapter 4, as well as possible techniques for improving the process, and improving image quality.

In Chapter 5 the conclusions of the viability of using a radionuclide filled flood phantom are presented

Feasibility study

2.1 Introduction

To measure the EPID response, independent from the linac beam, it is necessary to irradiate the EPID from another source. That source needs to produce an even dose and energy field to the EPID: this preconditions that a radionuclide be used, as bremstrahlung generation of x-rays is vulnerable to the mechanical tolerances which cause a distribution which is too uneven for our requirements and has a varying energy field. EPIDs are designed to operate in clinical situations, and expect a dose rate of approximately one half to six Gray per minute. If we to use a radionuclide with an activity that would produce this dose rate it would not be safe to handle it. This eliminates the possibility of using a high activity source at a distance.

An even and infinite plane source produces a homogenous distribution parallel to it. An approximation to this is close proximity to a finite plane but it has edge effects. Whilst in nuclear medicine solid flood phantoms, with Co57, are used to produce an even flood field, commercially available phantoms are not available in activities high enough to give the signal strength required [14]. Because engineering one locally was not practical, a simple way of producing an even distribution of a radionuclide was to use a liquid. The types of liquid radionuclide readily available in a hospital environment are I131 and Tc99m. Tc99m was chosen for this study as the preliminary tests showed that the EPID had a better response to it. Furthermore, Tc99m is easier to shield than I131 because it has a lower mean energy and has no electron emission (though the decay product of Tc99m is an electron emitter they are negligible).

The three things needed to produce suitable flood fields from a flood phantom are: to ensure the relative flood fields are not energy dependent; the dose response is linear or a calibration curve needs to be effected; and the size of the flood phantom needed to produce a flat flood field needed to be established. To understand these requirements it is essential to understand more about the EPID.

2.2 Varian aS500 portal imager

A Varian aS500 aSi EPID was used in this research, the active part consists of an amorphous silicon array of photo diodes, coupled to thin film transistors (TFT) (Figure 2.1). The photodiodes have a very poor DQE for high-energy photons. To increase the DQE, there is an approximately 0.5 mm thick layer of gadolinium scintillator (Gd_2O_2S), and a 1mm thick copper build-up plate [15], between the photo diodes and the radiation source[16]. The scintillator converts the high-energy photons into visible photons (Figure 2.2) which are detected in the photodiode and stored as charge until the TFT is triggered to conduct the charge collected into the ADC in the readout electronics.

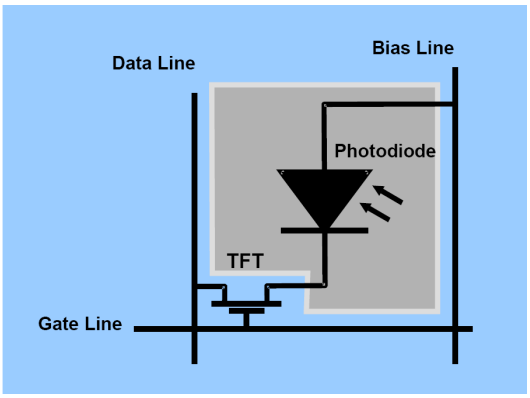

Figure 2.1 Illustration of the aSi pixel schematic [16]

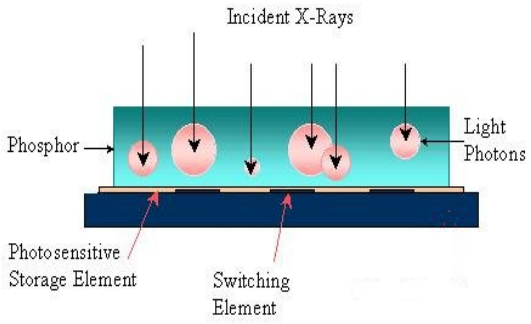

Figure 2.2 Functional cross-section of EPID [17]

The aSi500 has 512 (columns) x 384 (rows) pixels with a pixel size of 0.79mm and a bit depth of 14. It is read out one row at a time, each row is multiplexed and transferred to the IAS2 (image acquisition system 2), where it is converted to digital with a series of ADCs, one for each column (Figure 2.3). The readout is synchronized to a sync pulse (60-360 Hz) from the linac; the number of rows read out per sync pulse is dependent on the dose rate of the linac. Each full readout (512x384 pixels) is refereed to as a frame, in normal use more than one frame is readout by the IAS2 before exporting an image. The first frame is a reset frame to ensure that the time over which the photo diode is integrating photons (the time between two frames) is constant, and therefore is not included in the final image. The frames, following the reset frame, are averaged and exported as a single DICOM image. Each photodiode TFT (thin film transistor) pair, which becomes a pixel in the image, has different electronic properties resulting in different response characteristics, and for this reason it is necessary to calibrate the EPID to correct each pixel to give the same response.

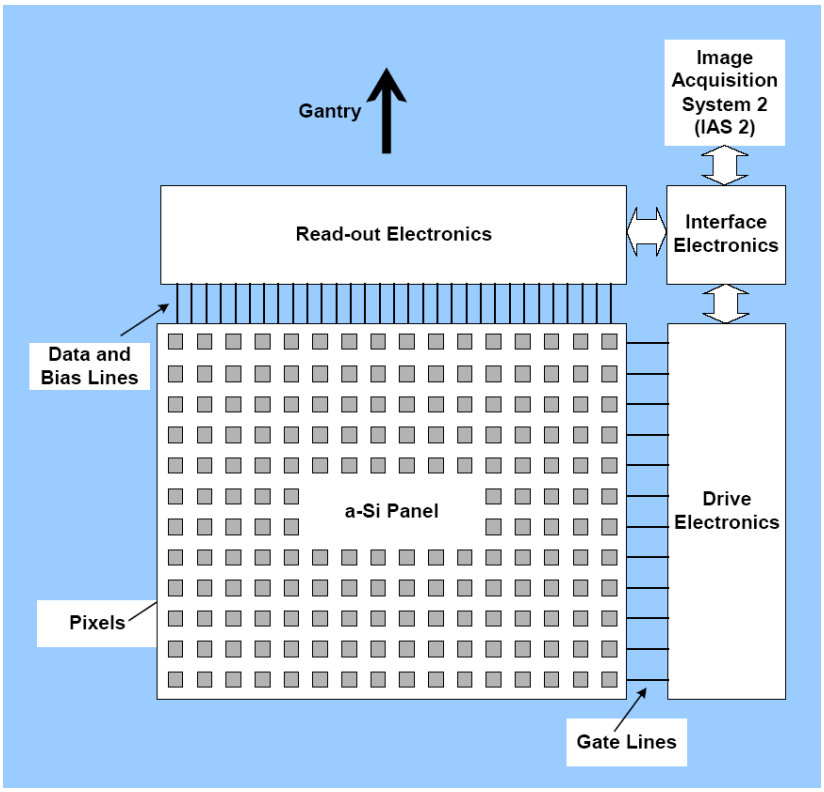

Figure 2.3 Block Diagram of EPID and IAS2

A relative calibration of each pixel requires both a zero value for each pixel and a value for every pixel exposed to the same dose, and as it is relative this dose does need to be precise. The manufactures recommended method, which is currently used for calibration, is; a dark field (DF) or offset correction and a flood field (FF) gain correction, see Eq 2.1, where CI is the corrected image, RI is the raw image, and k_{FF} is the mean of the flood field.

$$CI = \frac{[RI - DF]}{FF} k_{FF} \qquad \textbf{Eq 2.1}$$

The dark field is, an image from the EPID without any exposure, see Figure 2.4. The flood field is achieved by exposing the whole imaging cassette to an open field from the linac beam, see Figure 2.5. This is an adequate technique for treatment clinical imaging, but if the EPID is to be used for a QA tool of dosimetry a better method of flood field is needed. As the manufacturers specification of in plane flatness is ±3% (across 80% of the beam FWHM (full width half maximum) measured at 100mm deep in water [18]). The 3% flatness of the beam and the circular reference of calibrating the EPID using the linac beam, and measuring the same beam with the EPID, mean that a better method of producing a flood field is needed.

In clinical use EPID images are synchronized to the linac beam pulses which control the dose-rate. The image is corrected with the dark field and flood field within the IAS2, before being transferred to the portal vision workstation. The data format is DICOM file with a 16 bit tif (tagged image format) embedded. For obtaining flood fields with Tc99m, it is necessary to acquire uncorrected images without running the linac beam. To do this the setting in the IAS2 needed to be changed as described in appendix D.1.

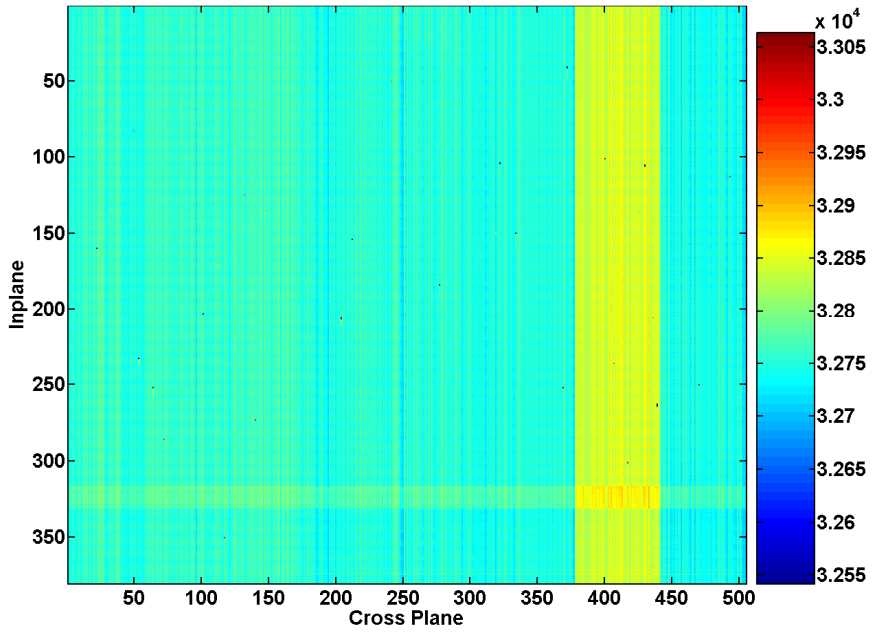

Figure 2.4 A typical dark field (DF).

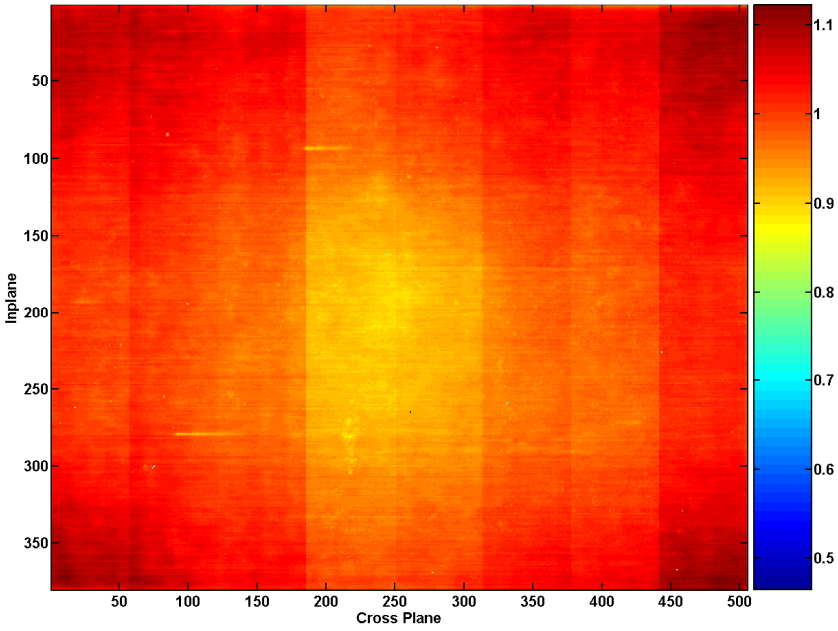

Figure 2.5 14 bit Flood field (FF) divided by mean of flood field (k_{ff})

2.3 Monte Carlo Modelling

If the EPID had a constant response with energy, the limitations on the tolerances of construction would not be problematic. Two factors need to be taken into account for the modelling which are, the energy response of the EPID, and the manufacturing tolerances of the elements of the imaging cassette. The energy response is due to the increased influence of the photoelectric effect at low energies [15, 19]. The exact tolerances of the active components of the EPID are commercially sensitive and are not readily available from Varian, but from the information available it is possible to estimate bounds for the tolerances. The copper plate has a density of 0.0896 g/cm^2 and is nominally 1mm thick [16, 19] and it is a safe assumption that it is cold rolled or produced by a more accurate technique, so this puts an upper bound for the tolerance of the Cu plate at 1% [20]. The gadolinium oxysulphide fluorescent layer is most probably constructed by drying a colloid on the Cu layer [21], consisting of approximately 25% Gd_2O_2S and 75% resin to give a nominal 0.5mm thick layer of 0.134g/cm^2 density [19]. The tolerance of the gadolinium layer is assumed to be no better than the absolute tolerance of the Cu, so we have a Cu plate that varies from 0.99mm to 1.01mm and a Gd_2O_2S layer varying from 0.49mm to 0.51mm.

To identify how the variance in thickness of the construction materials influences the signal from the EPID, DoseXYZnrc® Monte Carlo modelling was used. The DoseXYZnrc® Monte Carlo model uses, random number generation, and cross section data from the NIST (National Institute of Standards and Technology), to generate the path, and energy deposited of photons and electrons in any medium for which cross sections are available [22]. Monte Carlo was chosen as the EPID relies on electrons generated in the Cu layer being deposited in the Gd layer, which is difficult to physically measure.

DoseXYZnrc® is designed to model dose distributions in a phantom with rectilinear voxels, but it is not capable of modelling the visible light photons produced in the scintillator, that are integrated by the photo diode. The current practice is to model the dose deposited in the scintillator [15, 23, 24] and which is then modified with a convolution kernel for spatial investigations [19, 23].

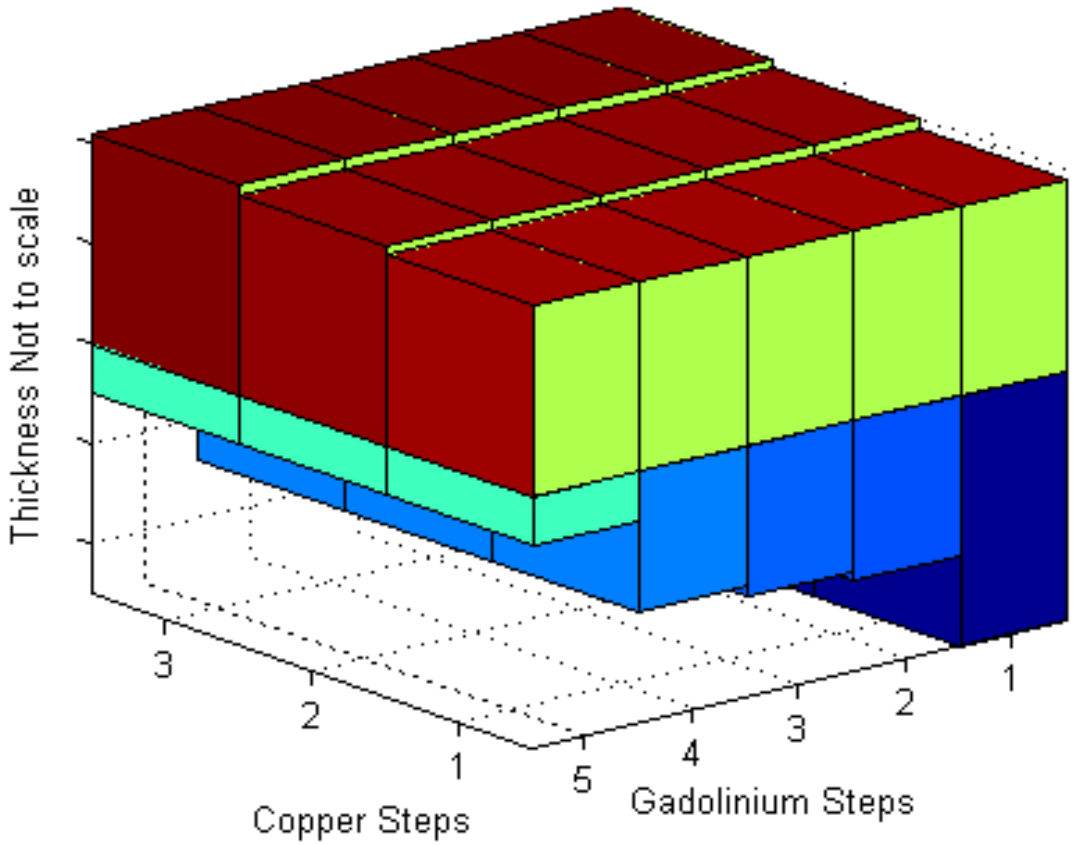

Figure 2.6 Depiction of MC phantom, not to scale.
Scale modified to magnify step size.

A phantom was designed in DoseXYZnrc® to cover 3 thickness (1.01mm ,1mm 0.99mm) of Cu build up, and 5 thickness' (0.4mm 0.49mm 0.5mm 0.51mm 0.6mm) of Gd. The voxels that make up the difference in thickness of the mediums were set to air (Figure 2.6), see appendix C.1.1 and C.2.1 for input file and 3ddose files. It was assumed the tolerance is in the order of 0.01mm but we wanted to investigate the affects of a larger variation, so thicknesses of 0.4mm and 0.6mm Gd were also modelled. The dose distribution in the phantom was calculated using 141KeV photons and an EGSnrc® spectrum called Mohan6 which is a nominal 6MV linac beam spectrum, 100,000,000 histories were used to give a mean voxel relative error of 0.07%. Because DoseXYZnrc® does not have the option of modelling a planar source; both the 6MV and Tc99m were modelled from a point source at 1m.

See Table 1 and Table 2 for relative visible photon fluence per unit area: obtained by taking the dose (J/kg), and multiplying by mass per unit area, since the density is uniform; this has the same relative affect as multiplying the dose by thickness of the gadolinium layer and summing the layers in each area, for Tc99m and 6MV spectrum respectively.

Table 1 Fluence from dose deposited in gadolinium from tc99m spectrum

	1.00 mm Cu			1.01mm Cu			0.99mm Cu		
0.4mm Gd	8.043	8.115	8.059	8.034	8.004	8.119	8.126	8.107	8.106
	8.091	8.111	8.072	8.086	8.098	8.128	8.138	8.094	8.137
	8.056	8.102	8.063	8.109	8.139	8.131	8.114	8.059	8.175
0.49mm Gd	9.926	10.022	9.967	9.911	9.932	9.883	9.882	9.843	9.900
	9.885	9.968	9.973	9.895	9.880	9.959	9.864	9.886	9.909
	9.859	9.981	9.843	9.862	9.889	9.835	9.965	9.967	9.894
0.50mm Gd	10.154	10.120	10.181	10.151	10.109	10.130	10.134	10.164	10.191
	10.073	10.066	10.215	10.109	10.143	10.188	10.091	10.167	10.181
	10.062	10.125	10.005	10.069	10.038	10.041	10.125	10.099	10.114
0.51mm Gd	10.298	10.336	10.326	10.293	10.309	10.294	10.236	10.322	10.264
	10.216	10.300	10.369	10.262	10.292	10.304	10.370	10.317	10.297
	10.257	10.202	10.338	10.287	10.310	10.345	10.369	10.314	10.332
0.60mm Gd	12.126	12.144	12.080	11.959	12.104	12.043	12.101	12.076	12.075
	12.011	12.001	11.921	11.975	11.985	11.987	11.978	12.008	12.007
	11.920	11.997	12.025	11.959	11.989	11.961	12.017	12.027	11.999

Table 2 fluence from dose deposited in gadolinium from 6MV spectrum

	1.00 mm Cu			1.01mm Cu			0.99mm Cu		
0.4mm Gd	2.026	2.092	2.078	2.092	2.071	2.009	1.982	2.034	2.025
	2.051	2.019	2.103	2.036	2.002	2.076	2.018	2.032	1.973
	2.070	2.016	2.100	2.030	2.003	2.008	1.979	2.008	2.036
0.49mm Gd	2.564	2.659	2.592	2.585	2.669	2.664	2.543	2.613	2.631
	2.640	2.700	2.576	2.603	2.651	2.618	2.606	2.649	2.759
	2.587	2.673	2.675	2.599	2.609	2.643	2.652	2.620	2.593
0.50mm Gd	2.667	2.663	2.688	2.715	2.752	2.603	2.734	2.667	2.723
	2.661	2.625	2.740	2.646	2.684	2.639	2.666	2.680	2.704
	2.647	2.675	2.714	2.669	2.764	2.773	2.675	2.625	2.662
0.51mm Gd	2.711	2.756	2.785	2.726	2.769	2.806	2.785	2.665	2.687
	2.726	2.795	2.752	2.681	2.751	2.734	2.825	2.758	2.761
	2.827	2.739	2.798	2.756	2.768	2.717	2.722	2.798	2.760
0.60mm Gd	3.400	3.366	3.397	3.313	3.357	3.379	3.414	3.425	3.346
	3.431	3.358	3.438	3.411	3.365	3.406	3.412	3.305	3.328
	3.372	3.344	3.182	3.387	3.290	3.304	3.361	3.309	3.381
Max, and minimum, of the 0.49-0.51 expected thickness of gadolinium.									

The raw data is not the most pertinent way of analysing the data as the flood field is the ratio of each pixel to the mean flood field pixel. So a matrix of the ratios of fluence for each pixel to every other pixel was created for the Tc99m (141KeV) and 6MV spectrum and then the ratios for the percentage difference between the 6MV and Tc99m ratios was calculated, see Eq 2.2., the results of this are in Table 3, Table 4 and Figure 2.7, see appendix B.1 and B.2 for MATLAB® code "d3dose" and "zeroair".

$$p_{ij} = \left(1 - \frac{\frac{Tc_i}{Tc_j}}{\frac{6MV_i}{6MV_j}}\right) \times 100 \qquad \textbf{Eq 2.2}$$

Table 3 Percentage difference between of 6MV pixel ratios to Tc99m pixel ratios

			Gadolinium in mm								
			0.49	0.50	0.51	0.49	0.50	0.51	0.49	0.50	0.51
			1mm Cu			1.1mm Cu			0.99mm Cu		
Gadolinium in mm	0.49	1mm Cu	0.00								
	0.50		0.33	0.00							
	0.51		0.35	0.03	0.00						
	0.49	1.1mm Cu	-0.01	-0.34	-0.37	0.00					
	0.50		0.70	0.37	0.34	0.71	0.00				
	0.51		-0.08	-0.40	-0.43	-0.06	-0.78	0.00			
	0.49	0.99mm Cu	1.49	1.17	1.14	1.50	0.80	1.56	0.00		
	0.50		0.72	0.39	0.36	0.73	0.02	0.79	-0.78	0.00	
	0.51		0.79	0.47	0.44	0.81	0.10	0.87	-0.70	0.08	0.00

Table 4 Percentage difference between 6MV pixel ratios to Tc99m pixel ratios for limits of variation.

			Gadolinium in mm								
			0.40	0.50	0.60	0.40	0.50	0.60	0.40	0.50	0.60
			1mm Cu			1.1mm Cu			0.99mm Cu		
Gadolinium in mm	0.40	1mm Cu	0.00								
	0.50		-1.44	0.00							
	0.60		-3.07	-1.61	0.00						
	0.40	1.1mm Cu	3.56	4.93	6.44	0.00					
	0.50		4.25	5.61	7.10	0.71	0.00				
	0.60		3.50	4.87	6.38	-0.06	-0.78	0.00			
	0.40	0.99mm Cu	8.82	10.12	11.54	5.45	4.78	5.51	0.00		
	0.50		8.81	10.11	11.53	5.45	4.77	5.51	-0.01	0.00	
	0.60		8.75	10.05	11.47	5.38	4.70	5.44	-0.08	-0.07	0.00

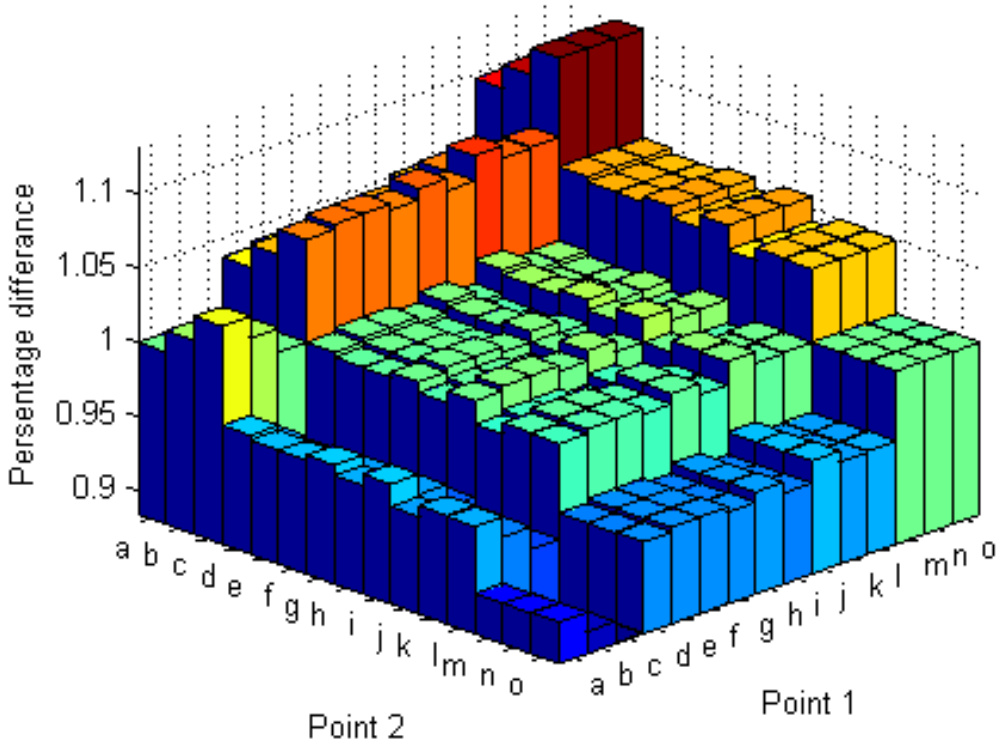

Figure 2.7 Relative ratio of Tc99m to 6MV, for the different combinations of thickness of gadolinium and Cu

Key					
	0.4mm Gd	0.49mm Gd	0.5mm Gd	0.51mm Gd	0.6mm Gd
1 mm Cu	a	d	g	j	m
1.01mm Cu	b	e	h	k	n
0.99mm Cu	c	f	i	l	o

While the difference between the max (1mm Cu 0.51mm Gd) and min (0.99mm Cu 0.49mm Gd) fluence for the 6MV spectrum is greater than 10% for a thickness tolerance of 2% for gadolinium and 1% for copper element, the ratio of maximum to minimum for Tc99m and max to min for 6MV the will be less than 1.6% ±0.1%. From Table 3 it can be seen that if the thickness are within 0.1mm tolerance then there will be less than 1.6% difference between the response of a 6MV spectrum and Tc99m. This means that the most accurate flatness that you can get from a Tc99m phantom is 1.6%. From Table 4 it can be seen that a change in thickness of gadolinium is least affective with 1mm of copper above it.

2.4 Linearity

The linearity of aSi EPIDs at linac beam energies and dose rates, has been well established [10, 13, 15, 25-31]. The bulk of the imaging in this research is done using Tc99m at lower dose rates than what is normally achievable with a linac. To determine if there is a difference, at low energy and dose rates, the linearity was investigated with Tc99m by spot checking the linearity with dose rate by placing 5 vials of different activities (93.7, 213, 387, 812, 1205 MBq) of Tc99m in 5 positions on the imaging cassette, see Figure 2.8, and rearranging so that images can be taken, see Figure 2.9 for sample image, with every vial in every position, see Figure 2.10.

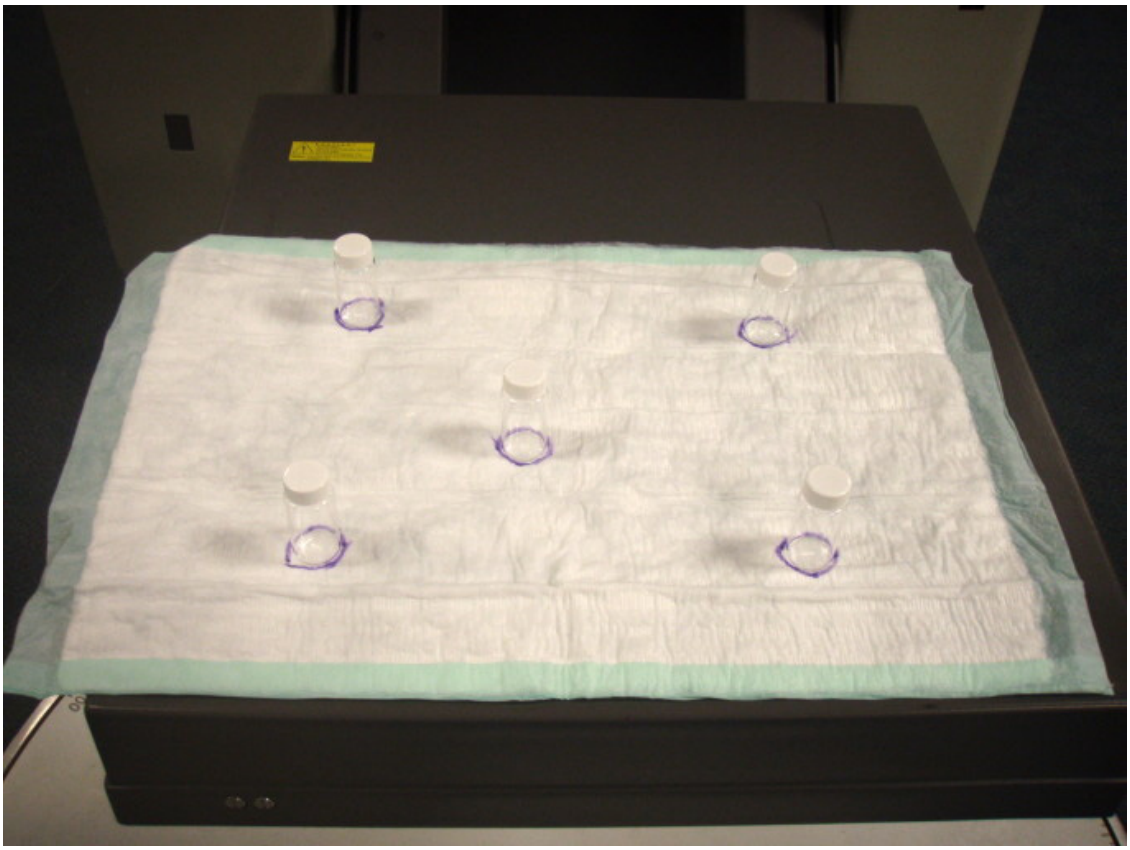

Figure 2.8 Tc99m vial placement on EPID cassette.

The imaging regime that was used was 100 images, of one frame average, were taken, for each arrangement of vials, for each of the linac "dose rate settings" (100MU/Min 300MU/Min and 600 MU/Min) for both energies (6MV and 18MV). The 100MU/Min setting had the most signal per frame so it was chosen as the primary modality for all further experiments and data analysis; the results for the other modalities were similar but had higher noise levels. Each image was read into MATLAB® and added together to get a single image for each geometrical arrangement of vials. The higher signal strength at the lower dose rate settings seam counter intuitive, but the dose rate the EPID is receiving from the Tc99m is the same for all settings. The "dose rate setting" changes the frequency of the sync pulse and the numbers of rows read out per pulse, therefore on the lowest setting (100MU/min) the EPID is integrating for longer between the reset frame and the image frame

For analysis an area of 15x15 pixels was selected for each position which was encompassed by the hotspot of each of the activities for that area. This was selected to be small enough that, small errors in placement of the vials did not produce a significant change in dose deposited in the area selected. The same pixels were used for each arrangement of vials to ensure that it was a measurement of pixel sensitivity, see appendix A.1.1 and A.1.2 for MATLAB® code. After dark field correction, the cross correlation (or r^2), between each of the 5 positions and the activity, was calculated. From the results in Figure 2.11 it can be seen that the response is linear.

To make the MATLAB® coding easier a 9 points of interest (POI's) were sampled, the 5 that had vials above them and 4 that were not exposed, marked dark red in Figure 2.10, it was noticed that the 4 unexposed POI's changed noticeably between configurations. When this change was plotted chronologically there was a definite drift in the background measurements. When it was corrected for the background drift the cross correlation coefficient increased from 0.995 to 0.998, see Figure 2.12. A cross correlation of individual pixels (the centre of each 15x15 area) and activity was taken to ensure that the linearity was an individual pixel phenomenon and not a global averaging effect, see Figure 2.13. The cross correlation of the single pixel measurement is still good even though it is much more susceptible to noise and fluctuations in the placements of the vials in the exact positions of measurement. The cross correlation of the background drift corrected relationship of the order of $r^2 = 0.9995$ is good enough to assume that the response is linear.

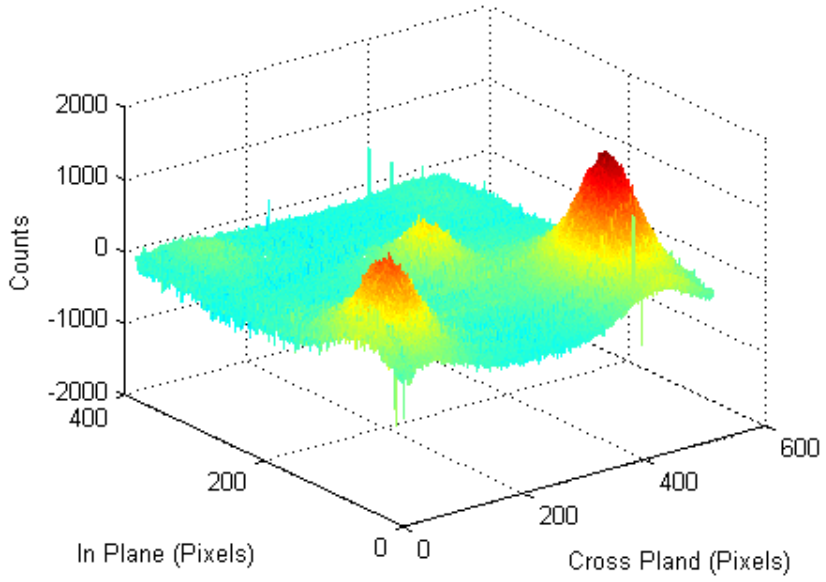

Figure 2.9 Dark field corrected peaks from vials of 5 different activities of TC99m of Tc 99m, inverted for aesthetics.

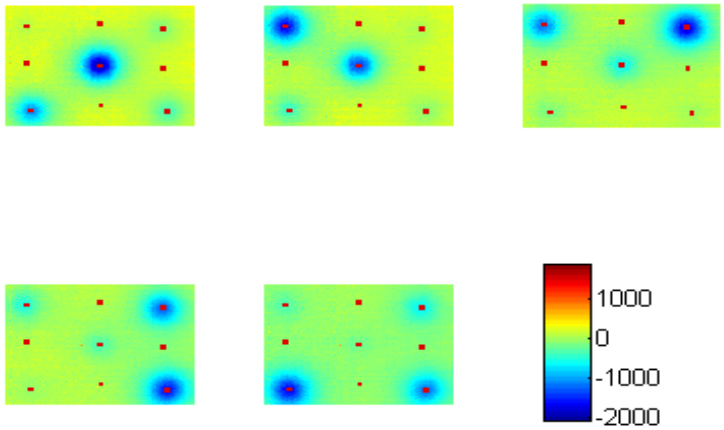

Figure 2.10 5 permutation s of locations for each vial, showing locations of 15x15 sampled pixels as +1500 (dark red)

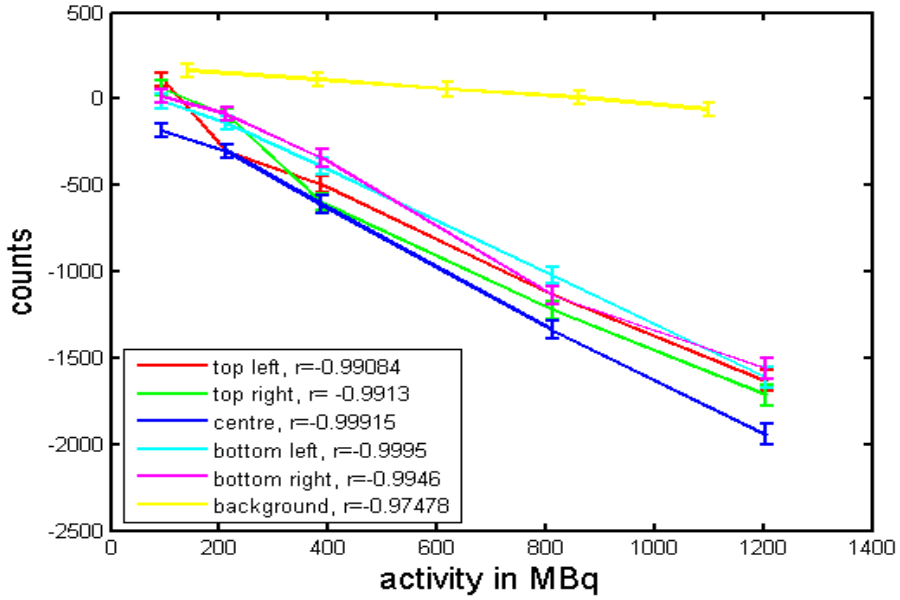

Figure 2.11 100 mu/min response of the mean of 15x15 pixels per plot, corrected with dark field but uncorrected for drift in background

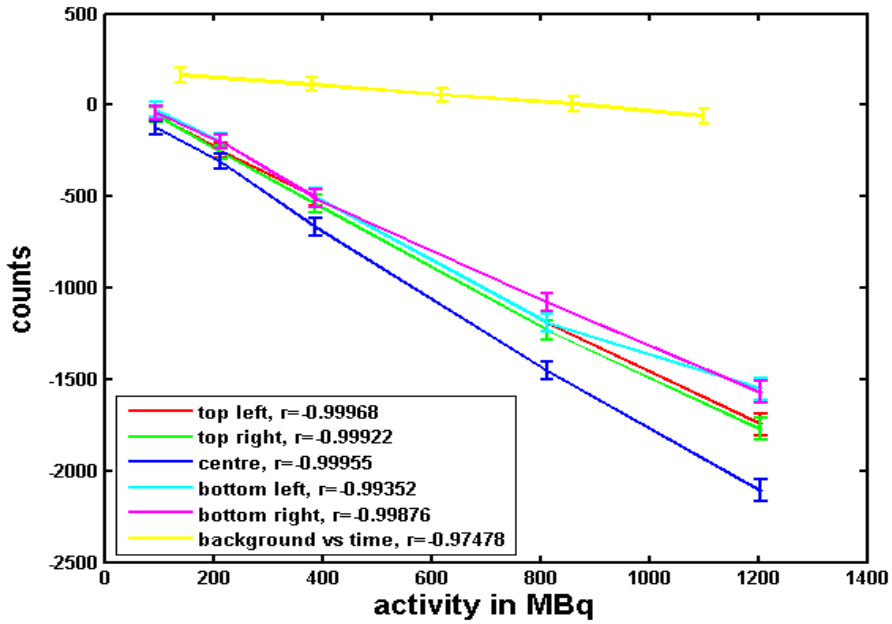

Figure 2.12 100 mu/min response of the mean of 15x15 pixels per plot, corrected with dark field and corrected for drift in background

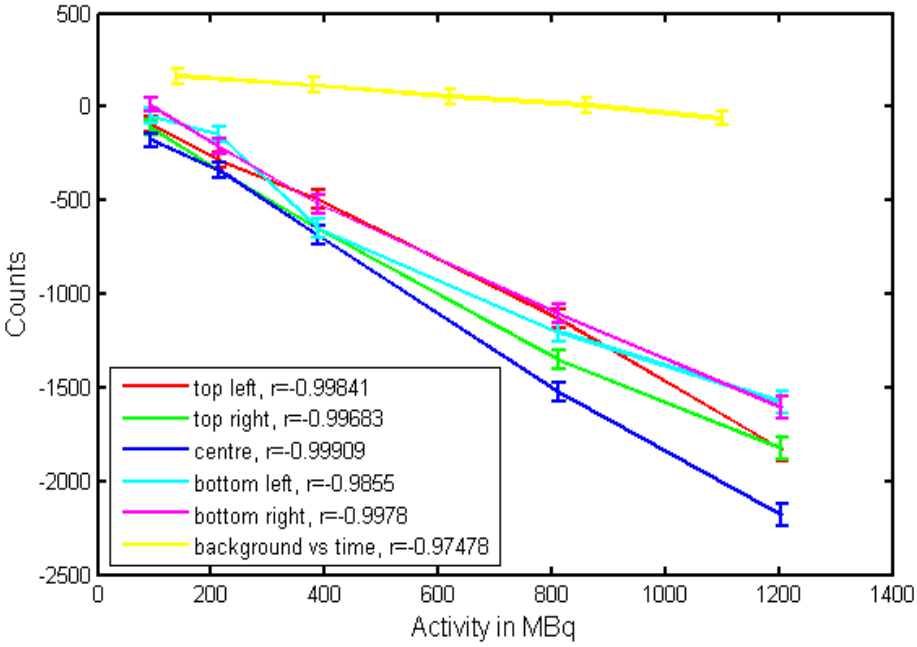

Figure 2.13 100 mu/min response of a single pixel per plot, corrected with dark field but uncorrected for drift in background

2.5 Ghosting and Drift

It was initially postulated that, the background drift in the linearity test was caused by ghosting from exposure during clinical usage prior to the measurements. Ghosting has been investigated under clinical conditions and it was found to contribute a signal remnant of approximately 1% to the next image [8]. 1% of the clinical beam is approximately 40 counts per frame; this corresponds to 700% of the count rate achievable from a technetium phantom. With the ghosting having a potential influence on the flood fields it was necessary to investigate the behaviour of the ghosting to mitigate its effects.

The EPID was left 24 hours without being exposed to a beam. Sporadically dark fields were taken to purge any residual signal. Then the EPID was exposed to a beam of 20MU at 6MV defined by the MLC (multi leaf collimator), see Figure 2.14, with the EPID using its internal trigger so it would carry on imaging once the beam had stopped.

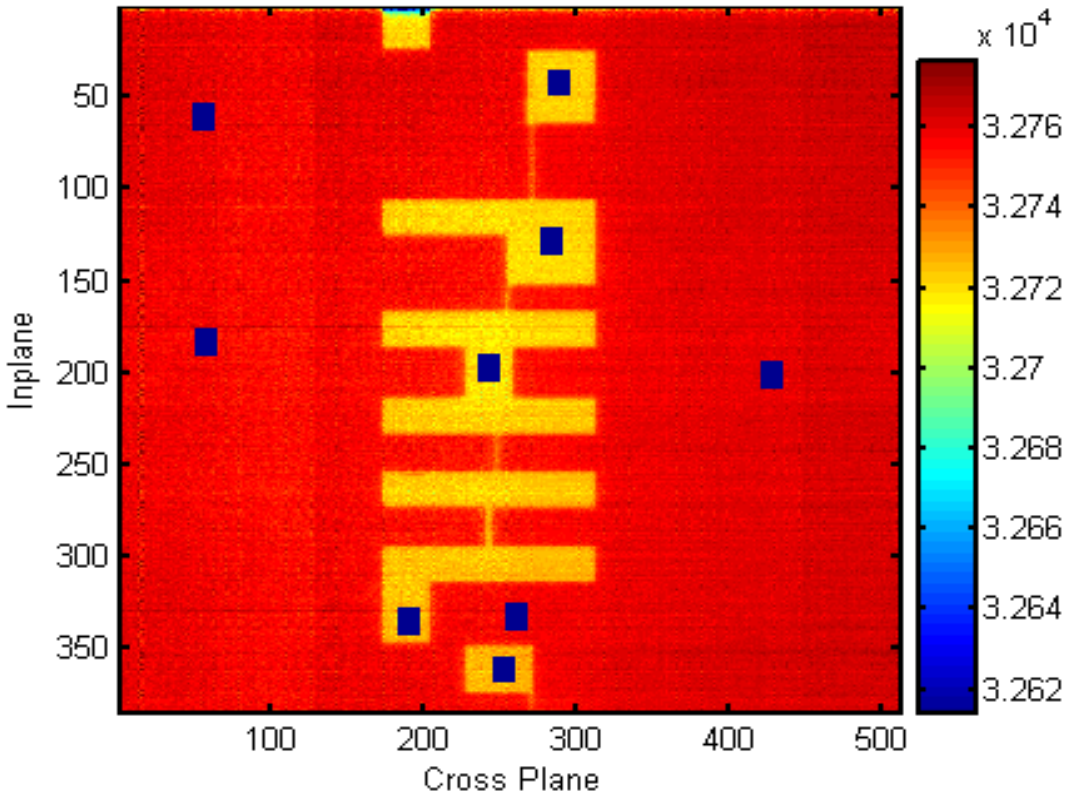

Figure 2.14 Locations of sampled points of interest (in blue) on ghosting pattern

Arbitrarily selected POI's within the beam and out of the beam, marked in blue in Figure 2.14, were sampled at the maximum rate possible, one frame per second, through-out the beam on time and then after the beam had stopped, until 1 minute after the beam was no longer visibly detectable on the portal vision screen, which took 1 minute. The DICOM images were imported into MATLAB®, see appendix A1.2 for code. The time stamps of the image were extracted from the DICOM headers, and the difference between the in-beam POIs and out-of-beam POIs was calculated, and the ghosting signal decay plotted, see Figure 2.15.

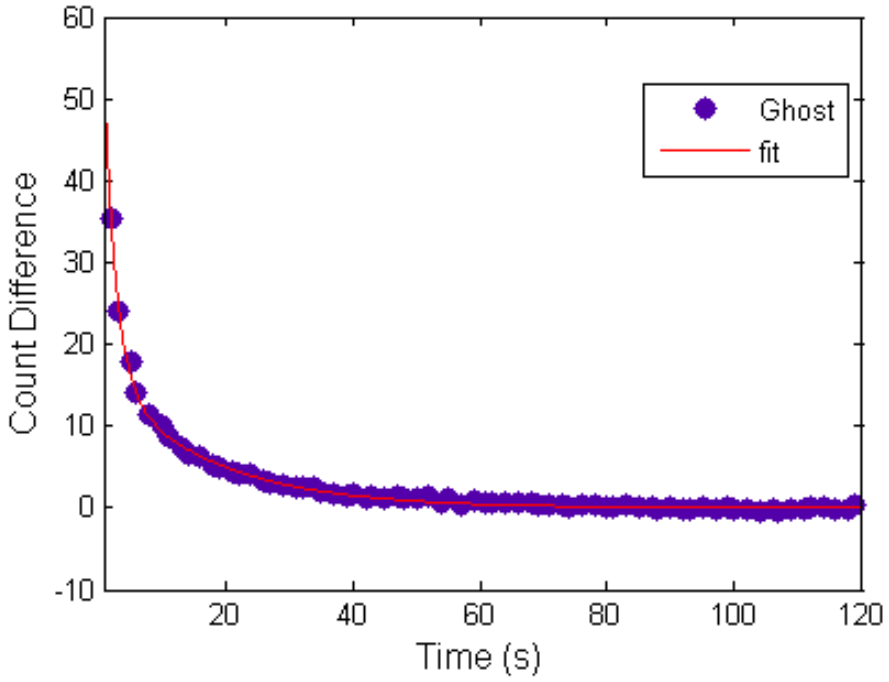

Figure 2.15 Ghosting duration after beam off, with an exponential decay curve fitted

It can be seen that the residual signal was quite clearly not to a long-term effect, indicating that it is not what was causing the drift in the background of the linearity measurements. By looking at the sporadically measured dark fields in Figure 2.16, a drift can be seen to be greater than the noise of any group of dark fields, which decreases after time. It was postulated that it could be caused by thermal effect but experiments to elicit this effect by increasing the temperature of the EPID proved inconclusive. So it was determined to mitigate the effect of drift by alternating periodically between taking dark fields and Tc99m flood fields.

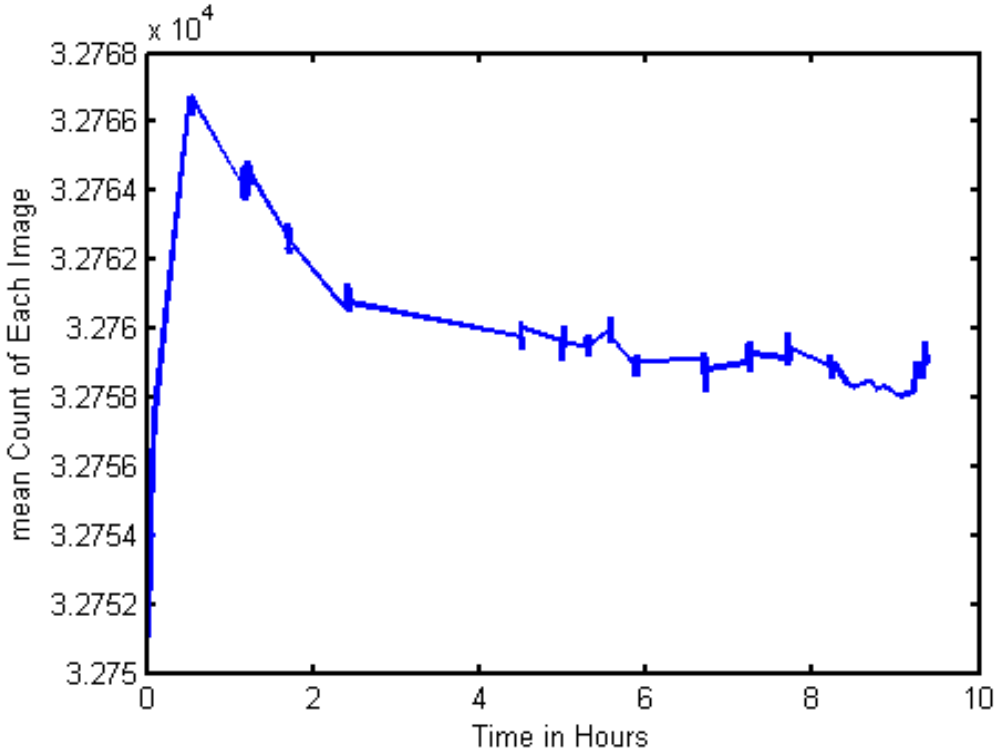

Figure 2.16 Mean EPID dark field drift

Experimental methods

This chapter describes the materials and methods used in using a flood phantom to achieve a flood field on and EPID. The first step in this is to calculate the size of the phantom needed to achieve a uniform dose deposition in the EPID. Then the practical considerations of a physical phantom are described and methods of comparing the dose distribution with the theoretical model. Last, we look at a method of taking a flood field with the Tc99m phantom and the statistical limitations.

3.1 Dose calculations

To predict what size phantom is needed, to achieve better than the 3 % flatness achievable with the linac, it is necessary to understand the relationship between the variables used in constructing a phantom (Width, Depth, Height, Distance, and Deformation). To calculate the relative dose deposited, in the EPID, by classical methods the two main factors are: inverse square law and attenuation within the build up of the EPID. With parallel geometry between the source and measurement plane the attenuation, in all layers, can be amalgamated into a single factor, for all layers, because the length of travel through a layer remains in the same proportion to the total travel as the angle of incidence changes. So the dose to a point can be calculated with a triple integral over the volume of the phantom, see Eq 3.1, where x y & z are coordinates in the phantom from the centre of the EPID, and a and b are the in plane and cross plane coordinates of the pixel in the EPID. The integral needs to be in Cartesian coordinates otherwise the bounds (ip, cp, and pt, these are dimensions of the phantom and h the height from phantom to EPID) become problematic.

$$\int_{z=h}^{z=h+pt}\int_{y=-cp}^{y=cp}\int_{x=-ip}^{x=ip}\frac{e^{-\mu t\frac{\sqrt{(x+a)^2+(y+b)^2+z^2}}{\sqrt{x_o^2+y_o^2+z^2}}}}{(x+a)^2+(y+b)^2+z^2}dx.dy.dz \qquad \textbf{Eq 3.1}$$

A solution to the indefinite integral could not been found analytically using dedicated mathematics software (i.e. Maple: Maplesoft Inc, Waterloo, Ontario, Canada.), so it was solved by numerical methods. Because the equation that is integrated changes for each pixel in the EPID, MATLAB was used to numerically solve the definite integral for each pixel. The dose distribution to the EPID can be calculated with 5 nested iterative processes (in plane, cross plane, x y and z), but this would involve calculation of many values more than once. As an example one would need to calculate the dose from the PVE (phantom volume element) above each pixel for every pixel, which is the same for all pixels. To avoid these unnecessary calculations a different conceptual approach was used. Rather than calculating the distribution from a point source and summing the contributions from each source to each pixel, it was calculated from the pixels perspective, this means the contributions to each pixel from each PVE (with PVEs the same area as pixels) was calculated. This allows the creation of a matrix, which was assigned the name *relative contribution matrix* (RCM). The value of each element in the RCM represents the dose deposited to an EPID pixel that is under the centre of the RCM from the PVEs above that element (Figure 3.1). To include all geometries between pixel and PVEs the dimensions of this RCM are: width being equal to, the width of the EPID plus the width of the flood phantom; and length being equal to, the length of the EPID plus the length of the flood phantom. The RCM contains the values for all geometries between every pixel and the vertical sum through the PVEs in the flood phantom. So for each pixel in the EPID there is a subsection, the size of the flood phantom, of the RCM that represents the dose from the flood phantom, see Figure 3.2 for the centre EPID pixel subRCM and Figure 3.3 for the bottom right EPID pixel subRCM, these subsections are summed to give the dose deposited in that pixel from the entire flood phantom. At first appearances this seams as though the subsection is moving the wrong way as you move the pixel of interest, but the centre peak will always be directly over the pixel of interest in the EPID, as depicted in the two dimensional example in Figure 3.4 .

As the system is symmetrical the dose distribution is only calculated for one quarter of the EPID and reflected twice to produce a whole EPID image. This takes the processing time down from over 24 hours to 1.7 hours to create a dose distribution for the EPID, see appendix A.2.2 for MATLAB® code “epddg4“.

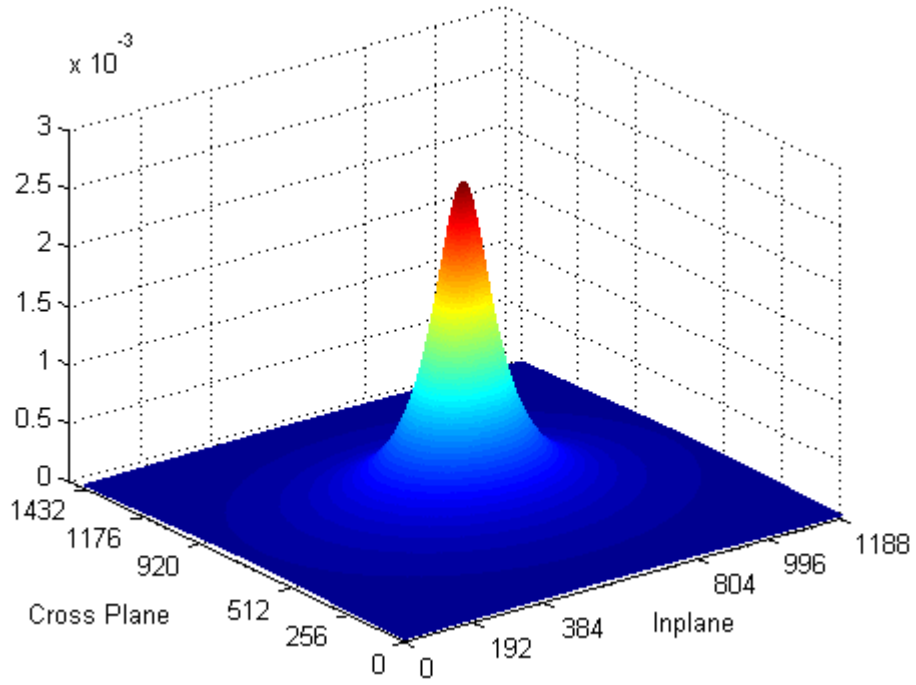

Figure 3.1 Relative contribution matrices the size of the phantom plus the EPID width, with edges of the centre and corner pixel sub matrices marked.

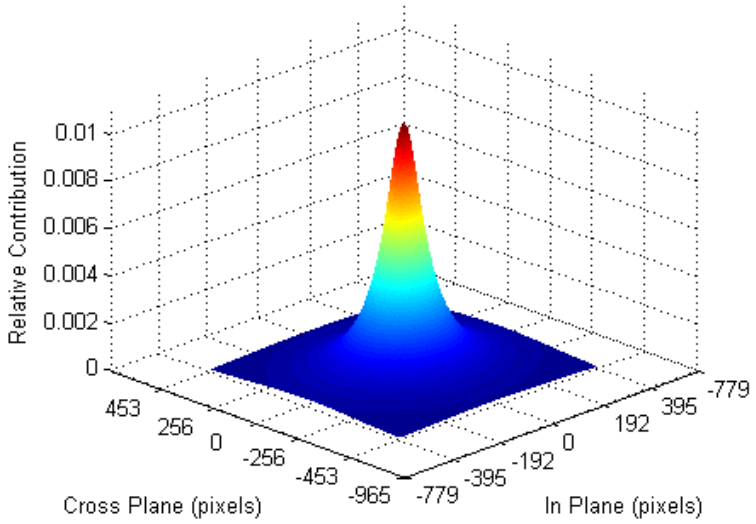

Figure 3.2 Relative contribution matrix for the centre EPID pixel

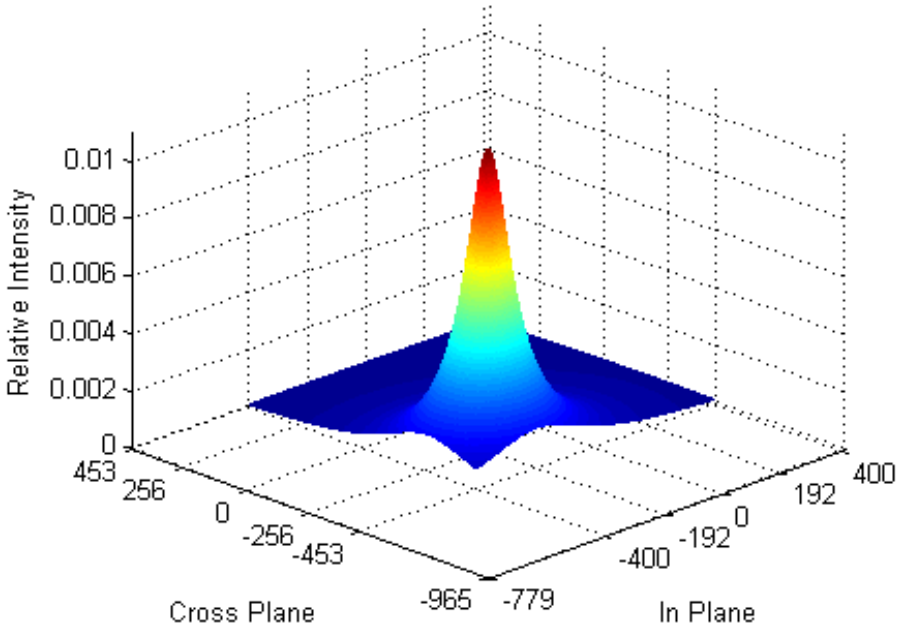

Figure 3.3 Relative contribution matrix for the bottom left pixel of the EPID.

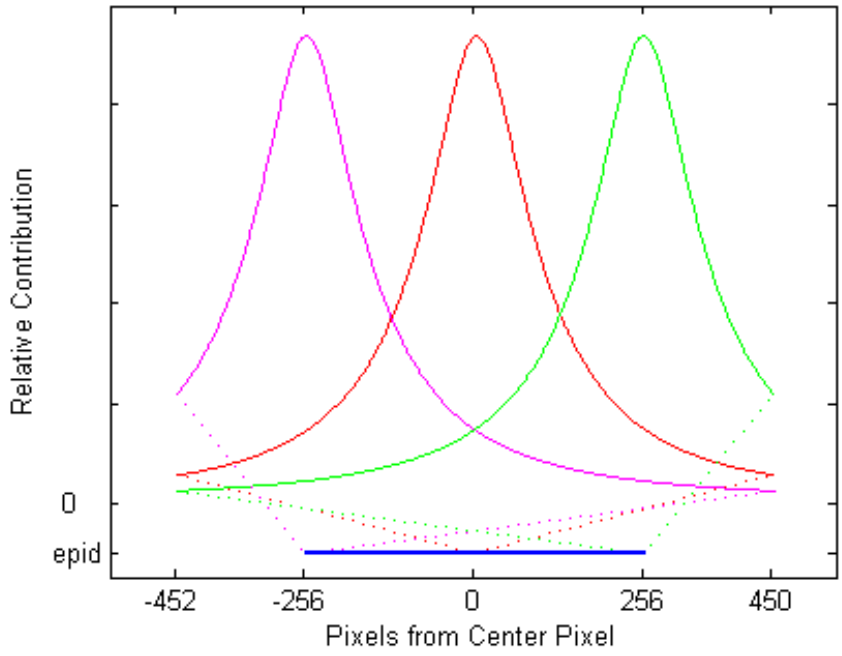

Figure 3.4 2D Relative contribution.

3.1.1 Optimising the phantom design

Now that we have constructed a model to predict the distribution of a given phantom, we can use that model to investigate how the dose distribution changes with different input parameters (phantom thickness (pt) distance away from the EPID (h), and overlap (cp & ip)). It is intuitive that the larger the overlap, of the phantom over the EPID, the flatter the flood field. For a point source the flatness increases with distance but an infinite flat source produces a flat field at all distances and it is intuitive that with overlap the closer you get to the source the closer approximation of infinite plane geometry is achieved. To understand how these factors affected each other and how they are affected by phantom thickness it was necessary to model the phantom for every combination over a range of all the input parameters. This was achieved by using the MATLAB code that iterated over a range of thicknesses, overlaps and distances, see appendix A.2.1 for code "Epipcpri6d.m". However to calculate the whole EPID for all of these iterations would have required excessive processing time, so just the in plane and cross plane profiles were calculated. This also reduced the amount of data storage needed, as running MATLAB® in a 32bit platform limits the amount of addressable memory to 3GB. Even with these processing techniques it still took over 40 hours to process.

In a perfect world this would indicate that the phantom should have as much overlap as possible be a thin as possible and as close as possible to the EPID. However the major limiting factor of using a radio nuclide is radiation protection. Therefore the limitation that all geometries have the same activity of radionuclide is necessary. Specific activity is not a limiting factor, because a fresh milking of a Tc99m generator can get over 100GBq in activity in 20ml and the smallest volume would be 240ml. So the relative intensity, of each combination of input parameters, is recorded by data-logging the EPID central pixel divided by the volume, of give a relative comparison of signal strengths for each combination.

The flatness could be improved on by shaping the phantom to make it thicker at the edges, to mitigate the edge effects. This would need to be a smooth deviation from the rectangular, if the system is to be used clinically to avoid derogation of image quality. To create a 20m radius curve in a 400mm wide object is not an easy task, so rather than machining a curve into the phantom, it was decided to bend the phantom into a deformed shape, because it is sealed for radiation protection reasons, the shape formed would be held in place by the hydraulic force of the sealed liquid. The shape that it was assumed to be formed on the phantom was a 2 dimensional extrapolation of the hyperbolic sine function [32]. When this was added into the model it was not possible to model the change in thickness directly while using the subset of the RCM, so the subset was multiplied by the ratio of deformed thickness divided by undeformed. This produces the greatest inaccuracy where the PVE is furthest away from the pixel where signal contributes least so this small discrepancy was ignored.

3.1.2 Physical geometrical considerations

In designing the flood phantom, it was noticed that the housing of the EPID was very close to the imaging cassette and would shield parts of the EPID from parts of the flood phantom. Sightlines, from the imaging cassette to the corner of cassette housing and on to the phantom, shown in Figure 3.5, define the areas of the flood phantom that are contribution signal to EPID. Therefore these need to be included in the model. Sightlines were included in the code to produce a new set of optimal conditions. By rewriting the code, to adjust size of the overlap to remain within sightline 90% of the EPID width, when the distance is adjusted so is the phantom size. For the model it is assumed that the contribution outside of the sightlines is zero as the EPID housing is 4-12 mm thick cast aluminium. To make the coding easier the cut off point is defined at the point where the sight line bisects the midline of the technetium volume. This over estimates contribution by the difference between the triangle section above the sightline that is outside the cut off point and the triangle inside the cut-off point that is below the sightline. See appendix A.2.2 for the MATLAB code “epddg4”.

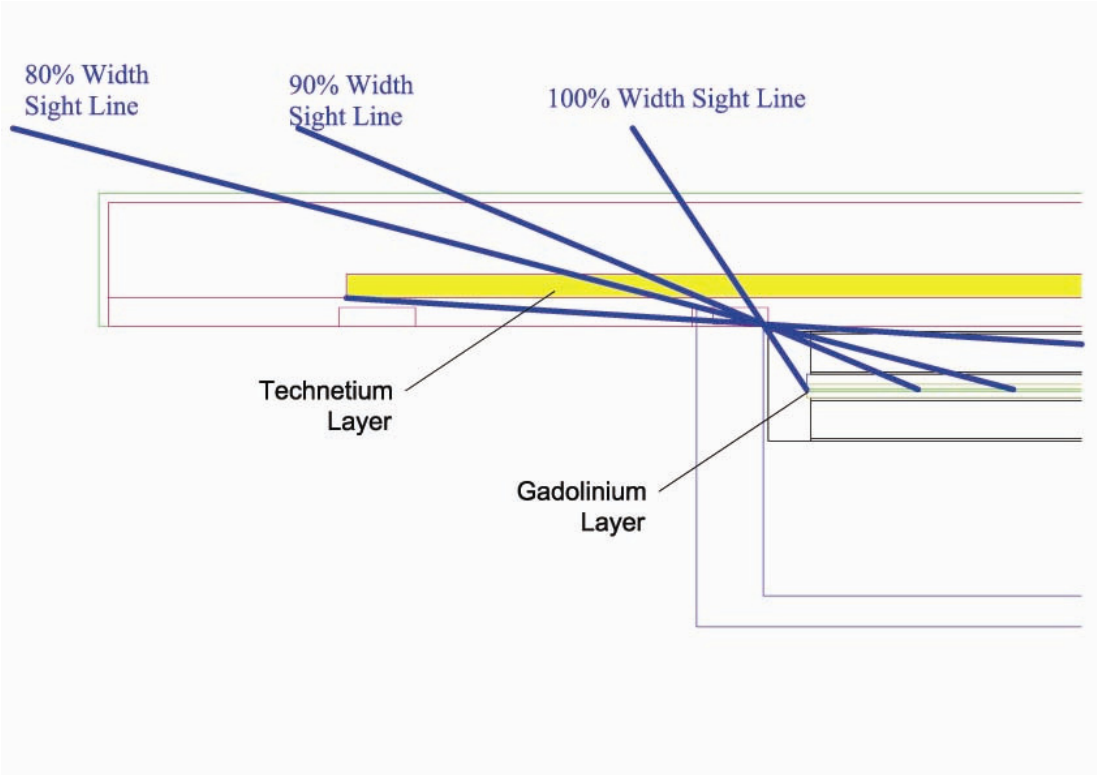

Figure 3.5 EPID and Phantom depicting sightlines past the edge of the EPID housing

3.2 Physical preparation and loading of the flood phantom

Based on the results of the computational modelling an existing nuclear medicine phantom was used. To load the phantom cavity with Tc99m and have the desired deformation it is necessary to find a way of predictably deforming the phantom and adding the technetium to the solution. Because the phantom deformed unpredictably unless it was supported, the phantom needed to be filled in a near horizontally position with a solid support, which requires a sealable filling whole in the top face of the phantom. To measure the deformation a DTI (Dial Test Indicator) was used by placing a steal beam across the phantom (Figure 3.6) when the phantom was undeformed and then placing weights (in an accurately reproducible position) on the phantom to deform it (Figure 3.7), then taking the difference as the value of the deformation. This allows us to find a weight we need for any deformation, so the desired weight can be placed on the phantom in a safe environment without the need for the DTI.

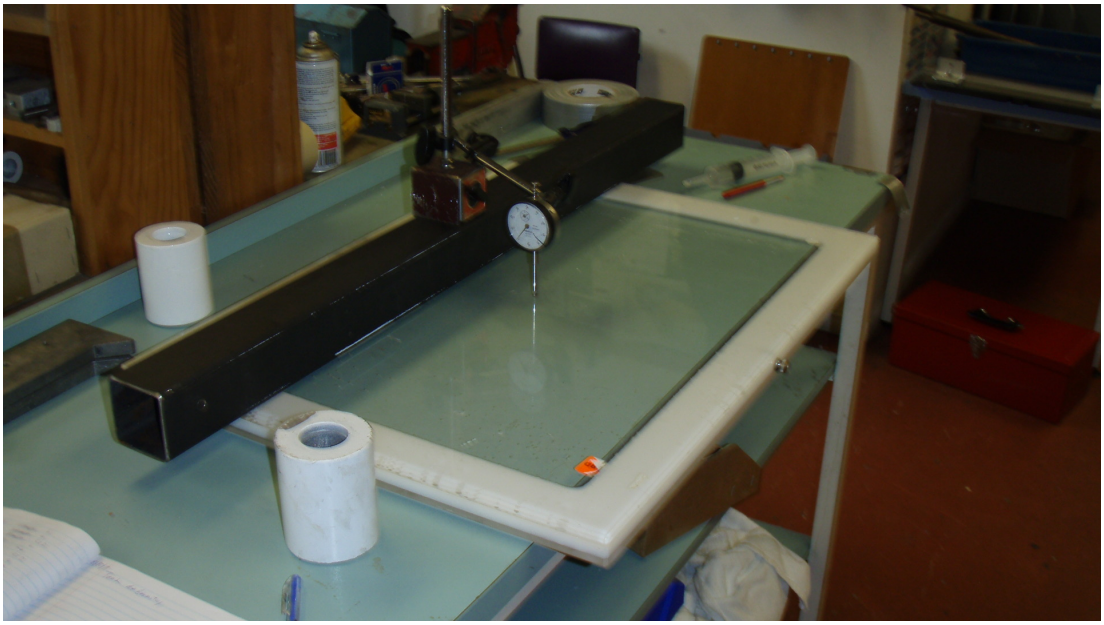

Figure 3.6 DTI on flood phantom to measure relative deformation

Figure 3.7 Weights placed on phantom to measure deformation. The DTI is obscured from view by the weights.

	The procedure for loading the phantom was to:
1	Deform the empty phantom, with specified weight
2	Fill it with deionised water
3	Seal the filling hole, remove the weight and move all the air bubbles to the filling hole
4	Place the phantom on a slightly angled support to ensure that the air bubbles remain at the filling whole
5	Reweight the phantom to maintain the deformation
6	Unseal the filling hole and top up the phantom with deionised water
7	Remove a volume of water equal to the volume of Tc99m plus 5ml
8	Add the Tc99m carefully to endure no air bubbles are introduced.
9	Fill with water leaving the smallest air bubble possible so when the plug is put back in it does not force the radioactive liquid out
10	Seal the filling hole, remove the weight
11	Agitate to mix thoroughly

The air bubbles needed removing in step 3 as they got trapped in local maximums in the top of the phantom due to irregularities in the surface, but steps 1-5 can be omitted if the phantom is not opened without the weights it was sealed with, and the deformation is changed carefully so that the air bubble did not get to far away from the filling hole.

The two largest faces of the phantom could not be shielded directly as the option to use either or both faces for flood field was required, but the edges were shielded with 1 mm of lead as a radiation protection precaution to reduce radiation exposure when handling the flood phantom, this does not affect the EPID exposure as the phantom is bigger than the EPID.

3.3 Comparison between flood phantom measurements to calculation

In this section the methods of producing a distribution in film from a flood phantom is described, then the film distribution is compared to what was calculated. To do the comparison a piece of software called Doselab4 [33] is used. DoselabV4 is a software tool that was designed to compare treatment planning system output to films taken on a linac for IMRT QA, but is extendable to more general applications and efficiently aligns and compares two images. Film was used as the response across the film is constant, also with Tc99m there is no energy dependence (of the film) to be concerned with. The most sensitive film available is Kodak T-MAT G/RA film, it was chosen over EDR2 and X-OmatV, but it does not have a linear response to optical density (OD) to dose [34]. Unfortunately the film could not be used in the cassette it is designed to be, because there is an anti-scatter grid inbuilt into the cassette. So a method of protecting the film from visible light was needed, so a preliminary method was designed using the X-OmatV film packet that had been opened on one edge with the T-MAT film in it. As the T-Mat film is larger than the X-OmatV film packets each piece of film was cut in half and placed in 2 film packets, the open edge was then folded over with a 4cm fold then a 2cm fold, to produce 3 180º curves in opposite directions to seal the light path these folds were held in place with 3 paperclips.

The OD to relative dose curve was created in a similar way to the linearity test in section 2.4, in that vials of different activities of Tc99m were place on the film in a makeshift packet and left to expose the film. To create the calibration curve a large number of points was needed, so lead pot were used to shield each vial so that they could be placed closer together without affecting each others point of interest, this allowed 8 vials to be used on each film. To obtain a wide range of points to fit a curve to, 4 films were taken with the same vials with decreasing exposure times and decreasing activities (due to decay). This gave a dose deposited in each POI proportional to the total number of decays that the film is exposed, to which henceforth will be called “corrected activity”. The background fog varied between the films so a reading was taken in an area selected to be as free as possible from influence from defects in the film packet and dose from the vials, this was subtracted from all POIs.

Calibration curves were determined for each film. It was found that each film had I different background fog, this was adjusted for by introducing a factor to align all 4 curves to form a single smooth curve. To allow for easy interpolation and extrapolation and smoothing an exponential curve was fitted to the log linear plot of the OD and corrected activity, this curve was then used in the DoselabV4 software to calibrate the films. Doselab4 is designed to compare two dose distributions, and the MATLAB model produces a normalised relative distribution, so to bring them into the dose domain a point in both the MATLAB calculated distribution and the film and the calibration curve was normalised to this point.

A series of films in their makeshift packet were exposed to the flood phantom with approximately 5GBq of TC99m in it. The films were taken off the phantom at intervals and developed to find the best length of time to expose the film to the phantom.

Unfortunately the size of the film is limited, and the whole phantom could not be covered with a single piece of film, so the film was placed overlapping the edge of the phantom as that is where there is the greatest range in the model and where the errors in the model are expected to be most evident. A film packet was then placed overlapping the edge of the phantom at 12mm, away, the thickness of the front face, and another film was spaced away from the phantom using 2 polystyrene sheets each 12 mm thick these were left to expose over night. The films were marked with the location edge of the phantom, which is 50mm away from the edge of the Tc99m, for registration purposes. The films were left to expose to a phantom containing 5GBq of TC99m, then removed and processed along with a film in a packet that had been left in the same conditions but not exposed to the phantom. These films were then scanned, with a Vidar Dosimetry pro film scanner, with 16 bit depth and imported into DoselabV4.

A modified version of the MATLAB code “epddg4” (see appendix A.2.2 for original) was used to create predictions of the relative dose deposited in the EPID as if it were at the location of the film. The code had to be modified for these predictions to remove the shielding of the phantom by the housing, and to allow for a bigger EPID than the phantom. The output was then converted to a 16 bit tif and imported into Doselab4.

Doselab4 takes two images and calculates gamma index images, distance to agreement images, relative percentages differences, and comparison profiles. So it is an effective tool for comparing my calculated distribution to the film distributions. The auto alignment tool was checked by aligning the two images with the inbuilt MATLAB function “normxcorr2”, which DoselabV4 calls, and comparing where the films were marked with the edge of the phantom and the edge of the phantom in the MATLAB model, this required rescaling the film image down from the 71 DPI (0.36mm pixel size) that it was scanned at to the 0.78 mm pixel size of the MATLAB model.

3.4 EPID measurements with the phantom

Once the phantom size was chosen and the flatness calculated (with the MATLAB model) flood fields for the EPID were obtained. To obtain flood fields using the phantom as a source the phantom needed to be accurately placed close to and parallel to the EPID. As the phantom deformed due its own weight, the phantom needed to be supported. So the easiest way to arrange the EPID and phantom was to turn the linac gantry to 180º and extend the EPID. Thus the phantom could be fully supported from underneath and the EPID could be exposed through the top face of the phantom. When the EPID hangs from the counter weight of the gantry the panel was not level, in the in plane direction. Consequently a method of adjusting the angel of the flood phantom, so that it is parallel to the EPID, is needed. To do this a plate larger than the EPID with an adjustable height leg in each corner was constructed. The top surface was covered with 1mm of lead for radiation protection and then covered in clear coat paint, to prevent lead contamination while handling. This was placed on the linac patient couch to adjust the height conveniently, see Figure 3.8.

Figure 3.8 Phantom support on couch

The procedure for taking flood fields is:

1. Set the portal vision "AM maintenance" software to "internal trigger" and "no correction", see appendix D.1
2. Start the EPID imaging continuously on a high (8-32) frame averaging rates with the AM maintenance software.
3. Extend the EPID and remove the fibreglass cover, remove the metal cover plate and replace it with two small cassette retention tabs to hold the non-electronics side of the imaging cassette in.
4. Rotate the gantry to 180º, carefully as the fibreglass cover is the collision detection system.
5. Place the adjustable plate on the couch and move it till it is under the EPID.
6. Using 4 spacers 12mm in height, one below each corner of the imaging cassette, on the plate raise the height of the couch until the closest spacer is almost touching the EPID, then use the adjustable legs to adjust the plate till all the spacers are touching and it is parallel with the EPID.

7. Move the couch away from the EPID so that the phantom can be easily placed on the adjustable plate.
8. Leave the system imaging for approximately 2 hours to let the drift come to a shallow gradient.
9. Fill the phantom as per section 3.2 and place it on the adjustable plate as far away from the EPID as the couch allows.
10. Stop continuous imaging and adjust the frame averaging to 1, and take 50 dark-field images,
11. Move the couch so the centre of the phantom is under the centre of the EPID and use the adjustable legs and the 12mm spacers to ensure that the phantom is parallel with the EPID, and take 100 dark field images
12. Move the couch so the phantom is as far from the EPID as the couch allows (approximately 1M) and take another 50 dark field images.
13. Repeat step 11 and 12, 30 times.
14. Import the images into MATLAB and subtract the adjacent dark fields from each set of flood fields them sum the 30x (100x) FF-(2x50x) DF.

The initial dark fields are needed to ensure that the output has become stable before the flood fields are calculated. The fibreglass cover, of the EPID, needs to be removed to ensure that the distance between phantom and EPID and alignment is accurate. The metal cover plate would produce a similar effect as the housing shielding in section 3.1.2, so it has to be removed. The only thing supporting the non electronics end of the imaging cassette is the metal cover plate so two small tabs were made to secure the imaging cassette when the plate was removed. By taking before and after dark field it is possible to mitigate the effects of the drift in the dark field provided that the gradient of the dark fields is not too great. In section 2.5 it can be seen that the dark fields has a shallow gradient after approximately 2 hours, so the flood field imaging is postponed till 2 hours after the cover has been removed. After the dark field has become stable the dark fields and flood fields were taken by consecutively alternating between 100 images of each to mitigate any drift in the dark fields. These images were imported into MATLAB using the code in appendix A.1.1 which produces a: mean; standard deviation; medium; and sum for each pixel in each group of images, as well as a graph of mean pixel for each image. The last step was to subtract the dark fields from the adjacent flood fields. Then sum all of these together to produce a flood field with bit depth and signal to noise ratios better than 3 %.

The main issue to be resolved in using Tc99m, is can you get the signal to noise ratio good enough. The metal cover that has been removed is part of the electromagnetic shielding, so to establish the effect of this on noise, dark fields were take with 1 and 2 reset frame and 1-11 image frames.

3.4.1 Statistical analysis

Because it is not practicable to achieve the dose rates of the beam with Tc99m, particular attention needs to be paid to the desired accuracy and the bit depth of each frame. The difference between the responses of each pixel was less than the resolution of the bit depth in any of the individual images this difference is undetectable, e.g. 5 +3% is still 5 when rounded, to an integer. However, due to the noise level being greater than bit depth the average of many images this difference is detectable. To better understand this, a Monte Carlo model was made in MATLAB to investigate the effects of how the accuracy and precision vary with number of images and frames averaged in each image. The code takes a range of numbers from 5 to 5 +3% and adds it to a series of random numbers and then rounds it to an integer and the checks the difference between the mean and the input number. To simulate frame averaging, groups of rounded numbers were averaged them and then rounded again. See appendix A.3.1 for MATLAB code “noi_add2”. The output of the model shows what noise level is high enough to carry the data thorough the ADC and how many needed for a given precision.

Results and Discussion

This chapter will present the results from the dose calculations with the MATLAB model and discuss the implications of the model as it relates to flood phantom images on the EPID. The calibration of a mass vs. deformation curve, which facilitates deformation of the phantom to what is optimally specified by the calculations, is presented. The comparison between the calculated and film measurements is presented, and the inherent limitations of the process are discussed, as well as some possible improvements to the process. Finally the measurements with the flood phantom and EPID area presented and the statistics to determine the accuracy and precision of the flood field are analysed. The flatness is calculated by taking the maximum value divided by the minimum value, so the minimum flatness possible is one.

4.1 Dose calculations

First to be discussed are the results for an optimal phantom without the complications of deformation and geometrical considerations. Upon analysis of the output, from the model, it can be seen from Figure 4.1 and Figure 4.3 that over the range from 14mm to 60mm the flatness varies with distance. 14mm was chosen as this is as close as possible to get to the Gd, as the active parts of the imaging panel are imbedded in 12mm of packing for structural support. The intuitive belief about overlap is confirmed by Figure 4.3 and Figure 4.2, but the thickness has very little effects shown in Figure 4.1 and Figure 4.2.

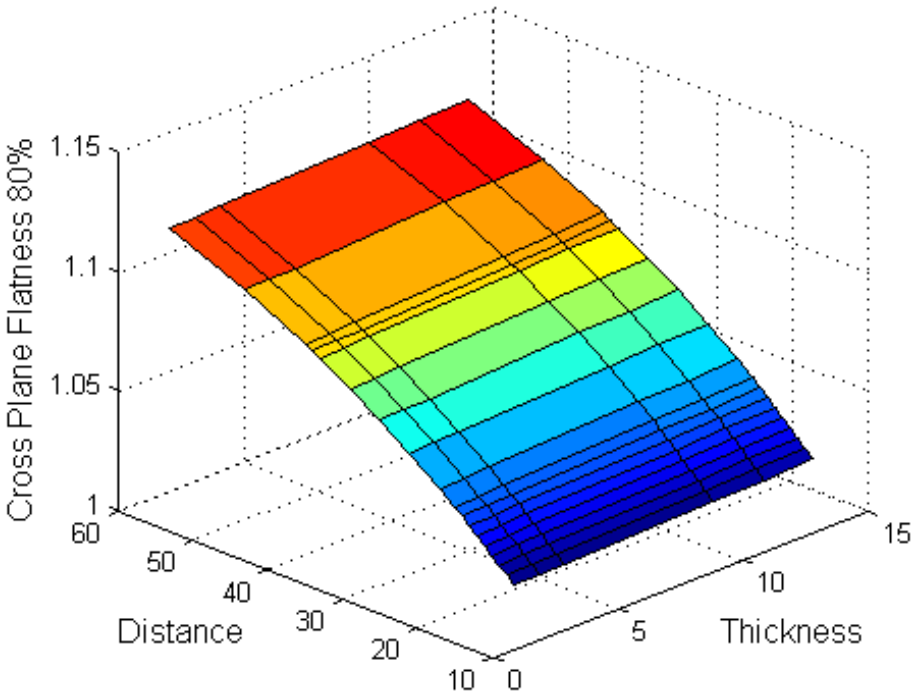

Figure 4.1 Computational prediction of flatness, calculated by max/min of 80% of the cross plane width, no deformation and an overlap at each edge of 145mm. All units in mm.

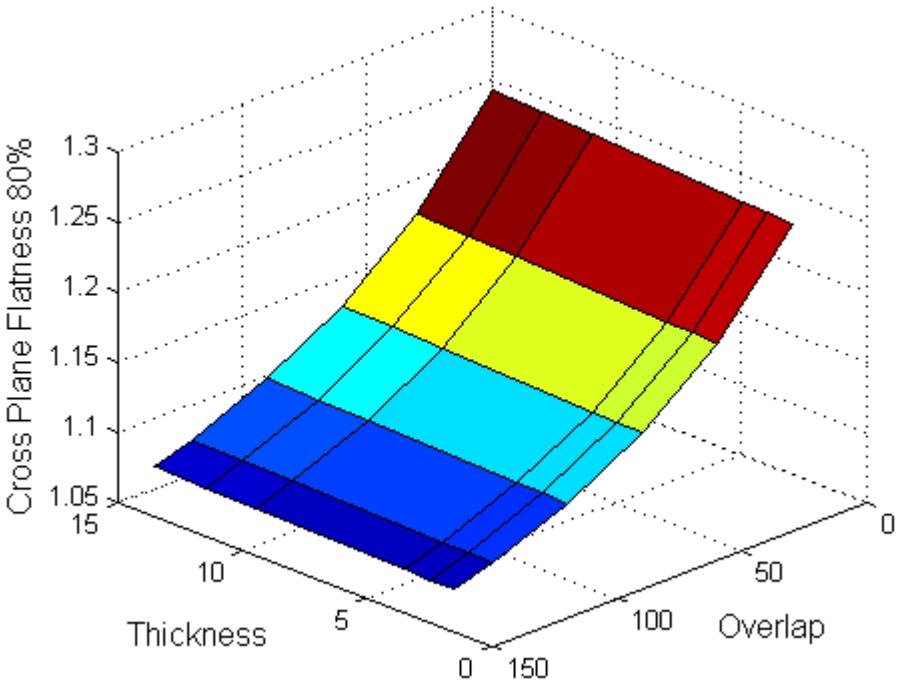

Figure 4.2 Computational prediction of flatness, calculated by max/min of 80% of the cross plane width, no deformation and a distance of 41mm. All units in mm.

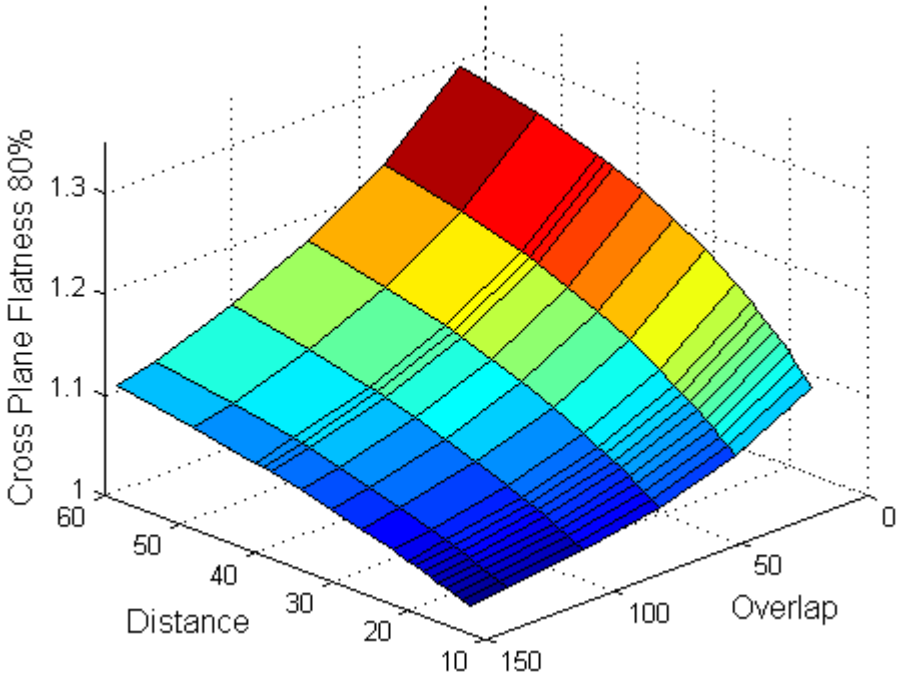

Figure 4.3 Computational prediction of flatness, calculated by max/min of 80% of the cross plane width, no deformation and a flood field thickness of 12mm. All units in

The signal strength decreases with a stronger dependence on overlap than thickness as can be seen in Figure 4.4. Figure 4.5 and Figure 4.6 show the dependence on distance to have a maximum that is dependent on thickness with its curvature dependent on thickness and overlap. This was originally thought to be an error in the MATLAB® coding. Intuitively one would expect to see the inverse square law result as depicted in Figure 4.7, but the absorption from the oblique angles dominate at close distances (Figure 4.8). Figure 4.9 shows the combined effect with the peak decreasing with distance but the Q (full width at half maximum) increasing, to give the integral result seen in Figure 4.5 and Figure 4.6. This effect is dependent on the attenuation coefficient in the absorption component of the formula (Eq 3.1), for which variation has not been modelled.

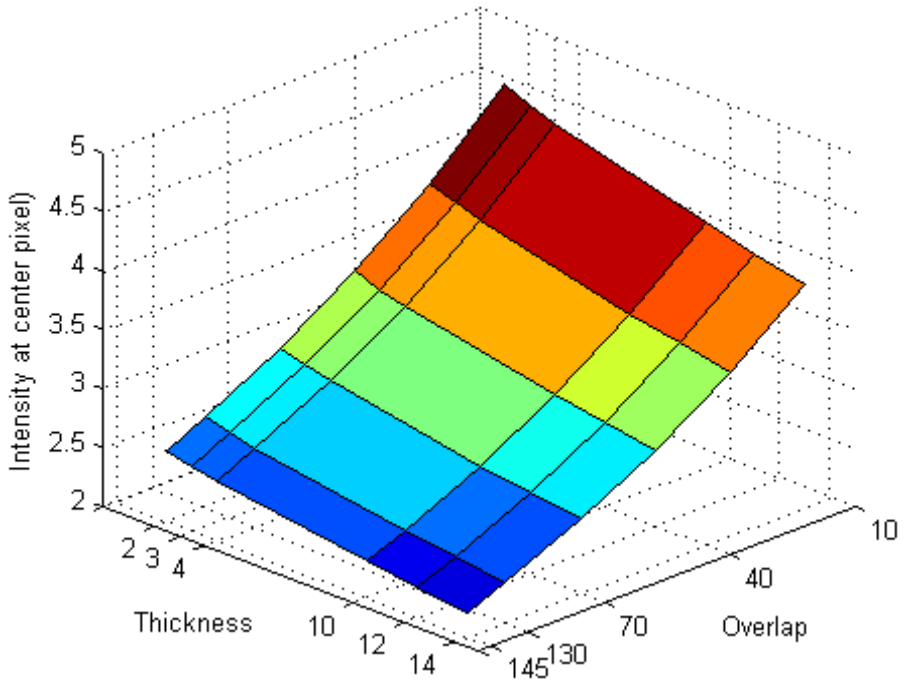

Figure 4.4 Computational prediction of relative intensity no, with deformation at a distance of 41mm. All units in mm.

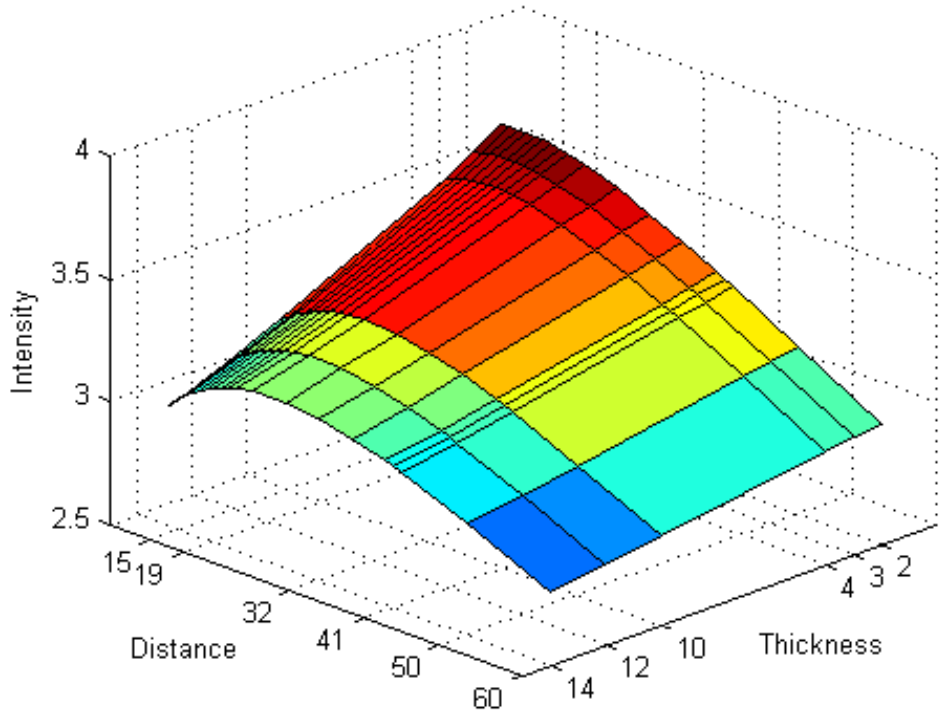

Figure 4.5 Computational prediction of relative intensity no deformation at an overlap of 145mm. All units in mm.

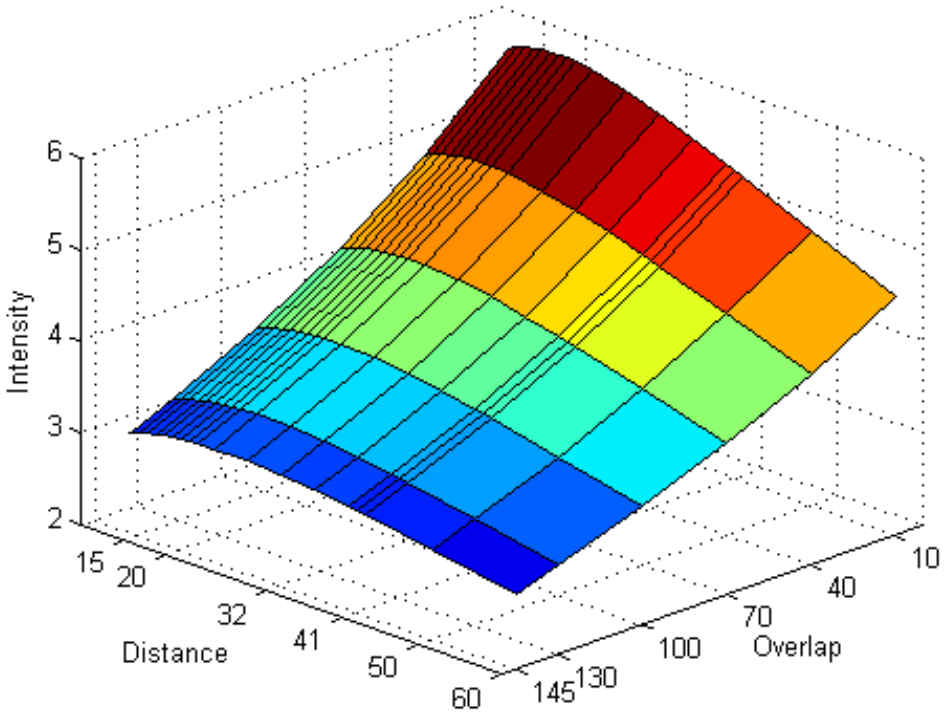

Figure 4.6 Computational prediction of relative intensity no deformation at a thickness of 12mm. All units in mm

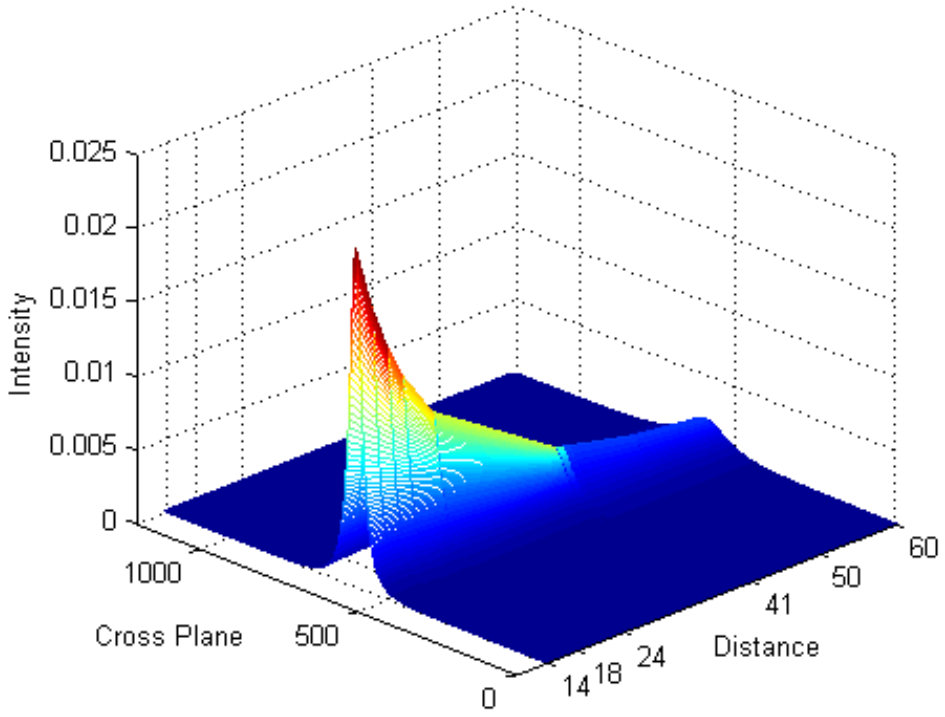

Figure 4.7 Cross plane of RCM of inverse square law, in mm

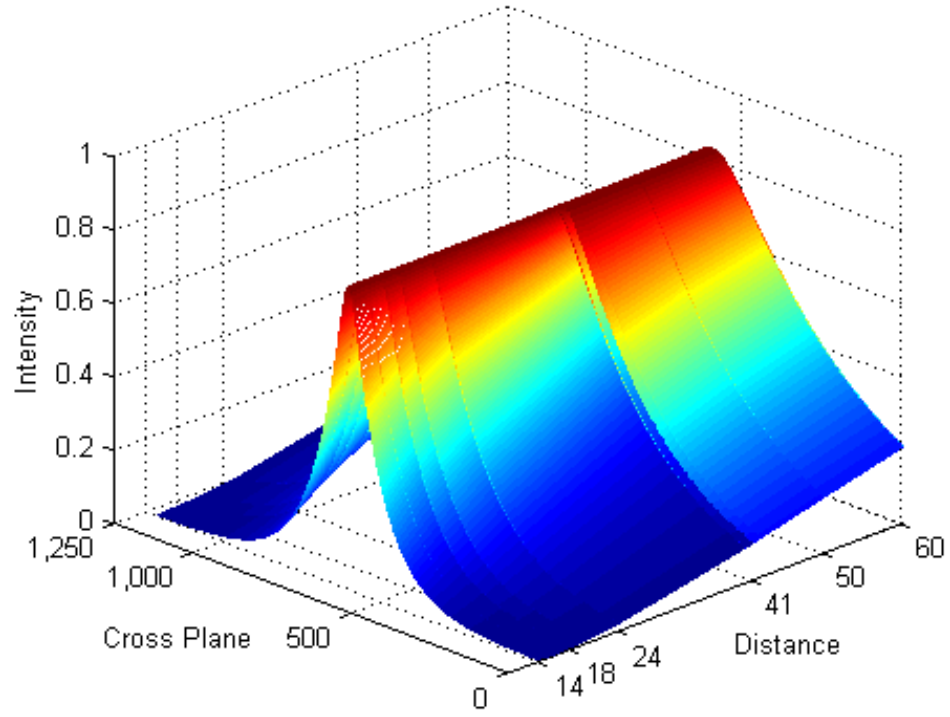

Figure 4.8 Cross plane of RCM of decrease signal from absorption, in mm

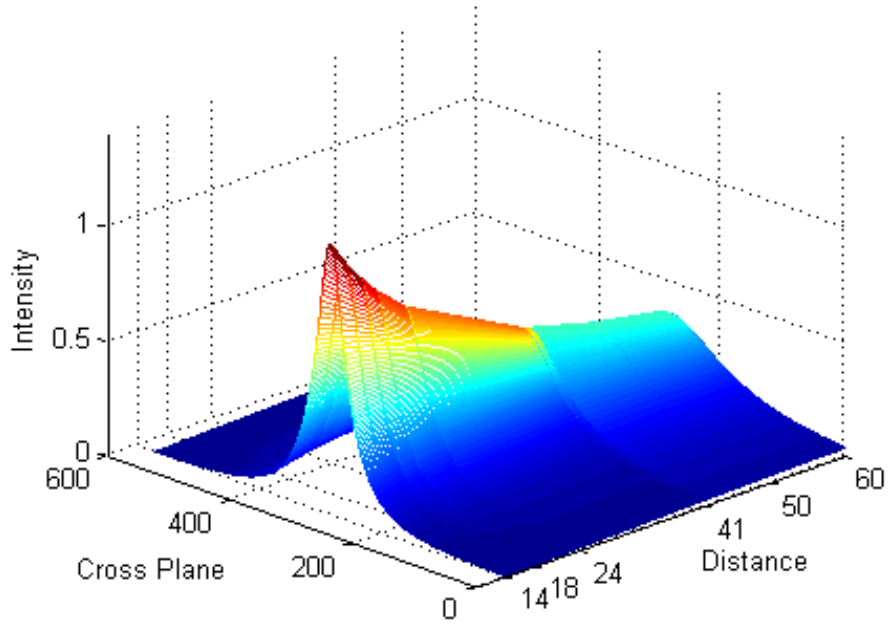

Figure 4.9 Cross Plane of RCM of absorption and inverse square law, in mm

4.1.1 Deformation

The variation of the deformation with respect to the three variables previously modelled all produced a minimum for flatness. The deformation is virtually independent from thickness (Figure 4.10), which is logical because the deformation is plotted as a ratio of the total thickness. In Figure 4.11, we see that the amount of deformation to achieve minimum flatness, as well as the curvature, is dependent on the distance. However, the dependence on overlap (see Figure 4.12) is inverted and the more overlap the less deformation needed to reach the minimum and the more the deformation the steeper the deformation curve. Thus, the optimal geometry depends on the relative weighting given to flatness and intensity. For simplicity if a minimum flatness of 3% is set an optimal result, with a 40mm overlap, 20mm distance, 2mm thickness, and 60% deformation, is obtained. If we assume a 0.5mm uncertainty, in the deformation of the phantom, we need at least 5mm thick or the uncertainty in deformation is greater than 10% which from Figure 4.10 will produce significant degradation of flatness. This is applicable even if no deformation is chosen as the 0.5mm convex phantom is possible and it is hard to measure the internal dimensions of the phantom. Looking at the intensity graphs, it can be seen that a 1mm tolerance in any of the other dimensions will not produce a significant change in the intensity, so a 1mm deviation from parallel or from centred will not significantly affect the overall flatness.

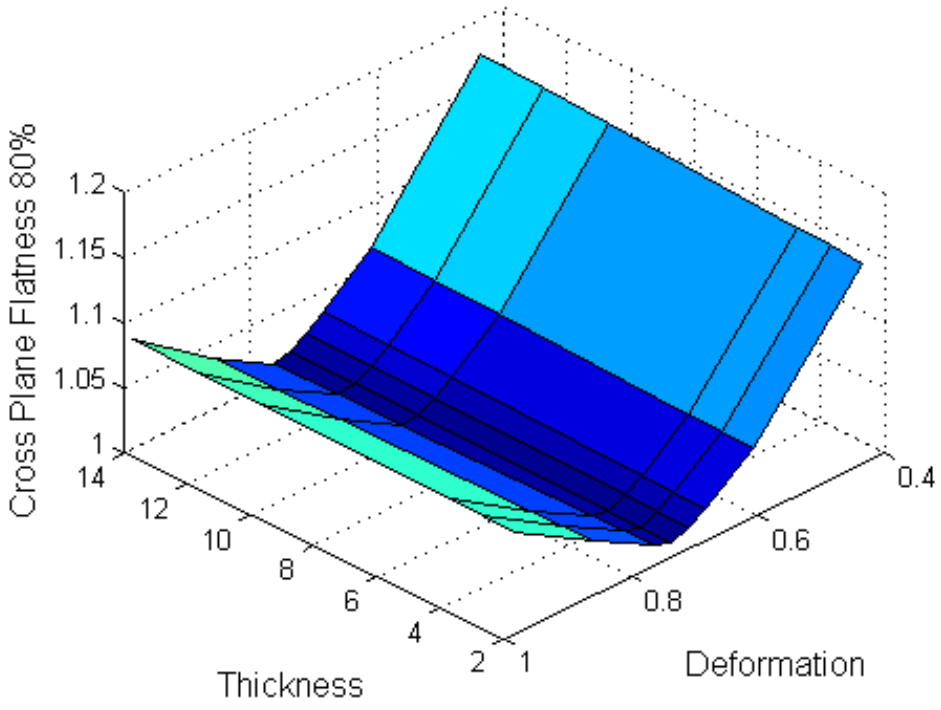

Figure 4.10 Computational prediction of flatness, calculated by max/min of 80% of the cross plane width an overlap of 145mm and a distance of 41mm, thickness in mm, and deformation as a ratio

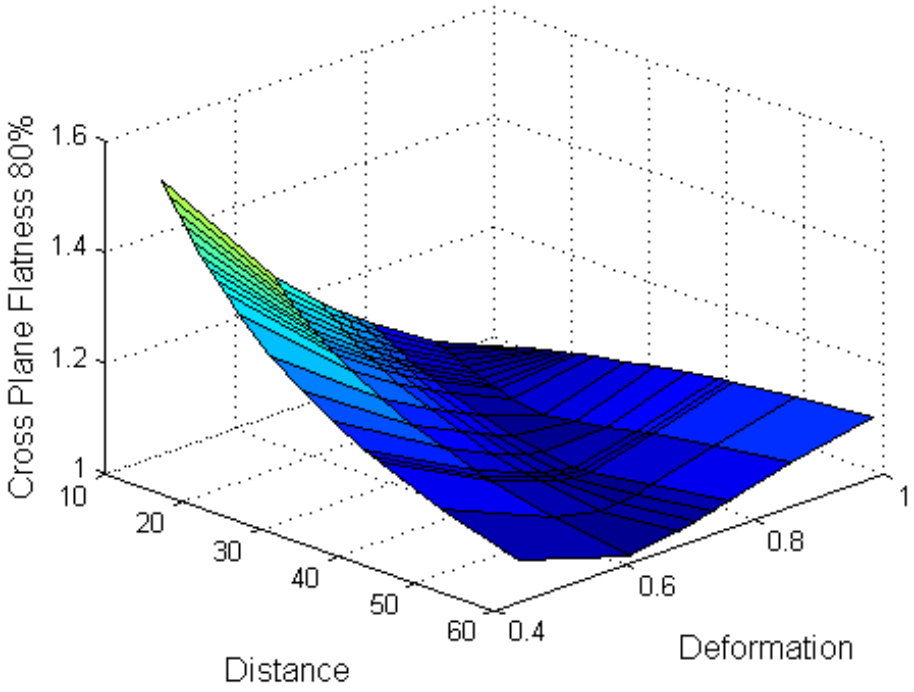

Figure 4.11 Computational prediction of flatness, calculated by max/min of 80% of the cross plane width an overlap of 145mm and .a thickness of 12mm, distance in mm, deformation as a ratio

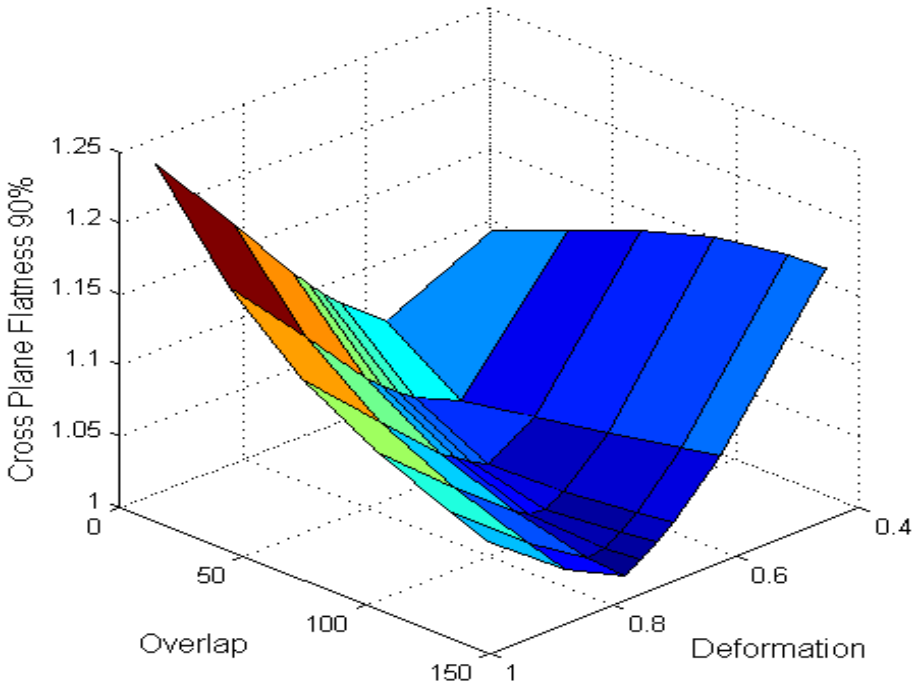

Figure 4.12 Computational prediction of flatness, calculated by max/min of 80% of the cross plane width a thickness of 12mm and a distance of 41mm. Over lap in mm, deformation as a ratio

4.1.2 Flood field prediction

In defining the size of the phantom by the sight lines from the EPID to the edge of the housing the problem reduces to three dimensions, from four. Note that there is a distinct minimum flatness for deformation for each of the combinations of thickness and distance. The intensity response, Figure 4.13, is slightly steeper version of the intensity response of the 4D model with respect to overlap and thickness which is as expected as overlap dominated intensity in Figure 4.6. In Figure 4.14 show the minimum 80% width flatness of 0.7% at a distance of 31mm and a thickness of 14mm deformed to 12mm (86%), Figure 4.16, in the centre, with a width of 555mm which is an overlap of 125mm. The irregularity is due to the low resolution in the deformation axis, because the deformation for minimum flatness is not calculated for all overlaps (or distances).

In comparing the flatness and intensity for an optimal phantom and an unused nuclear medicine phantom we see the difference is minimal, as the nuclear medicine phantom is 610mm x 420mm x 12mm. Thus gives a flatness of 1% and a relative intensity reduction of 25%. The deformation for minimum flatness for the nuclear medicine phantom was 72%, Figure 4.16 and Figure 4.15, and the distance dependence flatness for this deformation can be seen in Figure 4.17. Figure 4.18 shows the full intensity distribution of the geometry to be used, being that of the nuclear medicine phantom.

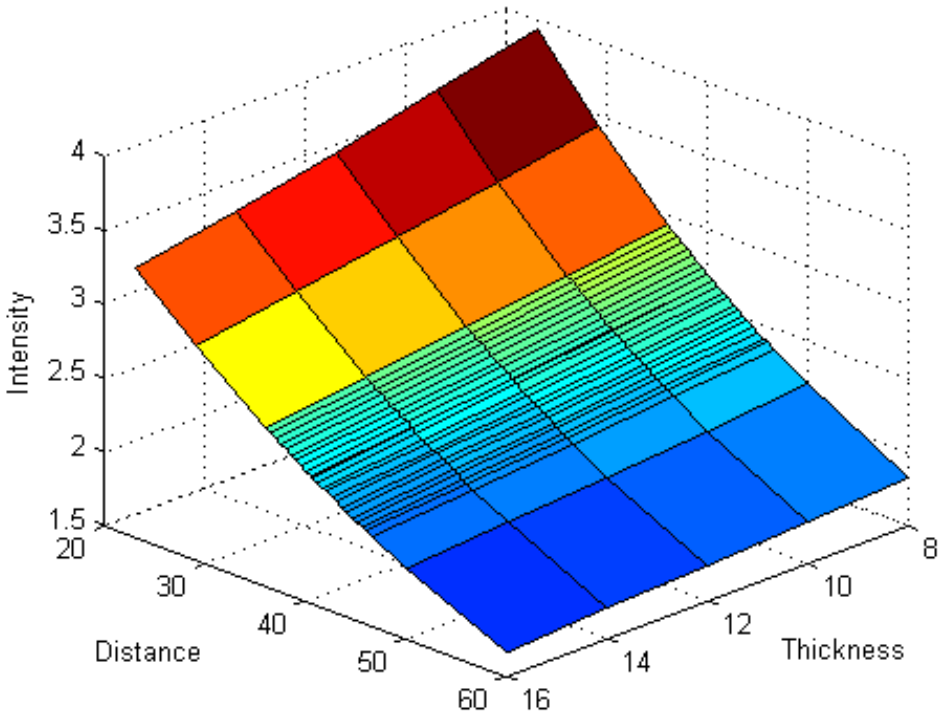

Figure 4.13 Relative intensity predicted in the centre pixel from the computational model. Units in mm

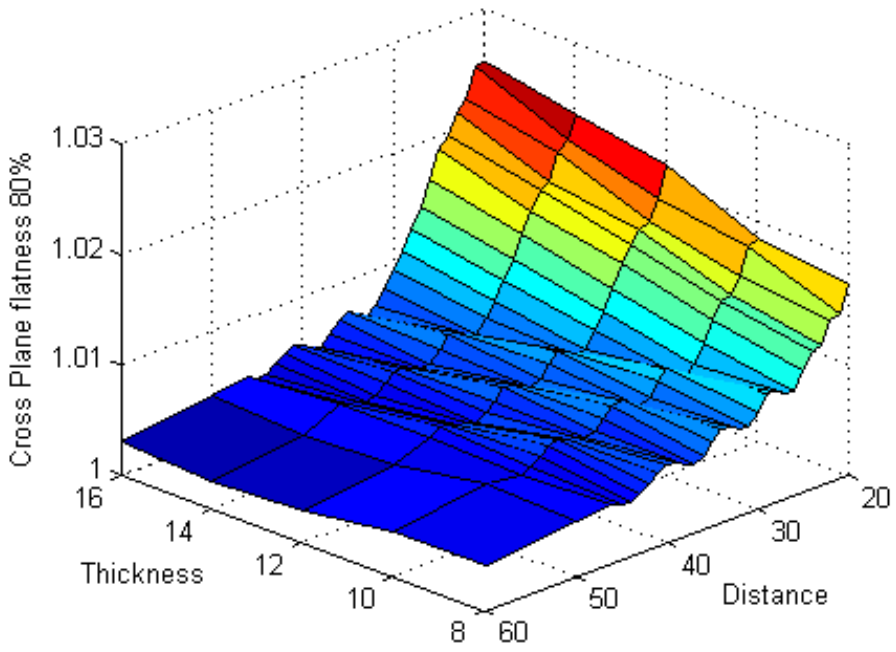

Figure 4.14 Computational prediction of flatness across 80% of the width with deformation selected to produce flattest possible, units in mm

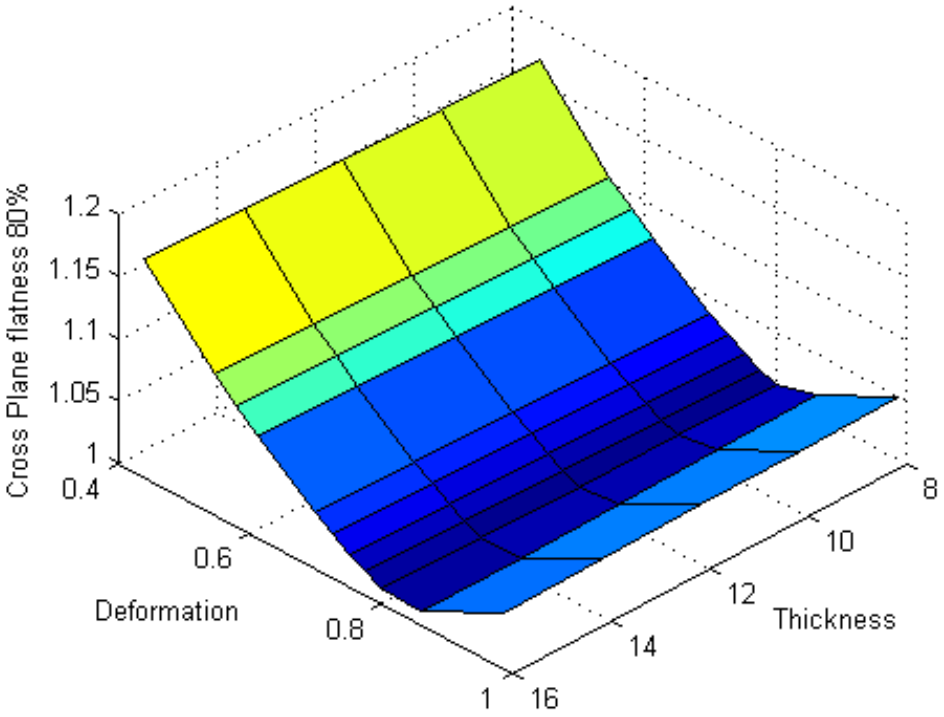

Figure 4.15 Computational predictions around nuclear medicine phantom size, distance 41mm, thickness in mm deformation as a ratio

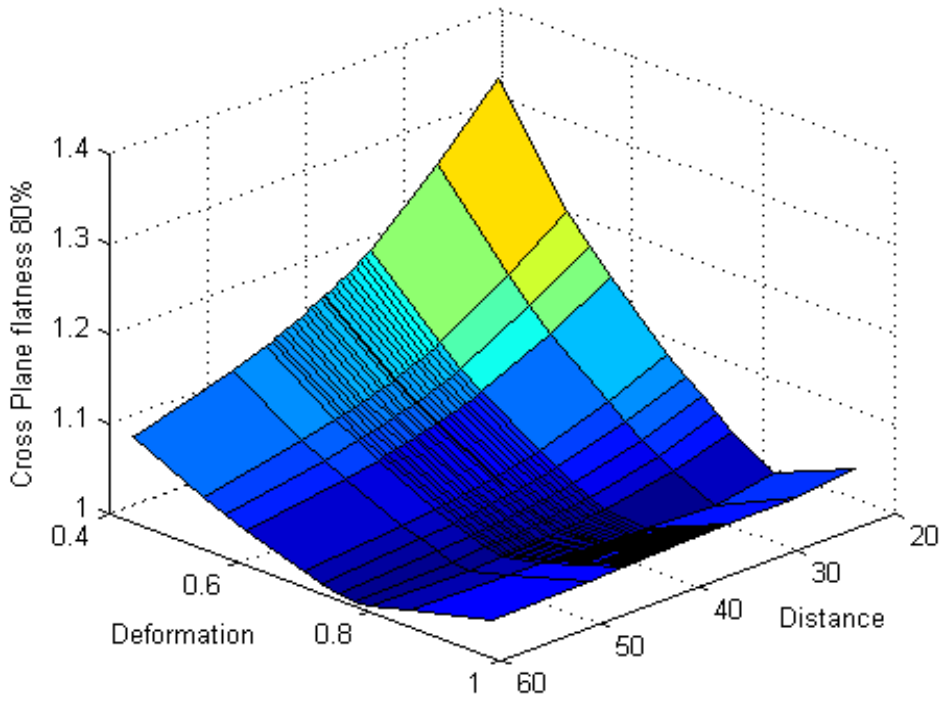

Figure 4.16 Computational predictions around nuclear medicine phantom size, thickness 12, distance in mm, deformation as a ratio

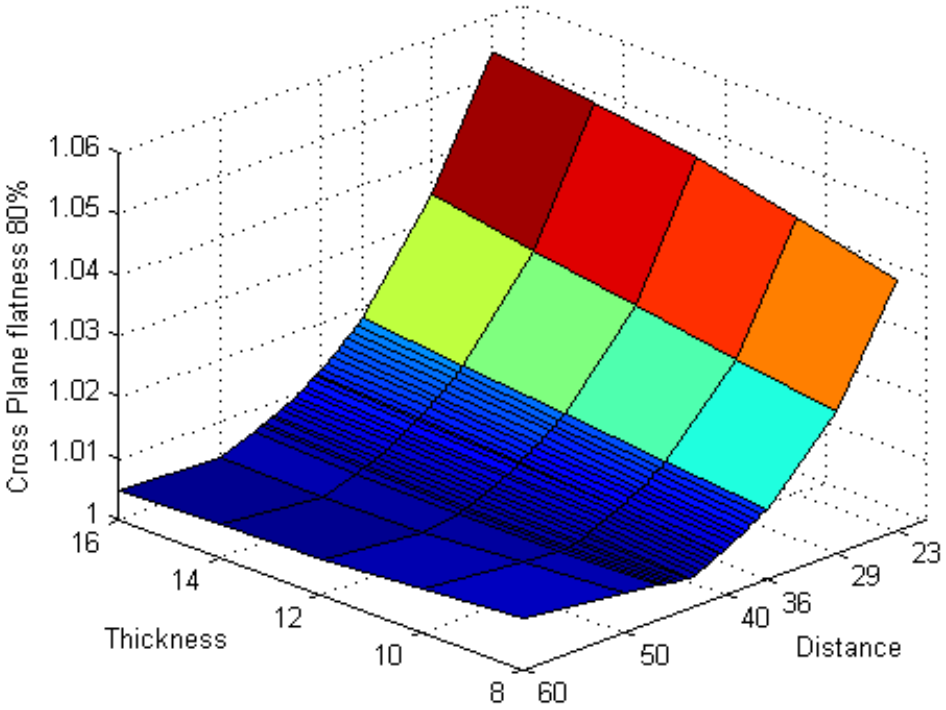

Figure 4.17 Cross plane flatness with a deformation of 72% with a phantom, in mm

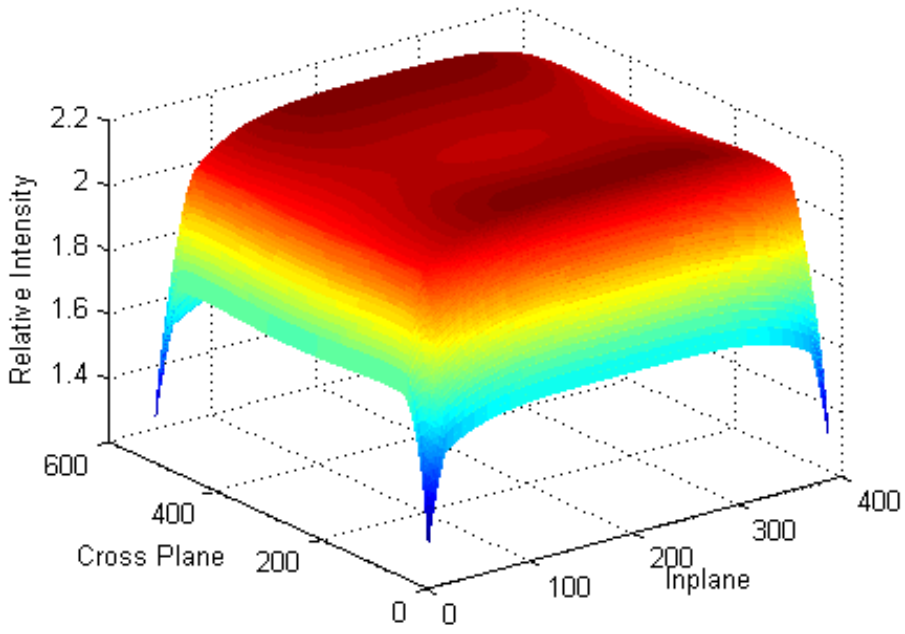

Figure 4.18 Computational prediction of full distribution to EPID form a phantom 610mm x 420mm x 12mm placed 41mm between the Gd layer and the front closest Tc99m

4.2 Phantom Deformation

To achieve the deformation model weights were placed on the phantom and the deformation measured with a DTI and plotted in Figure 4.19.

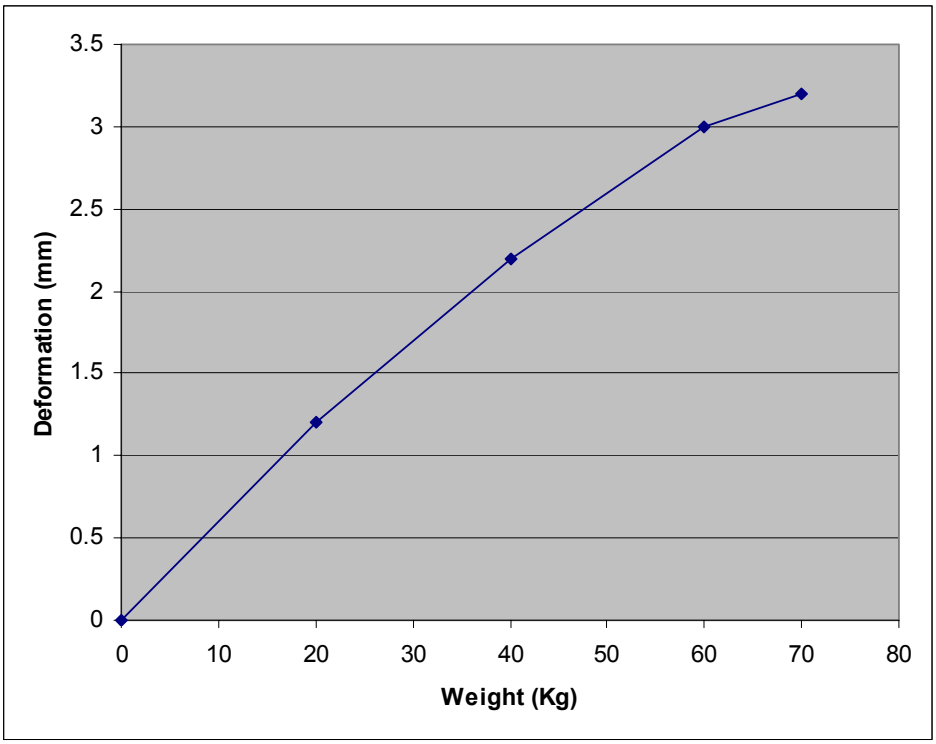

Figure 4.19 Deformation of the front face of the flood phantom with weight added as measured with a DTI.

To achieve the 72% deformation 70kg of lead weights were needed to be placed on the phantom. When the phantom was sealed and the weight removed, the deformation was reduced by half. This was due to the bottom face being pulled up until the tension on both faces was equal. However this is not a setback, as the deformation is modelled as a ratio of deformation, not the deformed thickness. The process of deforming the phantom could be made more practical using a screw press, with table large enough to fit the phantom, instead of the weights and a Coordinate Measuring Machine (CMM) to measure the deformation. Reproducibility of the position of the weights was checked by removing the weights and then replacing them, and measuring the volume change. The resulting volume change of 15ml relates to an estimated 0.2mm change in deformation.

4.3 Comparison between flood phantom measurements to calculation

4.3.1 Film calibration curve

The first step in comparison between calculated distribution, and the distribution measured with film is to create what would normally be called a dose calibration curve. However since it is relative distribution, it is simpler to keep the curve in the activity domain. Four different calibration films were taken as seen in Figure 4.20 with differing lengths of exposure and having been left to decay.

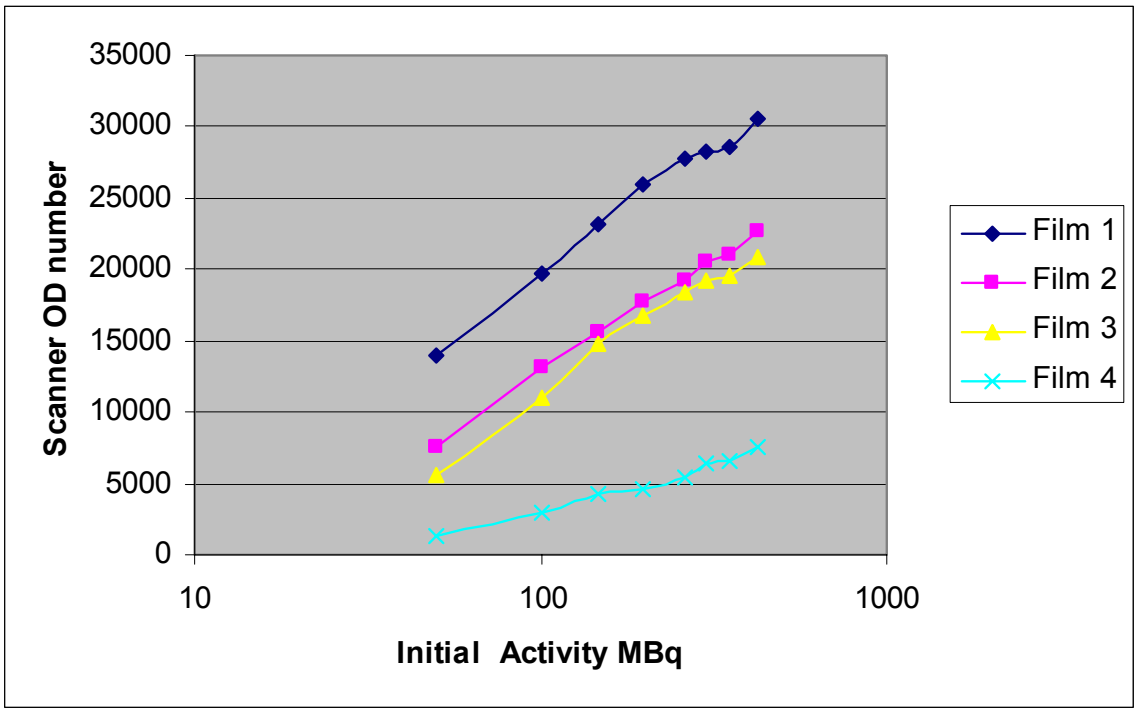

Figure 4.20 Kodak T-MAT G/RA film calibration for Tc99m not normalised for time ad decay.

Figure 4.21 shows the calibration curves adjusted for time, decay and background fog. Figure 4.22 shows the calibration data and the power series fitted and the data points used in for calibration in Doselab4

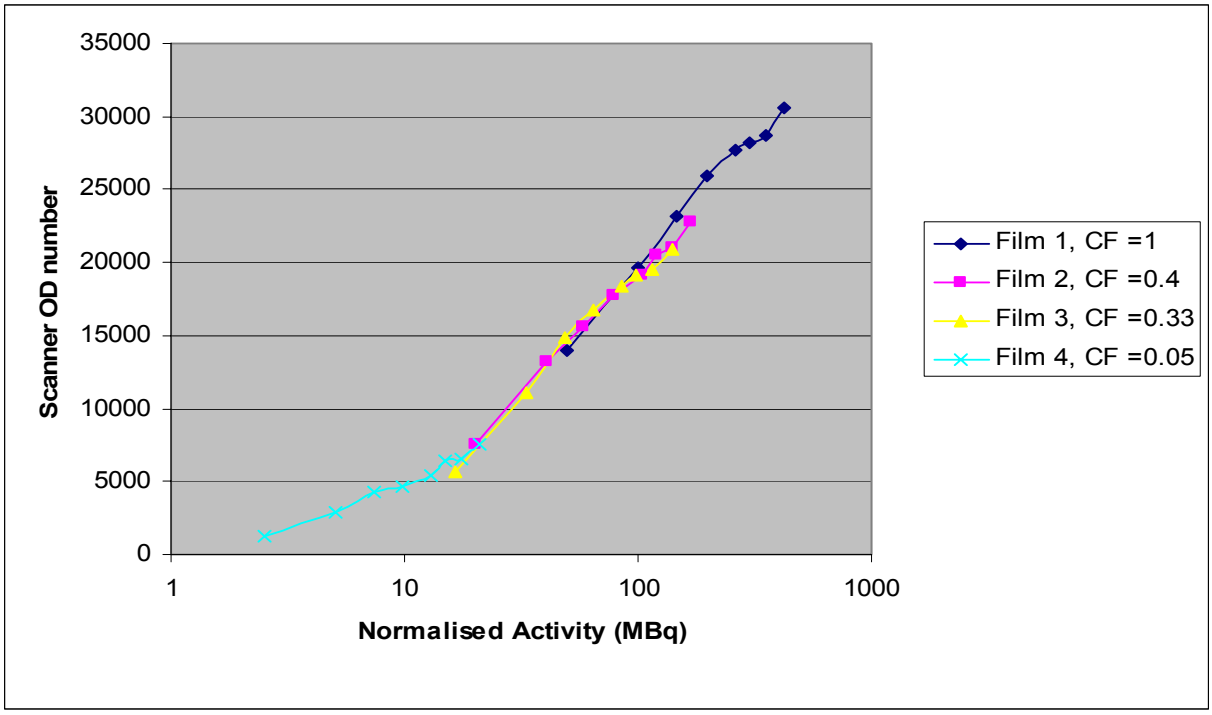

Figure 4.21 Kodak T-MAT G/RA film calibration

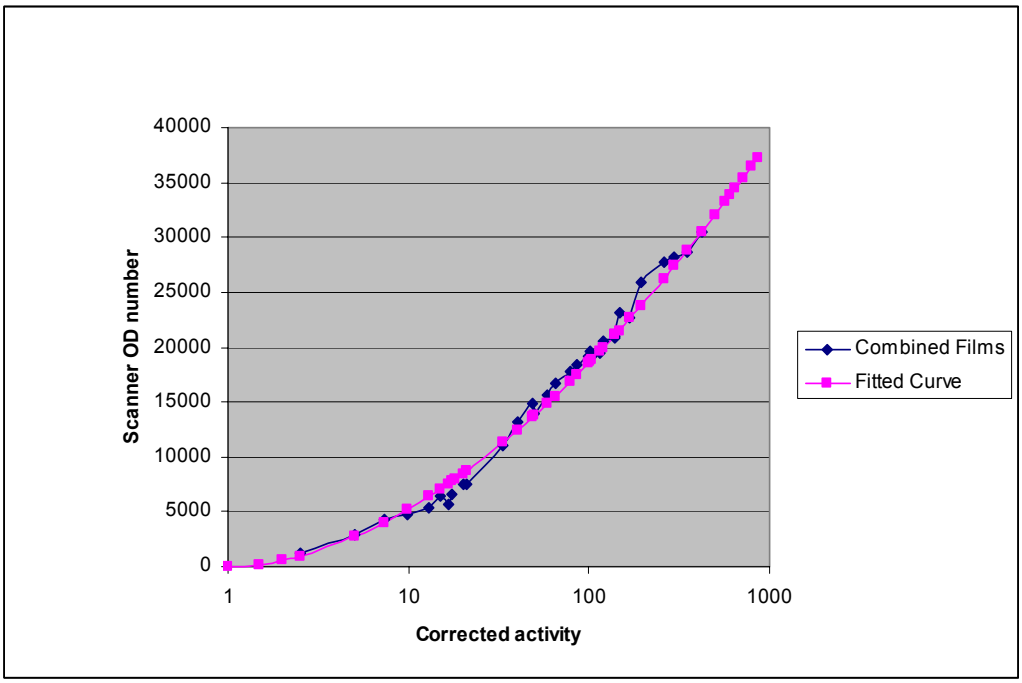

Figure 4.22 Kodak T-MAT G/RA film calibration showing best fit exponential curve

Figure 4.23 and Figure 4.24 show a sample profile comparison between the MATLAB calculated and the film measured at the close distance of 12mm tc99m to film. Figure 4.25 and Figure 4.26 show the profile comparison at 36mm distance.

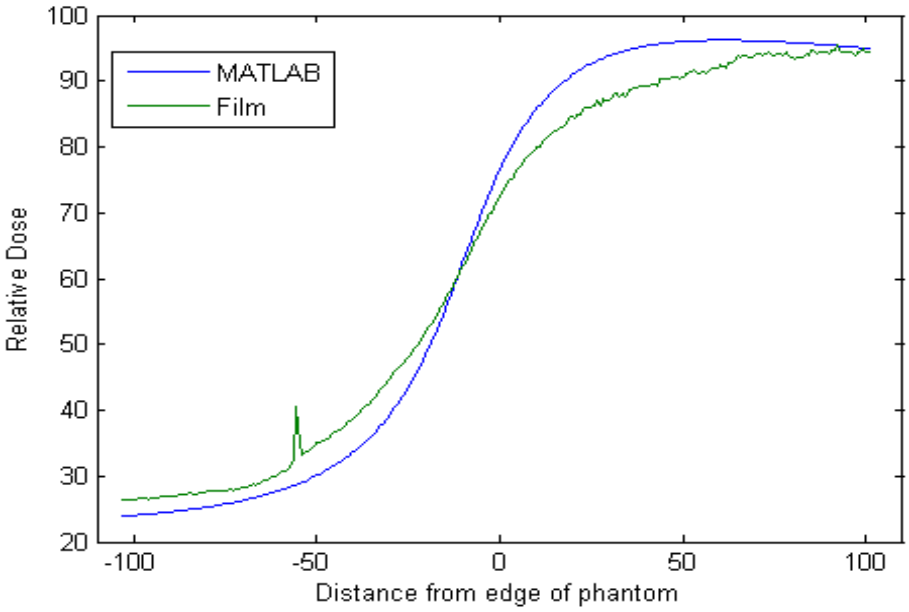

Figure 4.23 Comparison of the cross plane profile of the computational model and film at 12 mm distance.

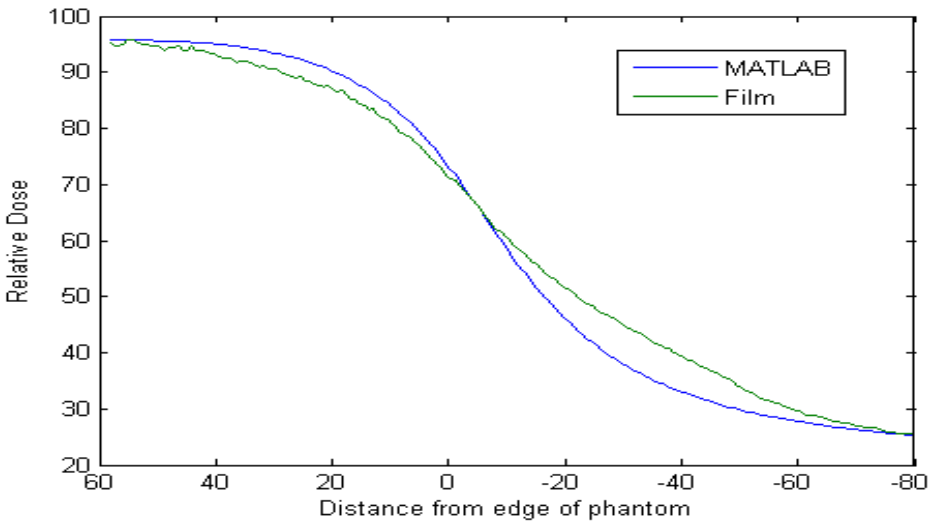

Figure 4.24 Comparison of the in plane profile of the computational model and film at 12 mm distance

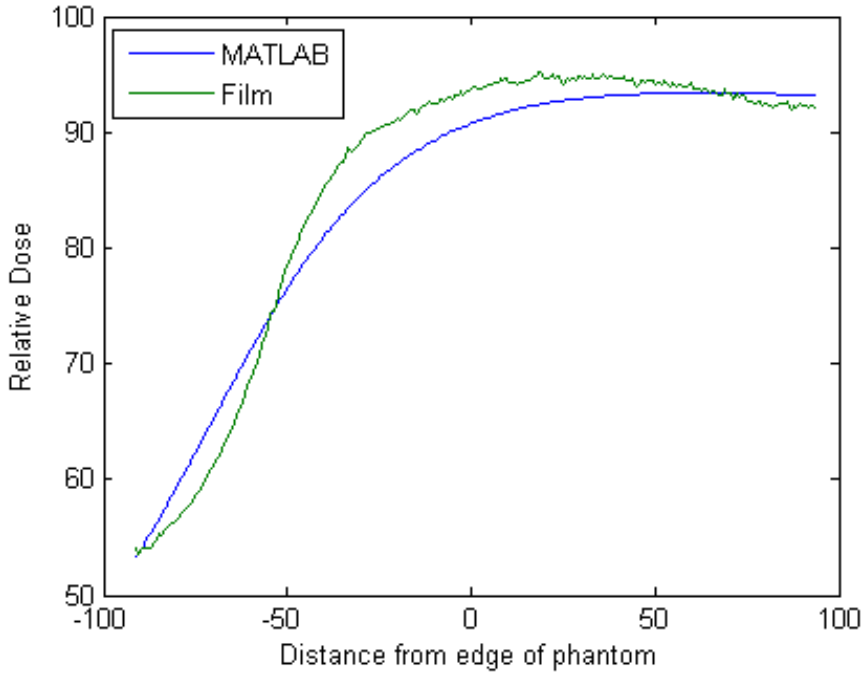

Figure 4.25 Comparison of the in plane profile of the computational model and film at 36 mm distance.

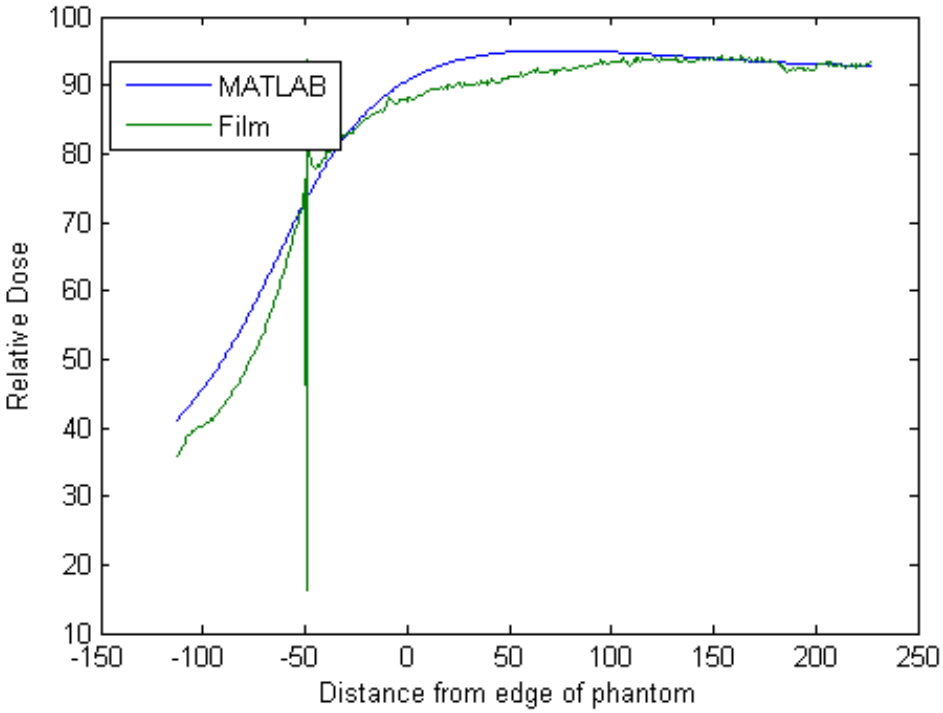

Figure 4.26 Comparison of the cross plane profile of the computational model and film at 36 mm distance.

Figure 4.27 and Figure 4.28 show the percentage difference at 12mm distance and Figure 4.29 and Figure 4.30 show the difference at 36mm distance.

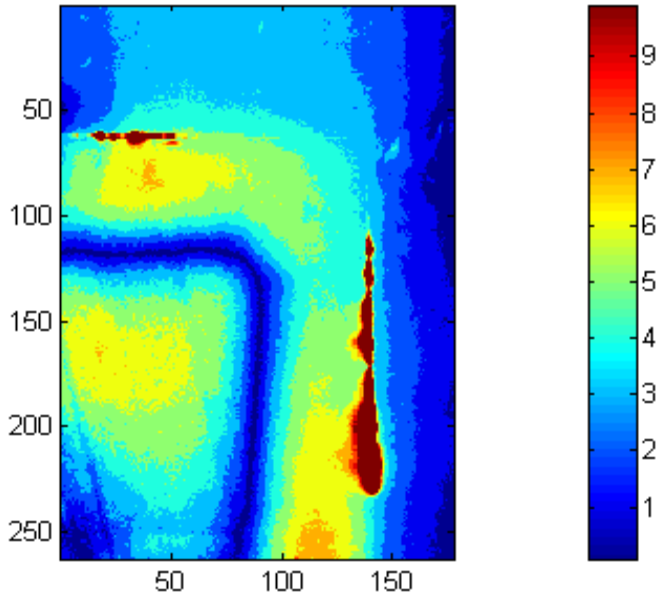

Figure 4.27 Relative percentage difference between film and the computational model 12mm

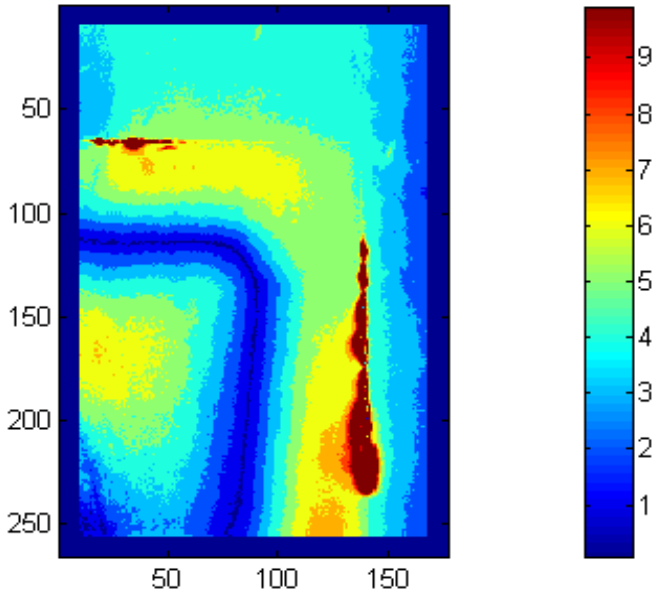

Figure 4.28 Gamma function between film and computational model and 12mm

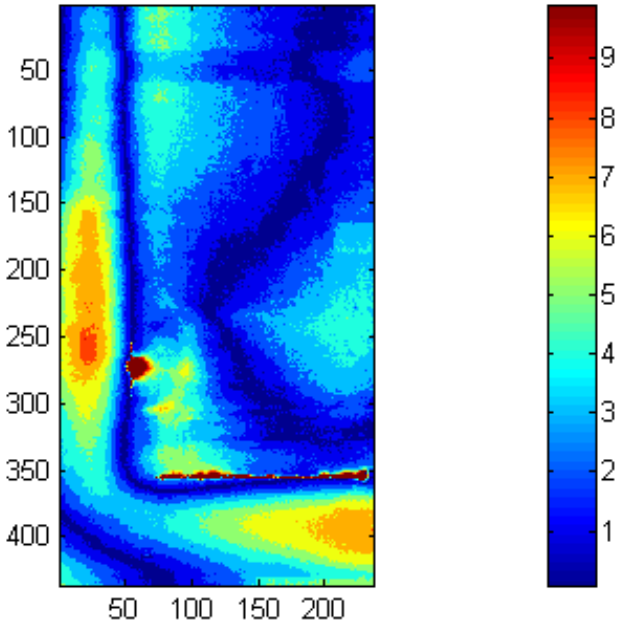

Figure 4.30 Relative percentage difference between film and the computational model at 36mm

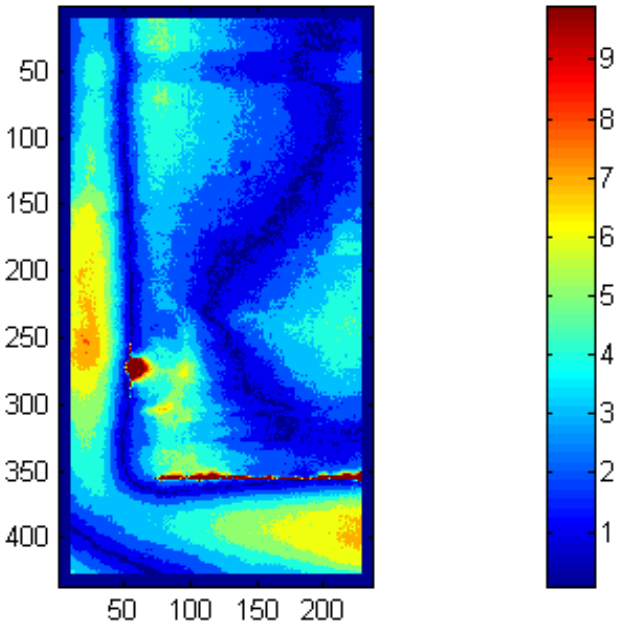

Figure 4.29 Gamma function between film and computational model and 36mm

While the distributions do not match perfectly, they are close considering the non-linear response of the film and the crude film packets. On the 36mm film a horizontal bar can be seen at the 50 pixel mark that is from a piece of tape used to seal old registration holes. The registration marking line can clearly be seen in both the profiles and the percentage and gamma images, when manual registration, with these lines, was compared to the to the automatic registration process the result was within 3 pixels. The fact that both distributions, 12mm and 36mm distance, match with the same calibration curve and that general shape of the profiles is comparable indicates that the differences are due to the imperfections in the calibration curve.

If the model or film work were to be used to mathematically correct for the edge effects, it would be necessary to improve the accuracy of this comparison method. The calibration curve could be improved by using a larger range of activities on a single film, and keeping the larges and smallest on every film, while using variety of intermediate activities. Instead of using a film packet, the manufacture of a cassette to emulate the EPID would improve the accuracy of the comparison: The cassette would need to have, one face made out of 1mm of copper, a securing the film horizontally so manual registration is possible, and a seal for the light.

4.4 EPID measurements with the Tc99m phantom

As there is no gold standard for EPID flood field flatness it is hard to rate the flood field flatness of using Tc99m and the only way is to compare it to the current methods to see what the differences are.

4.4.1 Derivation of optimal imaging parameters

The main issue that can be resolved for using Tc99m is can you get the signal to noise low enough to get a flood field with an accuracy of better than 3%. To obtain the lowest noise the dependence on reset frames and frame averaging was investigated. When comparing the standard deviation distribution; with the metal cover off (Figure 4.31) to with the cover on (Figure 4.32); it is evident that the noise is increased, in specific pixels, with the cover off. It was thought that the cover is part of shielding of the readout electronics, but unfortunately it was not possible to image with the cover on, without shielding the EPID from more of the flood phantom. Therefore a method of removing or mitigating this noise was need or a smaller area of adequate flatness would have to be accepted. It was noticed that the noise decreased more rapidly than would be expected with higher frame averages, so the hypothesis that there was more noise in the first frame was investigated by taking the mean standard deviation of images with 1 and 2 reset frame and 1-11 image frames, Figure 4.33. By comparing the standard deviation distribution with the cover on (Figure 4.32) and with the cover off and two frame averages (Figure 4.34) it can be seen that taking 2 frame averages mitigates the extra noise due to the metal cover being removed. Figure 4.35 shows that by taking more frame averages the distribution does not change significantly, but the standard deviation is decreased by the order of one over root N (mean squared error), as expected from Gaussian noise[35].

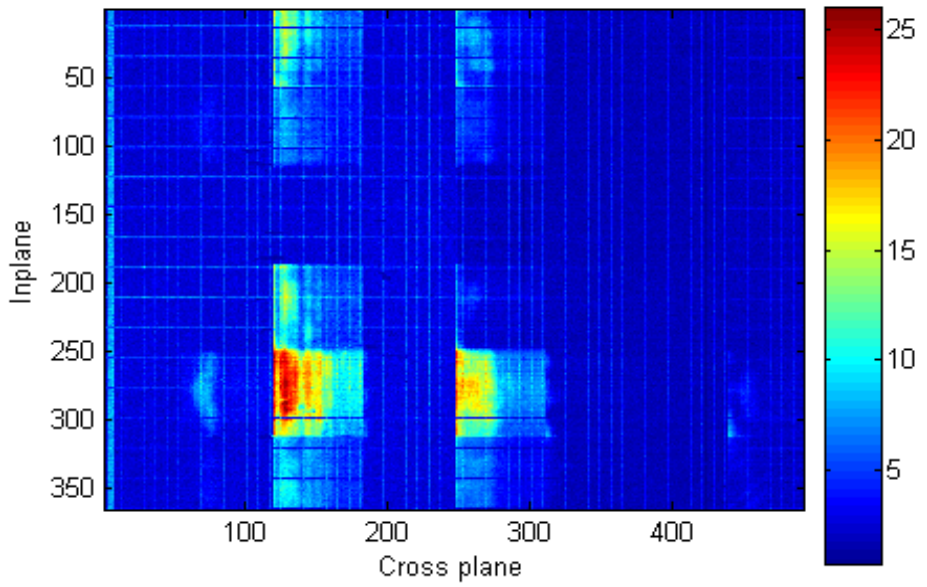

Figure 4.31 Standard deviation of each pixel in the EPID with 1 reset frame and 1 frame average with the metal cover off

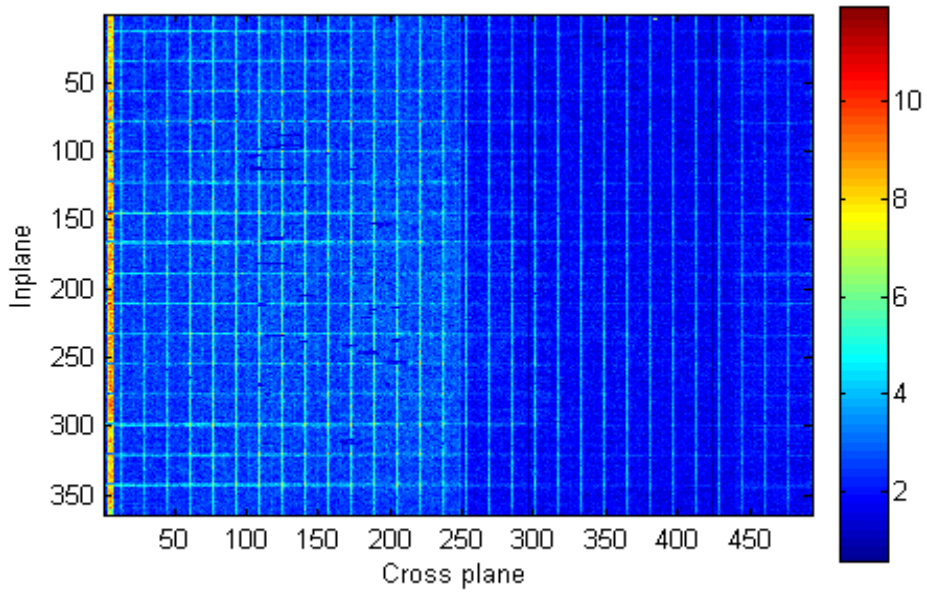

Figure 4.32 Standard deviation of each pixel in the EPID with 1 reset frame and 1 frame average with the metal cover on

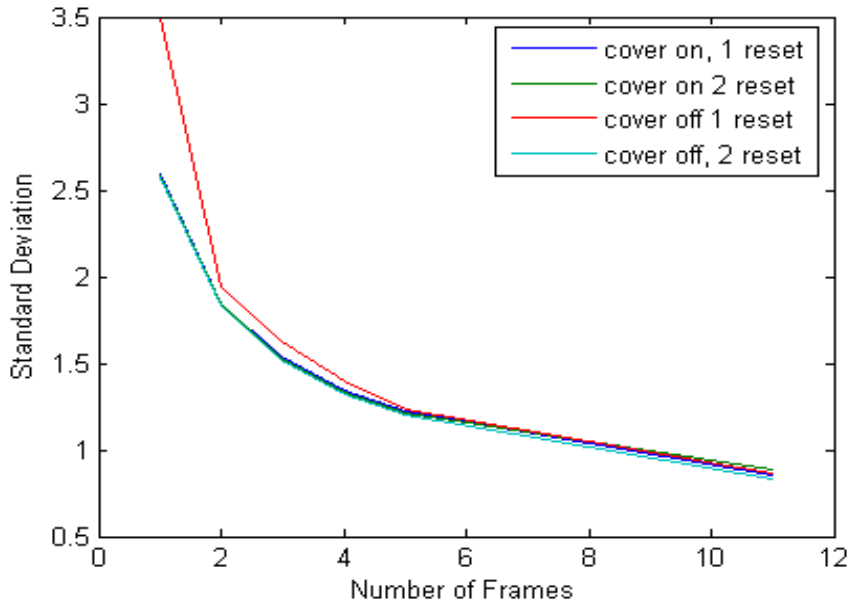

Figure 4.33 EPID mean pixel standard deviation in dark fields. (Flood fields are not significantly different)

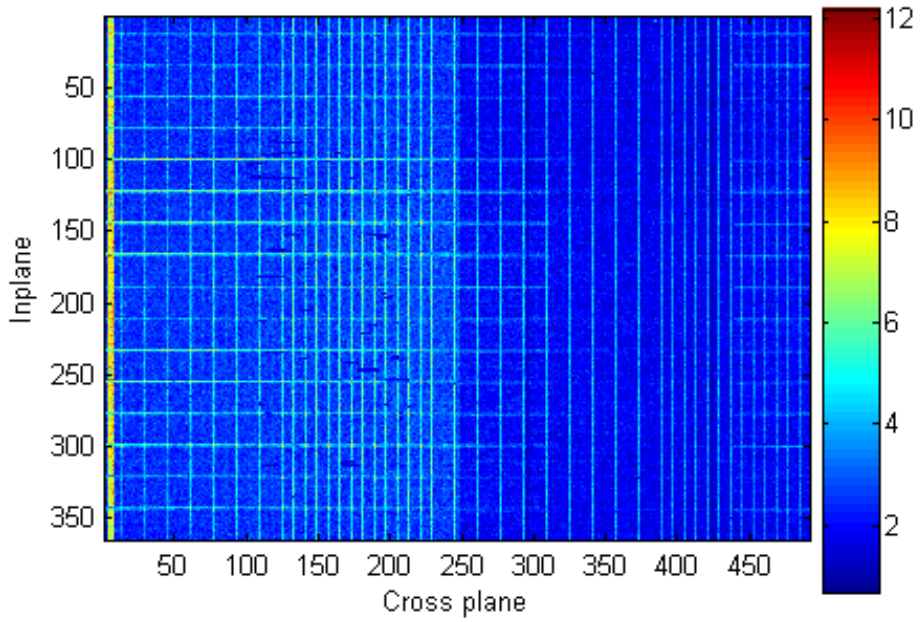

Figure 4.34 Standard deviation of each pixel in the EPID with 2 reset frame and 1 frame average with the metal cover off.

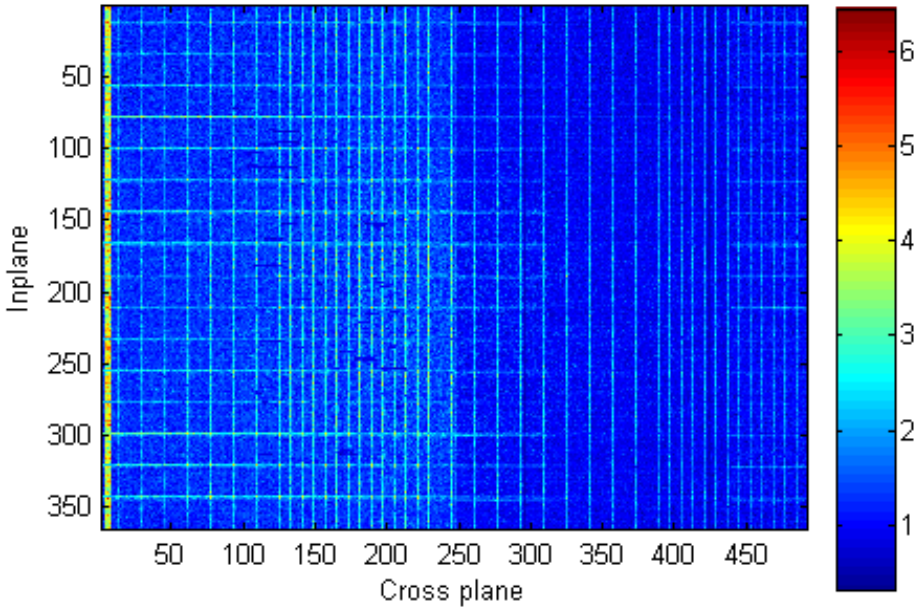

Figure 4.35 Standard deviation of each pixel in the EPID with 2 reset frame and 5 frame average with the metal cover off

The distinctive pattern, the horizontal bars at 22 row spacing and the vertical series of line, to the standard deviation was thought to be significant at first. The horizontal series of lines are spaced the same as the number of rows samples per pulse. But when looked for in a linac image they become insignificant compared to the variation, per beam pulse, in the linac beam, as can be seen in Figure 4.36.

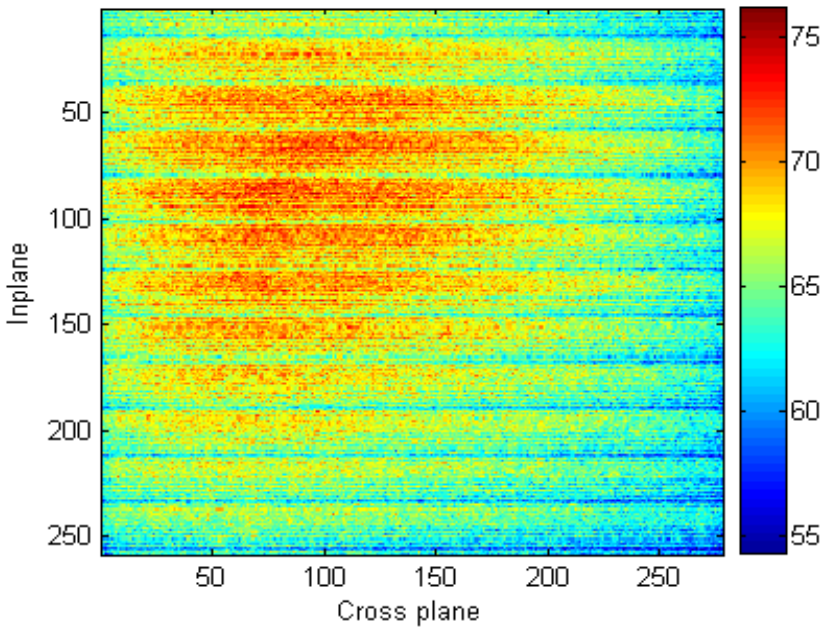

Figure 4.36 Standard deviation of each pixel in a section of the EPID exposed with the linac beam

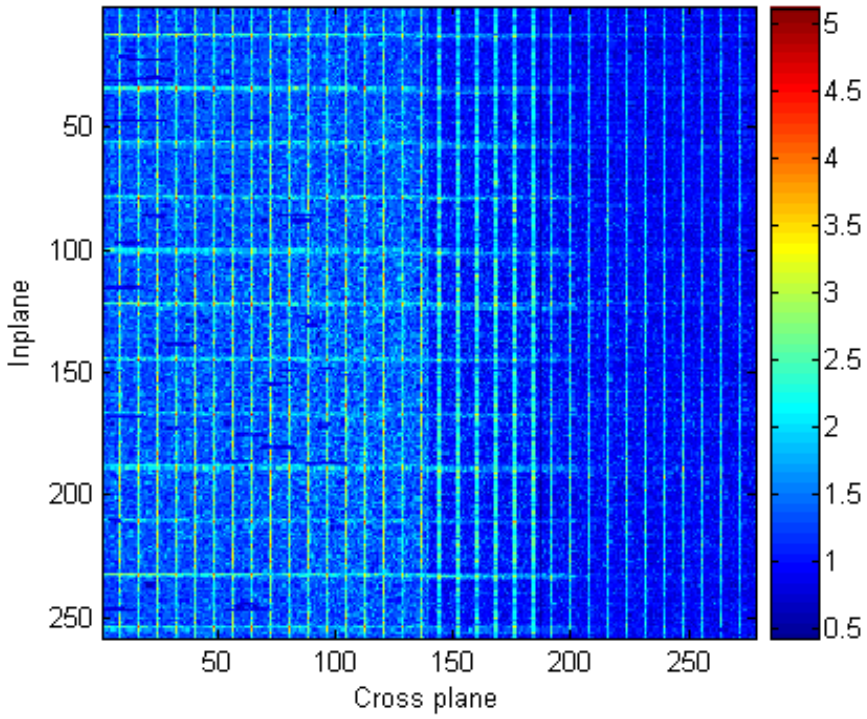

Figure 4.37 standard deviation of same section of EPID in Figure 4.36 for a dark field

4.4.2 Rounding errors

The number of samples needed to get an accuracy of better than 3% would normally be determined by the mean squared error[35], but the noise throughout the EPID images is not regular (Figure 4.38). The contribution from, rounding error of the ADC and from the frame averages, was investigated with a MATLAB model and the result can be seen in Figure 4.39 and Figure 4.40. The rounding error can be quit clearly seen in Figure 4.39, even with a large number of samples; a systematic offset of 0.125 counts can still be seen. Where as in Figure 4.40 there is no systematic offset. The offset occurred only with the even numbers of frame averages that were investigated, and the amount of the offset decreased with the number of frame averages. There was no offset with odd numbers of frame averages. Hence, it was determined that if frame averaging was to be used it would be best to use an odd number of frame averages

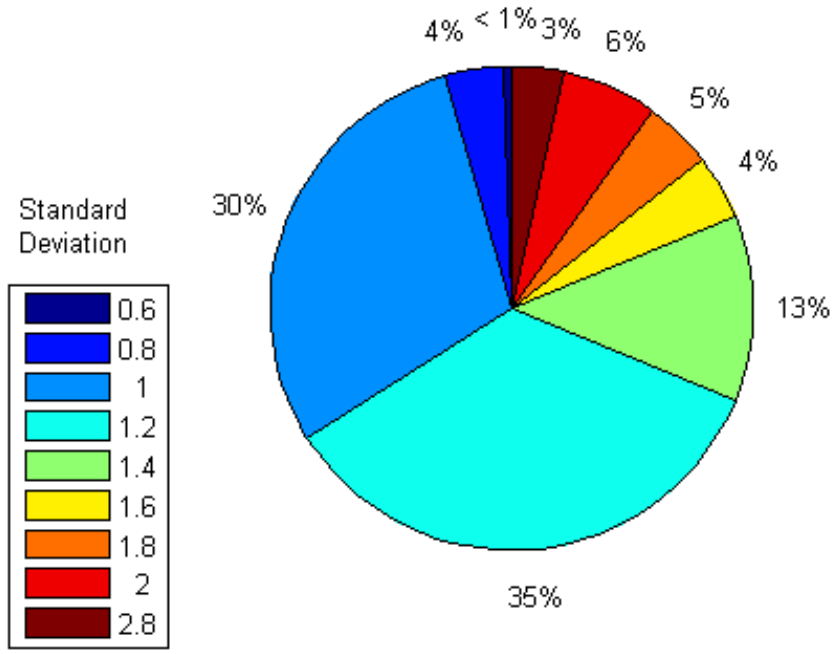

Figure 4.38 Standard deviations in a flood field with 2 reset frames and 5 frame averages

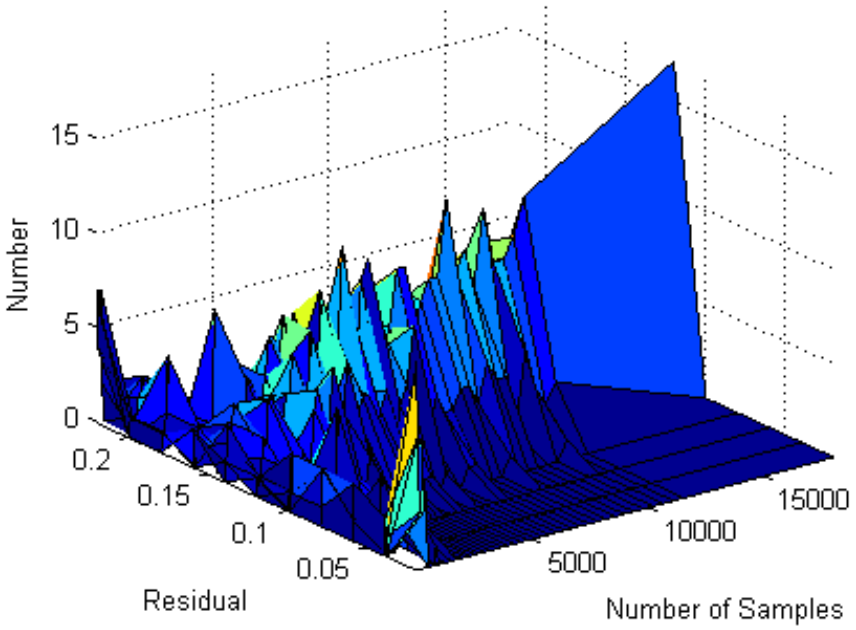

Figure 4.39 Histogram of difference between mean or output and the input of model (residuals), for a standard deviation of 2.5 and 4 frame averages.

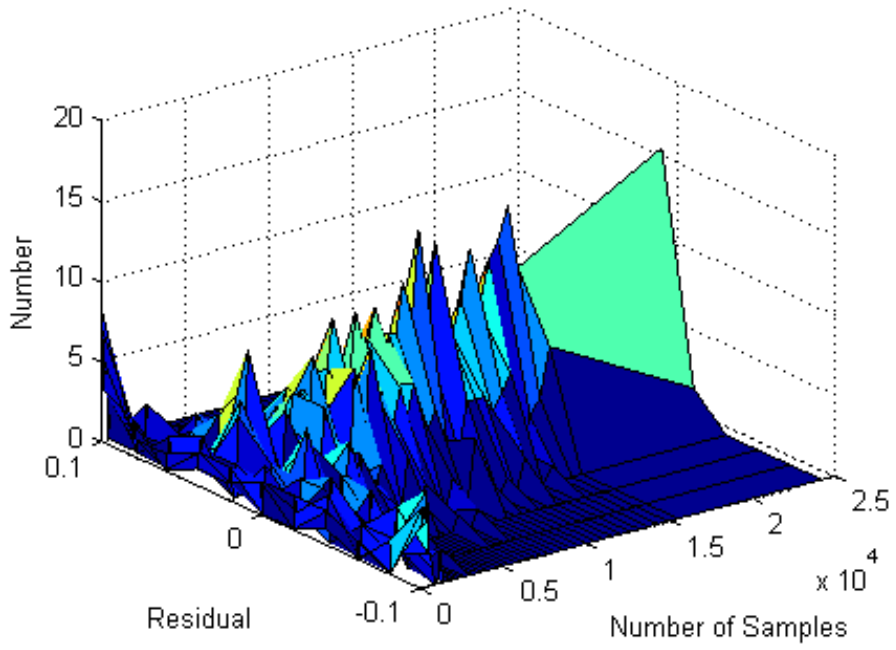

Figure 4.40 Histogram of residuals, for a standard deviation of 2.5 and 3 frame averages.

In the modelling of the rounding errors it was seen that if the standard deviation was to low it did not carry the sub rounding signal through to the rounding stage. Figure 4.41 and Figure 4.42, show the histograms for the residuals for one frame average and 5 frame averages respectively, for the same number of images, for the standard deviations present in a flood field. The standard deviation in these images are same raw noise levels, but are decreased in Figure 4.42 due to the frame averaging. Lower values of 0.4 and 0.2 were modelled to depict the phenomena, in Figure 4.42, but it is not evident in Figure 4.41, this is consistent with the corollary theorem [36]. This suggests that more frame averaging will introduce a systematic error.

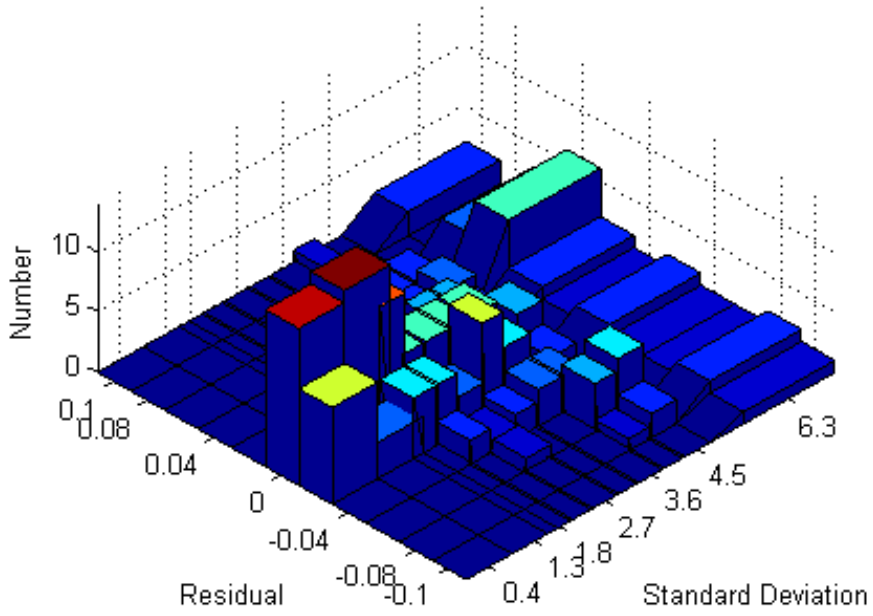

Figure 4.41 Histogram of residuals for 5000 samples and 1 frame average

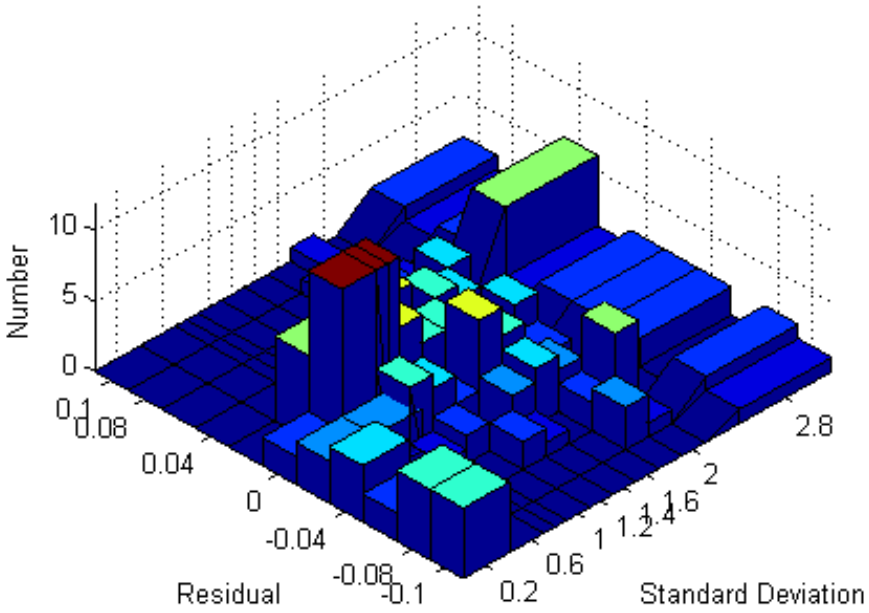

Figure 4.42 Histogram of residuals for 1000 samples and 5 frame averages

4.4.3 Contributions of drift to the signal

Because of the drift in the dark fields, it was necessary alternate the dark fields with the flood fields. The drift in dark field and the signal strength can be seen in Figure 4.43. From the subsection plots, of the top corner and bottom corner, of the EPID, it can be seen that the drift consistent over the mean and the pixels sampled, though there is a gain difference between the pixels that is evident during the warm-up section. It was noted that the dark fields became less stable at the 4.6 hour mark and the accuracy of measurements after this point is suspect.

To investigate if there were any systematic changes in the drift in any group (FF or DF) the first half of each group was subtracted from the second half, see Figure 4.44, and the odd images were subtracted from the even images to estimate the statistical error, see Figure 4.44 and Figure 4.45 for detail. Also plotted with the raw data is the FF data (Tc99m – DF). Clearly the systematic difference is larger than the statistical difference. The question is how much of this difference is propagated into the FF, and is it completely uniform or is the drift more dominant is some areas of the EPID. Figure 4.46 show the mean contribution from each flood field group and is much more variable than expected, from this we can conclude that there is a contribution to the flood field from drift.

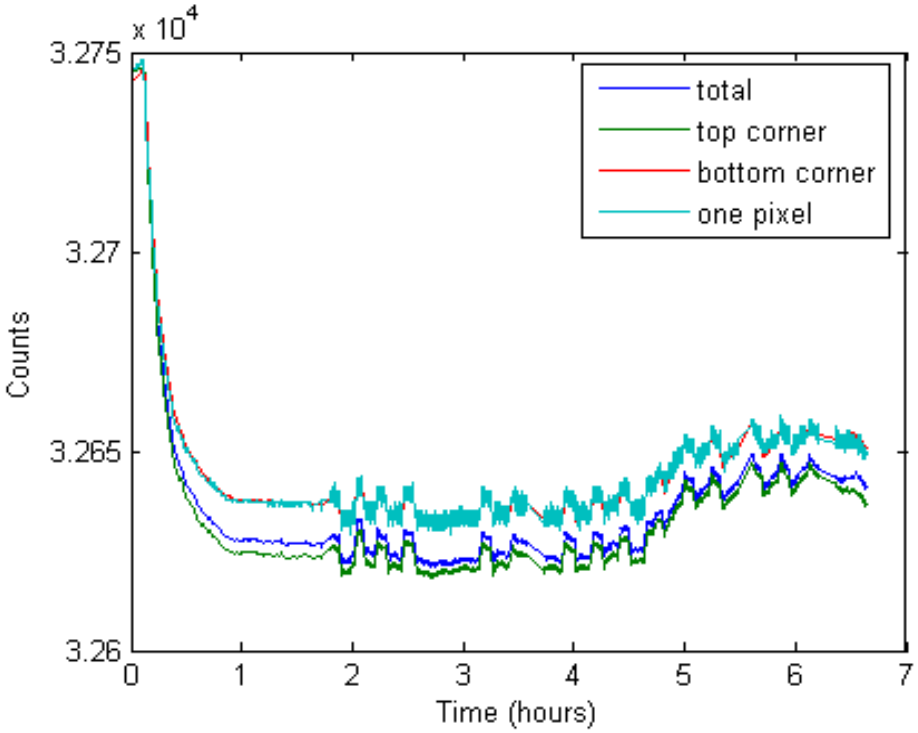

Figure 4.43 Mean counts of each image, and two groups of 625 pixels sampled and the centre pixel of the bottom corner group.

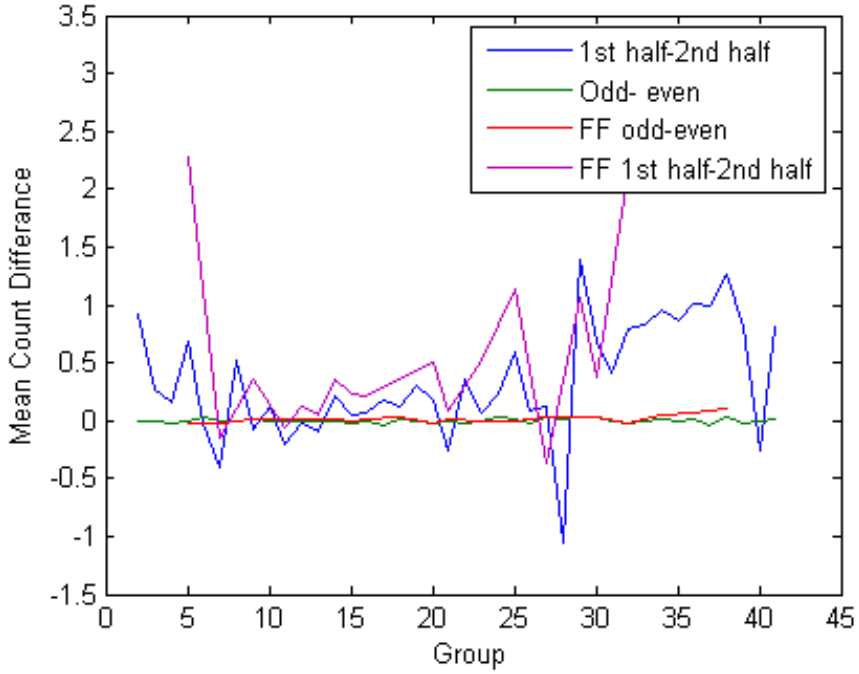

Figure 4.44 Effect of dark field drift within each series of images

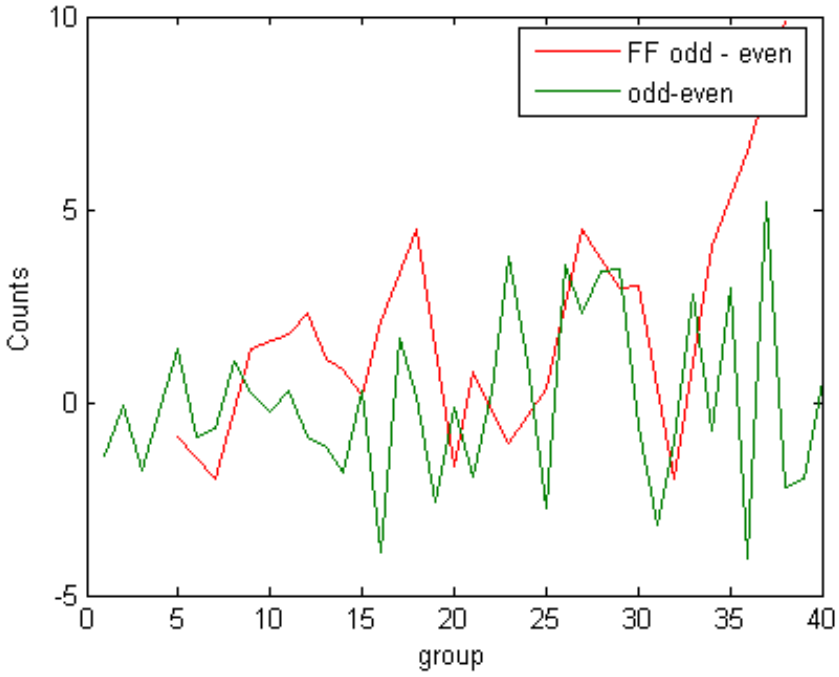

Figure 4.45 Statistical difference between one whilst imaging

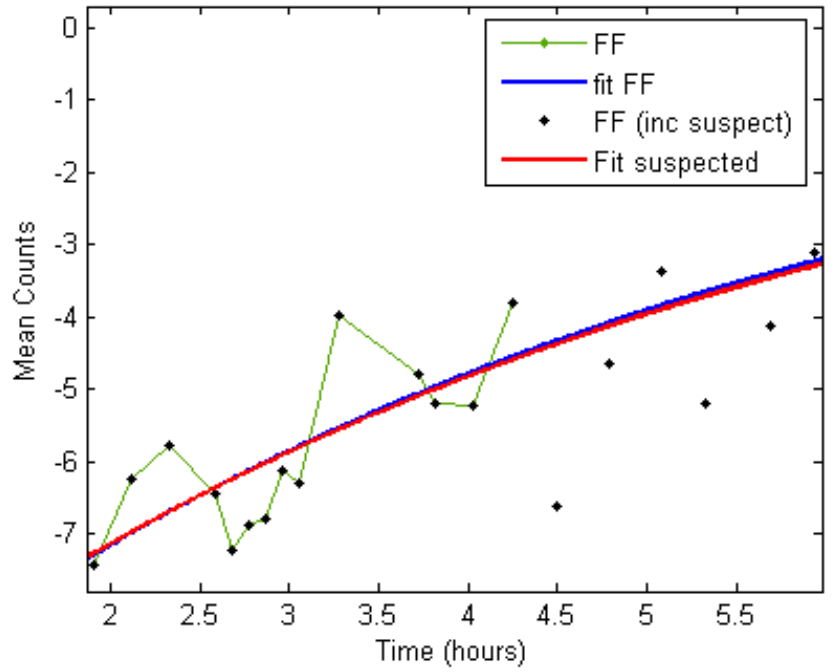

Figure 4.46 Correlation of activity decay, of the Tc99m, to average frame counts

To check that the theories about the effects of rounding were realistic, a group of images were taken with the flood phantom only over a quarter of the EPID (Figure 4.47), the image being continuous confirms that taking a mean of a large number of integers is capable of extracting a pre-rounding signal. As there were only two hundred images used, to take the quarter FF images, the noise level is higher than would be suitable for a flood field. Consequently a profile was taken averaging 20 rows (Figure 4.48) then the standard deviation was for those rows was added and subtracted form the curve and then smoothed to created bounds for expected values of the profile. The profile is predominantly within the bounds, which indicates that the noise is functioning as expected. Banding that looks similar to the banding in dark fields can be seen in Figure 4.48, on band from approximately 64-128 pixels and the next from 128-192 pixels, this and the negative signal indicates that they is significant contribution from the dark field. If we look at, the 6 hour onward part of Figure 4.43, when these image was take it can be seen that there is increased variation in the images in each group. Consequently it can be noted that the dark field is not as stable and the techniques to mitigate it need to be improved.

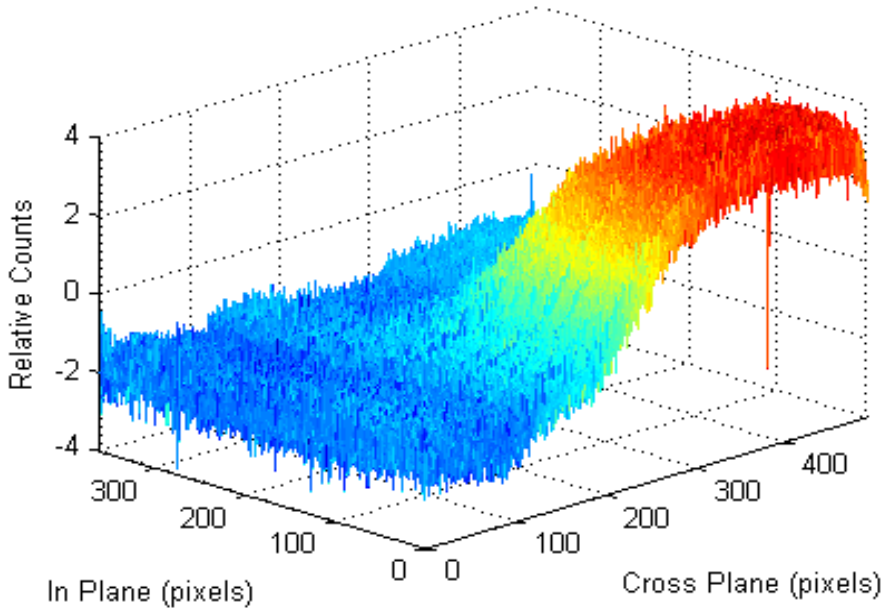

Figure 4.47 Flood phantom on the placed over only ¼ of the EPID, mean of two hundred images with dark field subtracted.

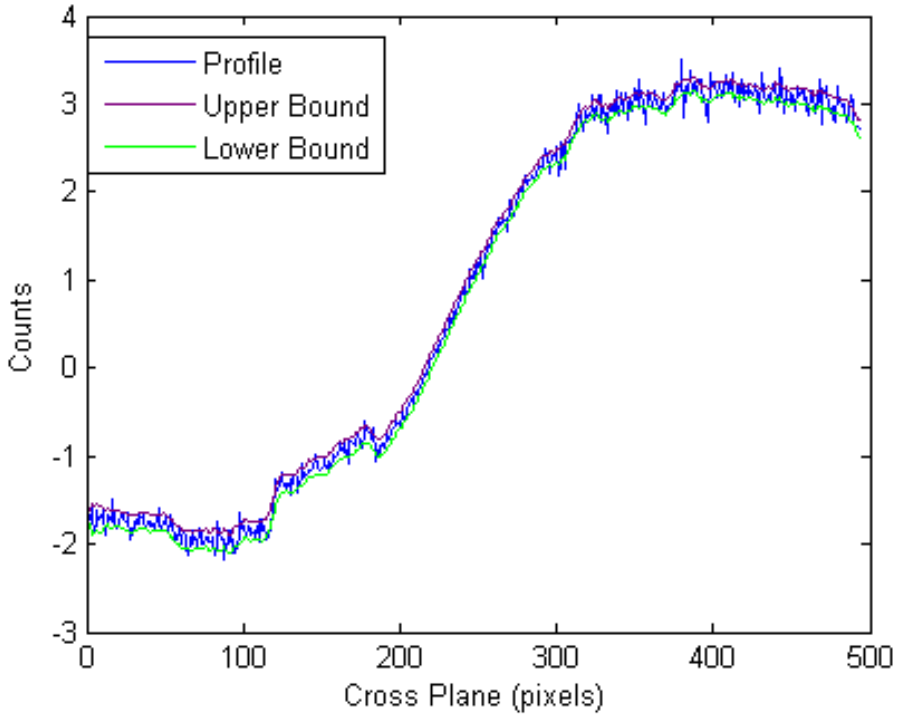

Figure 4.48 Profile through of ¼ flood phantom, showing bounds the standard deviation.

4.4.4 EPID flood field measurements

The culmination of all of this work is the flood field taken with the with the Tc99m flood phantom on the EPID. In order to construct a flood field with the flood phantom it was necessary to take alternating groups of dark field and flood image, then the difference between the flood images and adjacent dark fields was summed and its then normalized by dividing by the mean of the summed flood images. Before summing all the flood images, it was noticed in Figure 4.43 that the drift in the mean was noticeably drifting after the 4.6 hour mark, so these groups were excluded form the final flood field calculation. The metal cover being removed lead to visible light leaking in around the edges and contributing to the FF signal, so the outside 10 pixels have been removed from all images.

When comparing the normalised Tc99m flood field (Figure 4.49) to the normalised linac beam flood field (Figure 4.50) the difference is blatant. There are two major noticeable differences, the curvature in the linac bean FF, and the noise in the spatial domain in the Tc99m FF. The 8 bands, associated with the readout electronics grouping, can be seen in the beam FF but only one is clearly visible through the noise in the Tc99m FF. The noise level in the Tc99m phantom masks any pattern from the geometry of the flood phantom. The flood field was designed to produce a flatness range of 3% and the spatial noise level is approximately ± 2%, so it is not unexpected that the geometric pattern is not visible. Due to the low standard deviation pixels having a systematic error and the high standard deviation pixels having poor precision it was thought that they may be dominating the noise. Therefore, the pixels with a standard deviation less than 0.5 and more than 1.5 were set to 1 in the flood field in Figure 4.51, this is approximately $1/3^{rd}$ of the pixels (Figure 4.38). As a result, we get a picture of the tendency of the flood field, it can be seen that the Tc99m flood field is flatter even with the noise level. With flood fields being for the calibration of individual pixels it is not appropriate to apply smoothing or blurring to them, so the noise should not be removed in this way, for clinical use. However, for use as a QA tool many test, that the EPID could replace, a 0.6cc ion chamber is used and it has a cross section grater than 100 pixels, so there may be grounds for smoothing, of the flood field, for QA purposes.

It is ambiguous whether the noise is derived from systematic drift in the dark field or is random noise, but this was not investigated. The shape of the warm-up curve in Figure 4.33 indicated that the drift in the dark field was due to the change in temperature of the EPID, but attempts to stimulate this proved inconclusive.

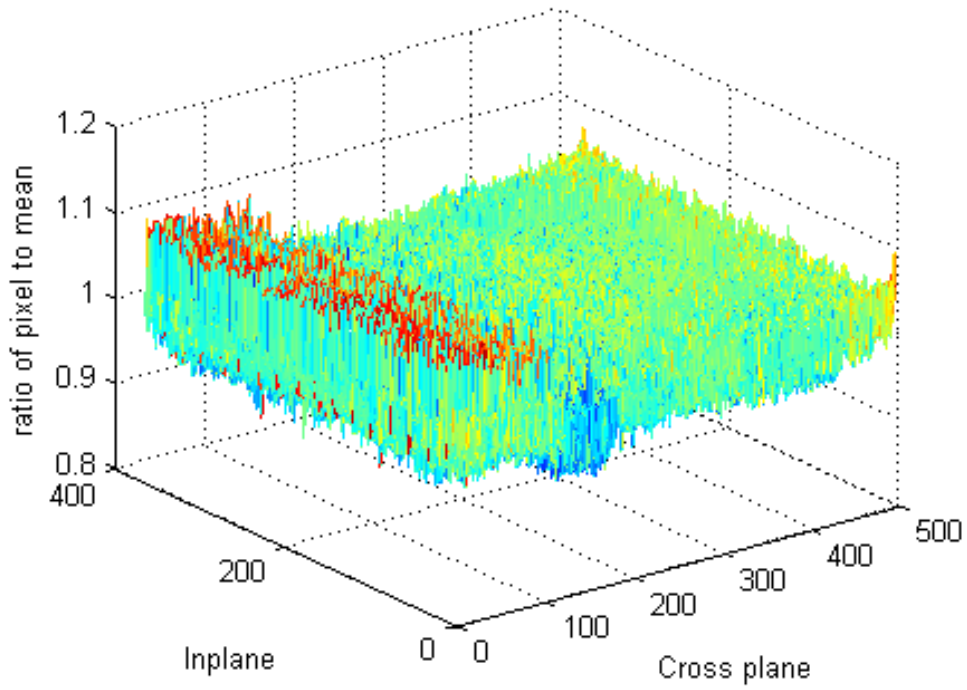

Figure 4.49 Tc99m flood field on EPID, with outside 10 pixels cropped

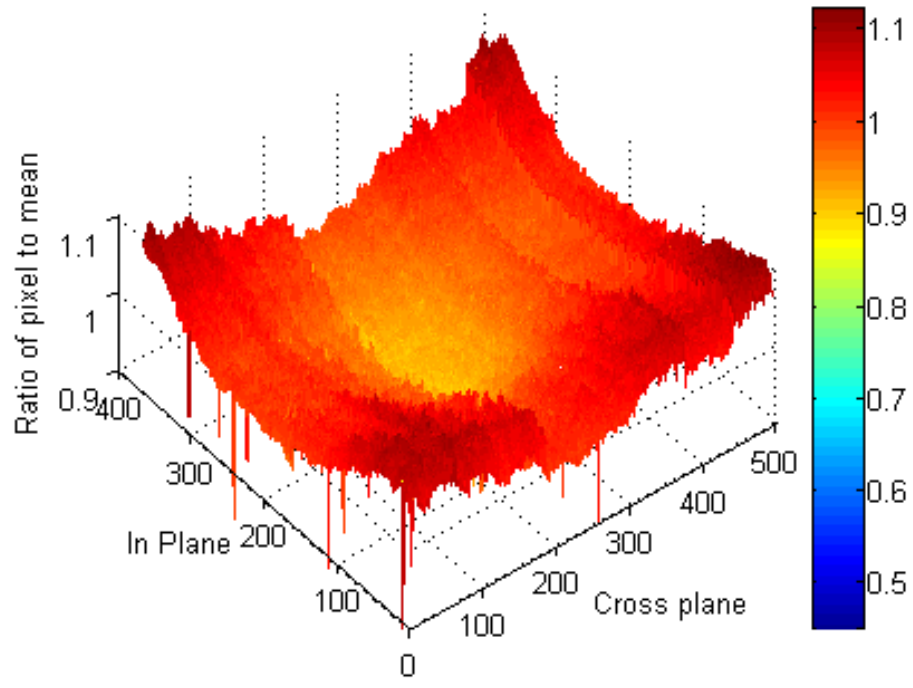

Figure 4.50 Flood field from linac beam, with outside 10 pixels cropped

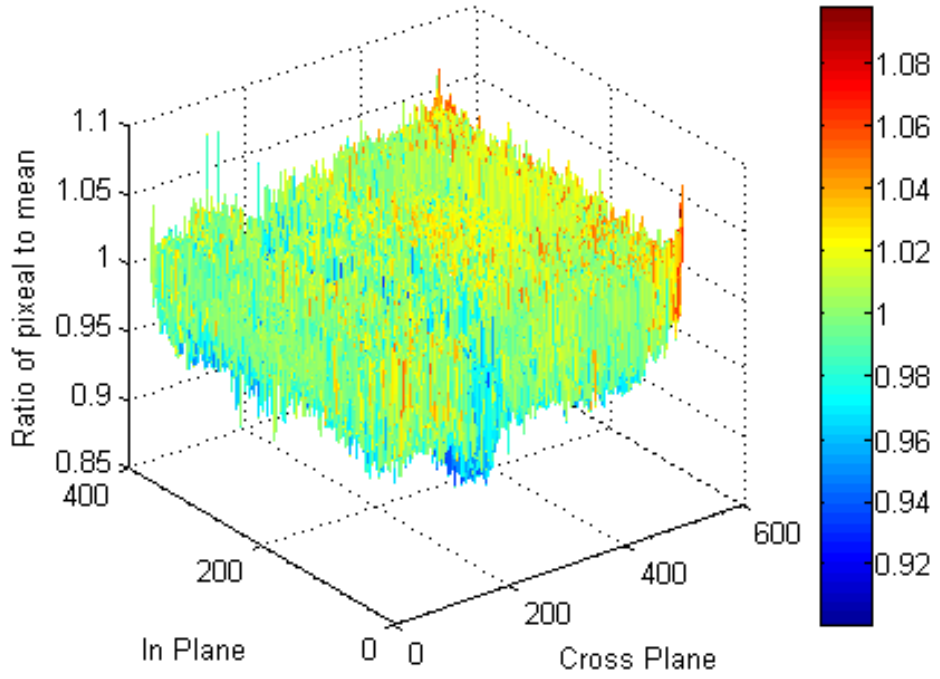

Figure 4.51 Tc99m flood field on EPID, with outside 10 pixels cropped, and outlier standard deviation pixels set to 1.

Future developments

While there is too much noise in the Tc99m flood field to use clinically it may be possible to use the technique analyse the stability of the flood field variables on long (monthly) time scale independent from beam fluctuations. The long term dosimetric stability of the EPID has been shown to have a standard deviation of 1.2% over an average of 800 pixels [37]. With the calculated, individual pixel, standard deviation of 3% (via the theory of standard deviation of the means), for the Tc99m flood field, a mean over 800 pixels would give a standard deviation of 0.1%. Therefore, using the flood phantom would be suitable for producing a long term stability test for the EPID independent of the linac beam. A comparison between the linac stability and the EPID stability could be made, if a linac beam stability test was done at the same time as the Tc99m test. If the EPID is stable, then the flood fields used for the stability could be combined into a mega flood field and used to asses other methods of taking flood fields.

It may be possible to increase the signal strength by changing the time between reset frames and imaging frames, by decreasing the number of frames per sync pulse, but this was not investigated as it was attempted to keep the imaging conditions as close as possible to the clinical conditions. However, this may introduce more noise into the image as in Figure 4.31.

A smaller phantom, the size of the hole in the metal cover, would approximately double the signal (Figure 4.6). Using the metal cover to align the flood phantom with the EPID reduces the potential for registration errors, to below the size of an EPID pixel. Using the smaller phantom would decrease the flatness, but this would not be relevant for stability tests. With improvement in the technique for confirmation of the model, and further development of the model to match what is measured, the shape of the flood field could be corrected for buy using the model.

The noise in the Tc99m flood field comes from both random noise and systematic change, in the dark field. By using, either multivariate or multiway analysis, on the flood fields it may be possible to separate the noise into its components of: row noise; column noise; pixels noise; and systematic change. It is suspected that a better understanding of the systematic noise will lead to a technique that will reduce the spatial noise in the flood field.

Conclusion

This thesis set out to investigate the possibility of using a radionuclide, technetium 99 m, in order to produce a flood field for the calibration of an EPID.

Because using Tc99m is radically different to what the EPID is designed for, preliminary tests were needed to ensure that the EPID responded appropriately with Tc99m. Gadolinium has increased absorption of x-rays at low energies due to the photo-electric effect. Because of the construction tolerances within the EPID, this spectral in response could have caused some pixels to have a significantly different ratio to that of the mean of the flood field when Tc99m is used, to that of when the linac beam is used. When modelled with Monte Carlo the ratios were within 1.6%, for the tolerances of ±0.01mm Cu and Gd, which is adequate for the use of a Tc99m flood phantom. There is a 10% difference between the max and min raw values, of the EPIDs response to 6MV spectrum in the Monte Carlo model: if the EPID had this range of thickness the pattern of varying thickness would be visible in the in the beam flood field. The EPID has a linear response to dose at the dose rates provided by the linac beam, provided it is not saturated, but the response at the dose rates achievable with Tc99m had not been established. The response of the EPID is found to be linear over all ranges measured ($r^2 = 0.994$).

The extraneous issue of ghosting was investigated as a possible cause of background drift. The results showed that the ghosting was only detectable for 90 seconds after the beam was finished so this was clearly not the source of the drift that changed over a 2 hour time period. This ghosting time could be significant in applications of where the EPID is used in continuous imaging mode for QA applications.

To build a flood phantom a model was used to predict the flatness resulting from variations in the geometry of the phantom. The model was then compared to diagnostic film exposed by the phantom. Due to the film not having a linear response with dose, and the preliminary nature of the film packet, the correlation was weak. The differences here were attributed to the film and film packet and the model was assumed to be accurate enough for a guide, but not to be used to correct for deviations from flat.

After taking the information from the preliminary experimentation into account, the flood field taken with the EPID and a Tc99m flood phantom. The Tc99m flood field had a spatial noise of approximately 3% which is the same as the noise predicted from the standard deviation. This is accurate enough to use for QA with pixel averaging, but is not accurate enough for clinical image correction.

Appendices

A MATLAB® code

A.1 DICOM Import

In order to import information from the DICOM header the MATLAB Dicom dictionary needs to be modified to include the EPID position information otherwise it will produce an error message.

So the file ‘dicom-dict.txt' needs to be modified with this line of code:

(3002,000d) LO epidpossition 1

This file was saved as ‘dicom-dictof.txt' to allow roll back.

A.1.1 Imports and groups DICOM Files

```
%% creates stack of data to do stat analysis on from a list
%% sets dictionary to alternate dictionary that has the info for r arm
%% position
Dicomdict('set','C:\MATLAB701\toolbox\images\images\dicom-dictof.txt');
% lists of start and stop numbers in file names to import
dcl;
if false;
%% takes lists and concatenates them to the ones used from dcl
[st b] = sort([st4 st5 st3b]);%%[stnt1,stnt3,stnt6,sttc1,sttc3,sttc6]);
en = sort([en4 en5 en3b]);%%[ennt1,ennt3,ennt6,entc1,entc3,entc6]);
nmt = [nm4 nm5 nm3b];%%[nnt1 nnt3 nnt6 ntc1 ntc3 ntc6];%%
nm = nmt(b);
else
st = stmv(1);
en =enmv(size(enmv,2));
nm ={'all'};
end
tcrono=[];  contentcrono=[];
lsttl= 0;   ll=size(st,2);    tconl=[];
for aa=1:ll;
    stnoxi =st(aa);  %% start
    ennoxi =en(aa);
    name= char(nm(aa));
    nmofxi =ennoxi-stnoxi+1;      %% nubber of images +1
  %% upolxi= 5;  %% number of standard dev above is replaced with mean
  %% dnolxi =8;
  %% no of stdv which below is replaced with mean used in rmol
    tic
    noi = zeros(384,512,nmofxi);
    toc

    %% make volume
    for fnm=stnoxi:ennoxi;
        if fnm >= 10000;
            fname = ['SPI',int2str(fnm),'.dcm'];
        elseif fnm >= 1000;
            fname = ['SPI0',int2str(fnm),'.dcm'];
```

```
        else
                  fname = ['SPI00',int2str(fnm),'.dcm'];
        end
        a = double(dicomread((fname)));
       %% a = rmol(a,upolxi,dnolxi);  %% removes outlyers
       noi(:,:,fnm+1-stnoxi)=a;
       infot = dicominfo(fname);
       ContentTime = infot.ContentTime;
       ContentTimesec = str2num(ContentTime(5:6))+60*...
           str2num(ContentTime(3:4))+3600*str2num(ContentTime(1:2));
       ContentDate = infot.ContentDate;
       Contentyear = str2num(ContentDate(1:4));
       ContentMounth = str2num(ContentDate(5:6));
       ContentDay = str2num(ContentDate(7:8));
       contentcrono(:,fnm-stnoxi+1)=[ContentTimesec; datenum([Contentyear...
                 ContentMounth ContentDay str2num(ContentTime(1:2))
...
           str2num(ContentTime(3:4)) str2num(ContentTime(5:6))])];
       avfrm=str2num(infot.RTImageDescription(134:135));

    end
         if isfield(infot,'epidpossition');
        contpos = infot.epidpossition;
        vide = findstr(contpos,'\');
        contposi(1)=str2num(contpos(1:(vide(1)-1)));
        contposi(2)=str2num(contpos((vide(1)+1):(vide(2)-1)));
        contposi(3)=str2num(contpos((vide(2)+1:size(contpos,2))))
        name
    else
        contposi(1)=0;
        contposi(2)=0;
        contposi(3)=0;
    end;
    toc

%% if to avoids out of memory error
if size(noi,3)<65;
    eval([name,'stdv = std(noi,0,3);']);
    eval([name,'mdi = median(noi,3);']);
elseif size(noi,3)<120
    eval([name,'stdv(:,size(noi,2)/2+1:size(noi,2),:)'...
        ,'= std(noi(:,size(noi,2)/2+1:size(noi,2),:),0,3);']);
    eval([name,'stdv(:,1:size(noi,2)/2,:) = '...
        ,'std(noi(:,1:size(noi,2)/2,:),0,3);']);
    eval([name,'mdi(:,size(noi,2)/2+1:size(noi,2),:)'...
        ,'= median(noi(:,size(noi,2)/2+1:size(noi,2),:),3);']);
    eval([name,'mdi(:,1:size(noi,2)/2,:) = '...
        ,'median(noi(:,1:size(noi,2)/2,:),3);']);
elseif size(noi,3)<180
    eval([name,'stdv(:,round(size(noi,2)*2/3)+1:size(noi,2),:)'...
        ,'= std(noi(:,round(size(noi,2)*2/3)+1:size(noi,2),:),0,3);']);
    eval([name,'stdv(:,round(size(noi,2)/3)+1:round(size(noi,2)*2/3),:)'...
        ,'= std(noi(:,round(size(noi,2)/3)+1:round(size(noi,2)*2/3),:)'...
        ,',0,3);']);
    eval([name,'stdv(:,1:round(size(noi,2)/3),:) = '...
        ,'std(noi(:,1:round(size(noi,2)/3),:),0,3);']);
    eval([name,'mdi(:,round(size(noi,2)*2/3)+1:size(noi,2),:)'...
        ,'= median(noi(:,round(size(noi,2)*2/3)+1:size(noi,2),:),3);']);
    eval([name,'mdi(:,round(size(noi,2)/3)+1:round(size(noi,2)*2/3),:)'...
      ,'= median(noi(:,round(size(noi,2)/3)+1:round(size(noi,2)*2/3),:)'...
        ,',3);']);
    eval([name,'mdi(:,1:round(size(noi,2)/3),:) = '...
```

```
        ,'median(noi(:,1:round(size(noi,2)/3),:),3);']);
else
    eval([name,'stdv(1:size(noi,1)/2,size(noi,2)/2+1:size(noi,2),:)=',...
        ' std(noi(1:size(noi,1)/2,size(noi,2)/2+1:size(noi,2),:),0,3);']);
    eval([name,'stdv(1:size(noi,1)/2,1:size(noi,2)/2,:) = ',...
        'std(noi(1:size(noi,1)/2,1:size(noi,2)/2,:),0,3);']);
    eval([name,'stdv(size(noi,1)/2+1:size(noi,1),',...
        'size(noi,2)/2+1:size(noi,2),:)= std(noi(size(noi,1)/2+1:',...
        'size(noi,1),size(noi,2)/2+1:size(noi,2),:),0,3);']);
    eval([name,'stdv(size(noi,1)/2+1:size(noi,1),1:size(noi,2)/2,:)',...
        ' = std(noi(size(noi,1)/2+1:size(noi,1),1:size(noi,2)/2,:)',...
        ',0,3);']);
    eval([name,'mdi(1:size(noi,1)/2,size(noi,2)/2+1:size(noi,2),:)=',...
      ' median(noi(1:size(noi,1)/2,size(noi,2)/2+1:size(noi,2),:),3);']);
    eval([name,'mdi(1:size(noi,1)/2,1:size(noi,2)/2,:) = ',...
        'median(noi(1:size(noi,1)/2,1:size(noi,2)/2,:),3);']);
    eval([name,'mdi(size(noi,1)/2+1:size(noi,1),',...
        'size(noi,2)/2+1:size(noi,2),:)= median(noi(size(noi,1)/2+1:',...
        'size(noi,1),size(noi,2)/2+1:size(noi,2),:),3);']);
    eval([name,'mdi(size(noi,1)/2+1:size(noi,1),1:size(noi,2)/2,:)',...
        ' = median(noi(size(noi,1)/2+1:size(noi,1),1:size(noi,2)/2,:)',...
        ',3);']);
end
    eval([name,'mni = min(noi,[],3);']);
    eval([name,'mxi = max(noi,[],3);']);
    eval([name,'sm = sum(noi,3);']);
    eval([name,'th = size(noi,3);']);
    save([name,'sm'],[name,'sm'])
    toc
    eval([name,'mei = mean(noi,3);']);
    toc
    eval([name '= noi;']);
    tcon(:,1)=squeeze(squeeze(mean(mean(noi,2),1)));
    tcon(:,2)=squeeze(squeeze(mean(mean(noi(38:105,78:125,:),2),1)));
    tcon(:,3)=squeeze(squeeze(mean(mean(noi(296:361,392:441,:),2),1)));
    tcon(:,4)=squeeze(squeeze(noi(10,10,:)));
    lsttl= size(tconl,1);
    tconl(lsttl+1:lsttl+size(tcon,1),:)=tcon;
    tcrono(:,lsttl+1:lsttl+size(tcon,1))=contentcrono;
    save([name,'sm'],'contentcrono','tcon',[name,'th'],[name,'sm']);
     if aa==ll;
        figure
        subplot(1,2,1);
        mesh(eval([name,'stdv']));
              title(['stdev ',name]);

        eval(['mns = min(',name,'stdv(:));']);
              eval(['mxs = max(',name,'stdv(:));']);
        h = [0,mns:(mxs-mns)/9:mxs];

        subplot(1,2,2);
        hist(eval([name,'stdv(:)']),h);
              title(['max = ',num2str(mxs),', min = ',num2str(mns)]);
        tcon2=tcon(:,1)-mean(tcon(:,1),1);
        figure;
        plot(tcon2(:,1),'b');
        title([name,' by layer'])
        xlabel('layer')
    else
        toc
```

```
        save(name)
        varlst = 0;
        cll=0;
        ncl = zeros(1,9); %%list of varables not to clear in each iteration
        varlst = who;
        ncl(1) = strmatch('aa',varlst,'exact');
        ncl(2) = strmatch('st',varlst,'exact');
        ncl(3) = strmatch('nm',varlst,'exact');
        ncl(4) = strmatch('varlst',varlst,'exact');
        ncl(5) = strmatch('cll',varlst,'exact');
        ncl(6) = strmatch('ll',varlst,'exact');
        ncl(7) = strmatch('en',varlst,'exact');
        ncl(8) = strmatch('tconl',varlst,'exact');
        ncl(9) = strmatch('tcrono',varlst,'exact');
        cll= varlst;
        cll(ncl) =[];%% remove not clear from clear list
              for s=1:size(cll,1) %%Clears the varirables in the var list
            clear(char(cll(s)))
        end
    end
end
toc
tconel=tconl;
tes=tcrono(2,:)-min(tcrono(2,:));
        save(name)
figure;
hold on
plot(tconel(:,1),'r')
plot(tconel(:,2),'g')
plot(tconel(:,3),'b')
plot(tconel(:,4),'color',[.5 0 .5])
legend('total','top corner','bottom corner','one
pixel','location','NorthEastOutside')

hold off
title({'mean of each slice in stack',char(nm(1))})
figure;
if max(tes)<2;
    div=24;
    xlab='time in hours';
else
    div=1;
    xlab = 'time in days';
end
plot(tes*div, tconel(:,1))
title({'Output of EPID ',char(nm(1))})
xlabel(xlab);
ylabel('mean count of each image')
```

A.1.2 Points of interest in linearity test

This code is modified to also find the points of interest for ghosting

```
%% creates a array of just the points of interest
 postfi = '_100';
fs=15;
ls=1.5;
%% snm={'g3','g4','g5'};
sasz=7 ;%%sample size
%% names of geometrical arrangements
snm={'g1','g2','g3','g4','g5'};
```

```
activi = [93.7 213 387 812 1205];
     %% locations of tc99 sources

lx = [57 255 426; 57 256 428; 70 260 439];
ly = [66 60 75; 183 192 201; 335 319 338];
 for x=1:size(snm,2)
          %% tmbsumg is the image - the background taken well after it.
          eval(['tempsorce = tmbsum',char(snm(x)),postfi,';']);


    temppoi = zeros(33,33);
    for y = 1:3;
        for z = 1:3
          thisselection = tempsorce((ly(y,z)-sasz):(ly(y,z)+sasz),...
              (lx(y,z)-sasz):(lx(y,z)+sasz));
          poi1p(y,z,x) = tempsorce(ly(y,z),lx(y,z));
          temppoi((y*(2*sasz+1)-2*sasz):(y*(sasz*2+1)),...
              (z*(2*sasz+1)-2*sasz):(z*(sasz*2+1)))= thisselection;
          tempsorce((ly(y,z)-sasz):(ly(y,z)+sasz),...
              (lx(y,z)-sasz):(lx(y,z)+sasz))=1500;
          %% creates the mean and stdv stacks
          poimean(y,z,x) =  mean(thisselection(:));
          poistd(y,z,x) = std(thisselection(:));
           end
        end
eval(['poi'   char(snm(x)),postfi,'=temppoi;']);
%%eval(['mnpoi',char(snm(x)),postfi,'=poimean'])
         %%eval(['stdpoi',char(snm(x)),postfi,'=poistd'])


figure(333);
    subplot(2,3,x);
    imagesc(eval(['poi',char(snm(x)),postfi]),[-1600,600]);
title(['points of interest of ',char(snm(x)),postfi])
    colorbar
     figure(444);
        subplot(2,3,x);
        imagesc(tempsorce,[-1800,1500])
        title(['points of interest of ',char(snm(x)),postfi])
        colorbar

end
poibg=(squeeze(poimean(1,2,:))+squeeze(poimean(2,1,:))...
    +squeeze(poimean(2,3,:))+squeeze(poimean(3,2,:)))/4;

poi1 = sort(squeeze(poimean(1,1,:)),'descend');
poi2 = sort(squeeze(poimean(1,3,:)),'descend');
poi3 = sort(squeeze(poimean(2,2,:)),'descend');
poi4 = sort(squeeze(poimean(3,1,:)),'descend');
poi5 = sort(squeeze(poimean(3,3,:)),'descend');
%% new  coding that does above for singel point
for x=1:size(snm,2)
    y=round((x*1.25)/2);
    z=(3-mod((x+1),3));
    poi1ps(x,:) = sort(squeeze(poi1p(y,z,:)),'descend');
    poi1psbg(x,:) =sort(squeeze(poi1p(y,z,:))-poibg,'descend');
end
ze=80 ;
covect = corrcoef([poibg'; poi1'; poi2'; poi3'; poi4'; poi5'; activi]');
covect0 = corrcoef([ze poibg';ze poi1';ze poi2';ze poi3';...
    ze poi4';ze poi5';0 activi]');
```

```
%% drift removed
poi1n = sort(squeeze(poimean(1,1,:))-poibg,'descend');
poi2n = sort(squeeze(poimean(1,3,:))-poibg,'descend');
poi3n = sort(squeeze(poimean(2,2,:))-poibg,'descend');
poi4n = sort(squeeze(poimean(3,1,:))-poibg,'descend');
poi5n = sort(squeeze(poimean(3,3,:))-poibg,'descend');

eb = [40 40 50 50 60];
covectn = corrcoef([poibg'; poi1n'; poi2n';...
    poi3n'; poi4n'; poi5n'; activi]');
covectn0 = corrcoef([ze poibg';ze poi1n';ze poi2n';...
    ze poi3n';ze poi4n';ze poi5n';0 activi]');
covect1n = corrcoef([poibg'; poi1psbg; activi]');


if postfi(1)=='_';
    postfi(1)=[];
end

%% plots uncorected
figure
errorbar(activi,poi1,eb,'r','linewidth',ls);
hold on
errorbar(activi,poi2,eb,'g','linewidth',ls);
errorbar(activi,poi3,eb,'b','linewidth',ls);
errorbar(activi,poi4,eb,'c','linewidth',ls);
errorbar(activi,poi5,eb,'m','linewidth',ls);
errorbar([140:240:1200],poibg,40,'y','linewidth',ls);
hold off
title({'Linearity of EPID with 5 diferent activities of Tc99',...
    ['in 5 different locations.  on 6Mv ',postfi,'MU per min']},...
    'fontsize',fs )
xlabel('activity in MBq','fontsize',fs)
ylabel('counts','fontsize',fs)
legend(['top left, r=' num2str(covect(7,2))],['top right, r= ',...
    num2str(covect(7,3))],['centre, r=' num2str(covect(7,4))],...
    ['bottom left, r=' num2str(covect(7,5))],['bottom right, r=',...
    num2str(covect(7,6))],['background, r=' num2str(covect(7,1))])
```

%% plots corected

```
Figure
errorbar(activi,poi1n,eb,'r','linewidth',ls);
hold on
errorbar (activi, poi2n, eb,'g','linewidth', ls);
errorbar (activi, poi3n, eb,'b','linewidth', ls);
errorbar (activi, poi4n, eb,'c','linewidth', ls);
errorbar (activi, poi5n, eb,'m','linewidth', ls);
errorbar ([140:240:1200], poibg, 40,'y','linewidth', ls);
hold off
title ({'Linearity - drift corrected ',...
    ['in 5 different locations.  on 6Mv ',postfi,'MU per min']},...
    'fontsize',fs)
xlabel('activity in MBq','fontsize',fs)
ylabel('counts','fontsize',fs)
legend(['top left, r=' num2str(covectn(7,2))],['top right, r=',...
    num2str(covectn(7,3))],['centre, r=' num2str(covectn(7,4))]...
    ,['bottom left, r=' num2str(covectn(7,5))],['bottom right, r=' ...
   num2str(covectn(7,6))],['background vs time, r=' num2str(covectn(7,1))])

%% plots corected single pixel
Figure
c0lr ={'r','g','b','c','m'};
```

```
errorbar([140:240:1200],poibg,40,'y','linewidth',ls);
hold on
for x=1:size(snm,2)
        errorbar(activi,poi1psbg(x,:),eb,char(c0lr(x)),'linewidth',ls);
end

hold off
title({'Linearity - drift corrected ',...
    ['in 5 different locations.  on 6Mv singel pixel',postfi,'MU per
min']},...
    'fontsize',fs)
xlabel('activity in MBq', 'fontsize',fs)
ylabel('counts','fontsize',fs)
legend(['top left, r=' num2str(covect1n(7,2))],['top right, r=',...
    num2str(covect1n(7,3))],['centre, r=' num2str(covect1n(7,4))]...
    ,['bottom left, r=' num2str(covect1n(7,5))],['bottom right, r=' ...
   num2str(covect1n(7,6))],['background vs time, r=' num2str(covect1n(7,1))])
```

A.2 Flood field prediction

A.2.1 Six dimensional calculation “epipcpir6d”

```
%% to model the output of a flood phantom on a EPID phantom + epid method *
%% deformantion  "epipcpir6d"
tic
%%epid size real
epw   = 400;%%401 epd   = 300;%%301
pxlstp = 1% must be binary    phstep=1;
%% epid size pixels
epwpxa = 512;%%12  EPID number of pixwls = 512 by 384
epdpxa = 384;%%4
epwpx = epwpxa/pxlstp;  %% number of pixels calculated for
epdpx = epdpxa/pxlstp;
tt = 0; %% count for number of points arc tan is undefind for
xx =[];     yy =[];
%% epid pixell size
pxw  = epw/epwpx;  %% sise of pixels in mm      pxd  = epd/epdpx; avps =
(pxw+pxd)/2;
mue= 0.1994;
%% resets variabesl to empty
trndi9 = [];      trndc9 = [];      trndi8 = [];      trndc8 = [];
      trddi9 = [];      trnddc9 = [];
trddi8  = [];     trddc8 = [];      defm=[];          distm=[];   thckm=[];
      intencnd=[];
intence=[]; volm=[];          volcm=[];   defslm=[];  olm= [];
      tsw=[];              tsd=[];

%% values that are calc for
overlap =[130,145] %%[10:30:130,145];
defv = [1,2];%% [1,3,3.9:.2:4.6,5,5.4,6];  %% 3 big led + 4 pots ~3.2mm
thckv = [10,12,14];%% [2,3,4,10:2:14];  %% nm tank 12mm
distv = [14,16,18,20,24,40,41,42,50,60]; %% nm tank 41mm
                                        %epid surface to gd = 12mm
overlaps =size(overlap,2);          defs = size(defv,2);    thcks =
size(thckv,2);    dists = size(distv,2);
ttlsz= overlaps*defs*thcks*dists
%% not enough mem
rs2ss=single(zeros(dists,thcks,2*round((epwpx+round(...
    (epw+overlap(overlaps))/pxw))/2),2*round((epdpx+round(...
    (epd+overlap(overlaps))/pxd))/2)));
obss=single(zeros(dists,thcks,2*round((epwpx+round(...
    (epw+overlap(overlaps))/pxw))/2),2*round((epdpx+round(...
    (epd+overlap(overlaps))/pxd))/2)));
  % ,epdpx+round((epd+overlap(overlaps))/pxd));
  % 2*round((epwpx+phwpx)/2) == phwpx = round(phw/pxw) ==epw+overlap(phol);
cpst=single(zeros(overlaps,defs+1,dists ,thcks,round(epwpx/2)));
avps = (pxw+pxd)/2;
%% mainfor loop
for phol = 1:overlaps;
    for thck =1:thcks;
        %%thicknes
        zthick =thckv(thck);  %%2+(thck-1)*.5;
        %% hight in pixels
        zpthick = (zthick/avps);
            for distl =1:dists;
            zmin = distv(distl );%%23+(distl -1)*3;
%distance between the bottom  %%of the tank to the closest =23
            zpmin = (zmin/avps);
```

```
            %% phantom size real
            phlp = 50;
%%nucular medcine tank is 530mm by 410mm internaly
        %% calculates the phantom size from the 90% epid width + gemometry
            %% based on hight to the midel of the phantom
            phw  = epw+overlap(phol); %%506; %% phlp + epw; %%600
            phd  = epd+overlap(phol); %%406; %% phlp + epd; %%  500;;
            if thck == thckv(1);
                tsw(distl )=(phw);
                tsd(distl )=(phd);
            end;
            %% phantom size in pixels
            phwpx = round(phw/pxw);       phdpx = round(phd/pxd);
            epro3 = zeros(epwpx/2,epdpx/2);     epro4 =
zeros(epwpx/2,epdpx/2);
             stpsz=1;
             olm(thck,distl )= phw-epw;
            for def = 1:defs;
              %% deformation calculations
               zz=defv(def);
              x1=(-phwpx/2):phwpx/2;
              x2=(-phdpx/2):phdpx/2;
              am=phwpx*phdpx/zz;
              y1 = (am*(cosh(x1/am)-cosh(phwpx/2/am)));
              y2 = (am*(cosh(x2/am)-cosh(phdpx/2/am)));
              slc=(1-(y2'*y1))';
              slcra =slc(round(phwpx/2),round(phdpx/2));
              %%slc=ones(phd,phw);  %% this line removes deformantion
              %%slc2 =zeros(phwpx,phdpx);
              slc3 =zeros(phwpx,phdpx);
              xw=phwpx;
              yw=phdpx;
             volajst= am^2*(-am*sinh(1/2*xw/am)+1/2*cosh(1/2*xw/am)*xw)*...
                  (-am*sinh(1/2*yw/am)+1/2*cosh(1/2*yw/am)*yw)-...
                 am^2*(am*sinh(1/2*xw/am)-1/2*cosh(1/2*xw/am)*xw)*...
                  (-am*sinh(1/2*yw/am)+1/2*cosh(1/2*yw/am)*yw);
              volc = (phwpx*phdpx*zpthick)/(epwpx*epdpx);
              vold = (phwpx*phdpx*zpthick-volajst)/(epwpx*epdpx);
               xofs = phd/(2)+1;    yofs = phw/(2)+1;
              %% matrix for invers sq law and absorntion for all the epid
              %%+ the phantome area
            bmw = round((epwpx+phwpx)/2);%%Total of the phantom and epid
              bmd = round((epdpx+phdpx)/2);
              slw = (phwpx/2);
              sld = (phdpx/2);
              %% rs  =  zeros((2*bmw),(2*bmd));
              rs2  =  single(zeros((2*bmw),(2*bmd)));
              ob  =  zeros((2*bmw),(2*bmd));
              znorm = sqrt(2+zpmin^2);
              unmod = ones(phwpx,phdpx)*(1/(zpmin)-1/(zpmin+zpthick));
               for x=1:(2*bmw);%%width
                  for y=1:(2*bmd);%%depth
                      rr = single(((x-bmw)^2+ (y-bmd)^2+zpmin^2));
                      %% rs(x,y)=1/rr;  %% single thick
                      ob(x,y)=single(exp(-1*mue*sqrt(rr)/znorm));
                      pnl= sqrt((x-bmw+.1)^2+ (y-bmd+.1)^2);
                      rs2(x,y)=single((atan(((zpthick+zpmin))/pnl)-...
                          (atan((zpmin)/pnl)))/pnl); %% multipl thivk
                    if and(x<=phwpx,y<=phdpx);
                        %generate deformation matrix
                       slc3(x,y)=(1/(zpmin+(zpthick*(1-slc(x,y))))-...
                      1/(zpmin+zpthick))/(1/(zpmin)-1/(zpmin+zpthick));
                    end;
```

```
                end; %% end y
            end; %% end x

            if phol==overlaps&&def==1;
                obss(distl,thck,:,:)=single(ob);
                rs2ss(distl,thck,:,:)=single(rs2);
            end

%% takes the peice of the peice of rs the inverse squar law and multiplys
            %% it by the deformation slc3
            for a=1:epwpx/2; %% crosplane/ width
                b=1;
                %def flat
               [epro4(a,b),epro3(a,b)]=pcdns(a,b,epwpx,epdpx,...
                    phwpx,phdpx,slc3,volc,vold,rs2,ob);
            end%% end a
            for b=2:epdpx/2;   %%inplane /depth
                a=1;
                %def flat
               [epro4(a,b),epro3(a,b)]=pcdns(a,b,epwpx,epdpx,...
                    phwpx,phdpx,slc3,volc,vold,rs2,ob);
            end %end b
            cpst(phol,def+1,distl ,thck,:)=single(squeeze(epro4(:,1)));
            if def==1
                cpst(phol,1,distl ,thck,:)=single(squeeze(epro3(:,1)));
            end

            %%Inplane not deformed
            inp90 = epro3(1,1:round(size(epro3,2)*.9));
            inp80 = epro3(1,1:round(size(epro3,2)*.8));
            trndi8(phol,def,distl ,thck)=max(inp80)/min(inp80);
            trndi9(phol,def,distl ,thck)=max(inp90)/min(inp90);
            %% Cross plane not deformed
            crp90 = epro3(1:round(size(epro3,1)*.9),1);
            crp80 = epro3(1:round(size(epro3,1)*.8),1);
            trndc9(phol,def,distl ,thck)=max(crp90)/min(crp90);
            trndc8(phol,def,distl ,thck)=max(crp80)/min(crp80);
            intencnd(phol,def,distl ,thck)= epro3(1,1);
            %% inplane
            inp80 = epro4(1,1:round(size(epro4,2)*.8));
            inp90 = epro4(1,1:round(size(epro4,2)*.9));
            trddi8(phol,def,distl ,thck)=max(inp80)/min(inp80);
            trddi9(phol,def,distl ,thck)=max(inp90)/min(inp90);

            %% crosplane
            crp90 = epro4(1:round(size(epro4,1)*.9),1);
            crp80 = epro4(1:round(size(epro4,1)*.8),1);
            trddc9(phol,def,distl ,thck)=max(crp90)/min(crp90);
            trddc8(phol,def,distl ,thck)=max(crp80)/min(crp80);

            intence(phol,def,distl ,thck) = epro4(1,1);

            defm(def)=zz;
            defslm(phol,def,thck)=slc(round(phwpx/2),round(phdpx/2));
            volm(phol,def,distl ,thck)=vold;
            volcm(phol,def,distl ,thck)=volc;
            if mod(phol+def+thck+distl ,10*pxlstp)-1==0;
               fprintf(['Overlap = ',num2str(phol),', def = ',...
          num2str(def),',  distl  = ',num2str(distl ),', thck = ',...
                    num2str(thck),', time = ',num2str(toc),'\n']);
                vold;
                volc;
                volajst;
```

```
            end
          end; %% end of def
          distmp(distl )=zpmin;

      end;  %% end of distl

      zpt(thck)=zpthick;

   end; %% end of thck
end% end of phol
thckm=thckv;

%% finish an print
def=round(size(defm,2)/2);
thck=round(size(thckm,2)/2);
distl =round(size(distmp,2)/2);
phol=round(size(overlap,2)/2);

zz=defv(def);%%round(size(defv,2)/2));
zmin = distv(distl );
zthick =thckv(thck);
ol= olm(thck,distl );
slcra = defslm(phol,def,thck);
tm=toc
```

A.2.2 Full EPID dose "epddg4"

```
%% to model the output of a flood phantom on a EPID phantom + epid method *
%% deformantion  and semetrical tank sheilding "epddg4"
tic
%%epid size real
epw   = 400;%%401 epd   = 300;%%301
pxlstp =1   phstep=1;
%% epid size pixels
epwpxa = 512;%%12  EPID number of pixwls = 512 by 384
epdpxa = 384;%%4
epwpx = epwpxa/pxlstp;  %% number of pixels calculated for
epdpx = epdpxa/pxlstp;

tt = 0; %% count for number of points arc tan is undefind for
xx =[];           yy =[];

%% epid pixell size
pxw  = epw/epwpx;  %% sise of pixels in mm
pxd  = epd/epdpx;
%% phantom size real
phlp = 50; %%nucular medcine tank is 530mm by 410mm internally
phw  = 610; %% phlp + epw; %%600; %%
phd  = 420; %% phlp + epd; %%  500;;

%% phantom size in pixels
phwpx = round(phw/pxw);
phdpx = round(phd/pxd);

zmin = 41;  %% distance between the bottom of the tank to the
zthick =12;
%% hight in pixels
avps = (pxw+pxd)/2;
zpmin = (zmin/avps);
zpthick = (zthick/avps);
```

```
hi = 13 ;%% avreage hight to sheilding that blocks the phantom
sightlines
hipx =hi/avps;
f = 10.5;%% average distance to sheilding
fpx =f/avps;

epro = zeros(epwpx/2,epdpx/2);
epro2 = zeros(epwpx/2,epdpx/2);
epro3 = zeros(epwpx/2,epdpx/2);
epro4 = zeros(epwpx/2,epdpx/2);
mue= 0.1994;
stpsz=1;

volajst= am^2*(-am*sinh(1/2*phwpx/am)+1/2*cosh(1/2*phwpx/am)*phwpx)*...
                (am*sinh(1/2*phdpx/am)+1/2*cosh(1/2*phdpx/am)*phdpx)-...
             am^2*(am*sinh(1/2*phwpx/am)-1/2*cosh(1/2*phwpx/am)*phwpx)*...
                (-am*sinh(1/2*phdpx/am)+1/2*cosh(1/2*phdpx/am)*phdpx);

volc= phwpx*phdpx*zpthick/(epwpx*epdpx);
vold= (phwpx*phdpx*zpthick-volajst)/(epwpx*epdpx);

%% deformation calculations
zz=4.1;
x1=[(-phwpx/2):phwpx/2];
x2=[(-phdpx/2):phdpx/2];
am=phwpx*phdpx/zz;
y1 = (am*(cosh(x1/am)-cosh(phwpx/2/am)));
y2 = (am*(cosh(x2/am)-cosh(phdpx/2/am)));
slc=(1-(y2'*y1))';
slcra =slc(round(phwpx/2),round(phdpx/2));
%%slc=ones(phd,phw);  %% this line removes deformantion
slc2 =zeros(phwpx,phdpx);
slc3 =zeros(phwpx,phdpx);

xofs = phd/(2)+1;
yofs = phw/(2)+1;

%% matrix for invers sq law and absorntion for all the epid + the phantome
%% area

bmw = round((epwpx+phwpx)/2);  %%Total of the phantom and the epid
bmd = round((epdpx+phdpx)/2);
slw = (phwpx/2);
sld = (phdpx/2);
rs  =  zeros((2*bmw),(2*bmd));
rs2  =  zeros((2*bmw),(2*bmd));
ob  =  zeros((2*bmw),(2*bmd));
znorm = sqrt(2+zpmin^2);
unmod = ones(phwpx,phdpx)*(1/(zpmin)-1/(zpmin+zpthick));
for x=1:(2*bmw);%%width
    for y=1:(2*bmd);%%depth
        rr = ((x-bmw)^2+ (y-bmd)^2+zpmin^2);
        rs(x,y)=1/rr;  %% single thick
        ob(x,y)=exp(-1*mue*sqrt(rr)/znorm);
        pnl= sqrt((x-bmw+.1)^2+ (y-bmd+.1)^2);
        rs2(x,y)=(atan(((zthick+zmin)/avps)/pnl)-(atan((zmin/avps)/pnl)))...
            /pnl; %% multipl thivk
        if and(x<=phwpx,y<=phdpx);
          slc3(x,y)=(1/(zpmin+(zpthick*(1-slc(x,y))))-1/(zpmin+zpthick))...
                /(1/(zpmin)-1/(zpmin+zpthick));
        end;
          end;  %% end y
```

```
    end;  %% end x


toc

%% takes the peice of the peice of rs the inverse squar law and multiplys
%% it by the deformation slc3
for a=1:epwpx/2; %% width
    aomn = (epwpx/2+a-1);
    aomx = (epwpx/2+a-2)+phwpx;
    for b=1:epdpx/2;   %%depth
        %def flat
        [epro4(a,b),epro3(a,b)]=pcd(a,b,epwpx,epdpx,zpmin,phwpx,phdpx,...
            zpthick,slc3,volc,vold,fpx,hipx,rs2,ob);
        [epro(a,b),epro2(a,b)]=pcd(a,b,epwpx,epdpx,zpmin,phwpx,phdpx,...
            zpthick,slc3,volc,vold,fpx,hipx,rs,ob);
%                             pcd(a,b,epwpx,epdpx,zpmin,phwpx,phdpx,...
                    %zpthick,slc3,volc,vold,fpx,hipx,rs2,ob)
       if and(mod(a+b-2,100)==0,mod(a-1,20)==0); %%progres counter
            fprintf([' a = ',num2str(a),' of ' num2str(epwpx/2),' b = ',...
         num2str(b),' of ' num2str(epdpx/2),'time = ',num2str(toc),' \n']);
       end;
    end;
end;
pltg3;
```

A.2.3 Point dose calculation “PCD”

This function is used in A.2.2 "epddg4" and a simpler version is used in A.2.1

```
function [def flat] = pcd(a, b, epwpx, epdpx, zpmin, phwpx,...
  phdpx,zpthick,slc3,volc,fpx,hipx,rs2,ob)
%% calc the dose to a point in the EPID from the phantom by moving the
%% section of rs2 and summing it.
xa =round(1/2*phwpx-a-zpmin*(1/2*epwpx-a+fpx)/hipx);
aomn1 = (epwpx/2+a-1);
naomn = aomn1 +xa;
aomx = (epwpx/2+a-2)+phwpx;
xan =max(xa,0)+1;
aomn = max(naomn,aomn1);
xb=round(1/2*phdpx-b-zpmin*(1/2*epdpx-b+fpx)/hipx);
bomn1 = (epdpx/2+b-1);
nbomn = bomn1 +xb;
bomn = max(nbomn,bomn1);
xbn=max(xb,0)+1
bomx = (epdpx/2+b-2)+phdpx;
thp3 = rs2(aomn:aomx,bomn:bomx).*ob(aomn:aomx,bomn:bomx); %% multiple thick
thp4 = thp3.*slc3(xan:size(slc3,1) ,xbn:size(slc3,2)); %% multiple deformed
def = sum(thp4(:))/volc; %% deformed multiple normalised to thickness
flat = sum(thp3(:))/volc; %% Multiple thick normalised to thickness
```

A.3 Statistical analysis

A.3.1 Rounding error “add_noi2”

```
%% adds noise and rounds and tien compairss the average "noi_add2b"
%% no of samples
noss =160;  maxss=640000;     risidtotal=[];    resbip=[];  resfa=[];
t=[];       tt=[];
varst =5;   varsp =.01;       varen =5.2; fa=5; %% list of values
sva=stdrg ;%[0.5:0.5:3];%standard deviations in epid image
    nos=round(1550*fa*2^.5) % number of sampels
VN=varst:varsp:varen;
%VN = 5.13*ones(1,21)
ends=50;
for a=1:size(sva,2);
    sv=sva(a);
    [notused VNa]=meshgrid(1:nos, VN);%
    %imput varabels VNa + random no with standarddeviation SV
    inprand=round(sv*single(randn(size(VN,2),nos))+VNa);
    framesm= inprand(:,1:fa:nos); % averaging frames
    for b=2:fa
        framesm=framesm+inprand(:,b:fa:nos);
    end
    frameave=round(framesm/fa);
    risiduals=inprand-VNa;
    risidtotal(a)=mean(abs(roundn(mean(inprand,2),-3)-VN'));
    resbip(:,a)=(roundn(mean(inprand,2),-3)-VN'); %% residual by input
    resfa(:,a)=(roundn(mean(frameave,2),-3)-VN'); % residual frame average
fprintf([num2str([max(risiduals(:)),min(risiduals(:)),mean(risiduals(:)),nos,
risidtotal(a),std(inprand(:))]),'\n'])
end
[T10 ,T11] = hist(resbip,[-.1:.02:.1]);
mn=roundn(mean(mean(resfa(:)))/2,-2)*2;
[T12 ,T13] = hist(resfa,[mn-.1:.02:mn+.1]);
```

B Importation of and analysis of Monte Carlo output

B.1 d3dose

```
%%  converts 3ddose, with paragraph marks removed, file to a stack
%% And the thickness of each layer in that stack
function [mtx th] = d3dos(vtr);
dp = vtr(1);      wd = vtr(2);      hi = vtr(3);            os= 6+dp+wd+hi;
mtx= zeros(dp,wd,2*hi);       th=vtr(6+dp+wd:os);
for c=1:2*hi;
    for a=1:wd;
            mtx(:,a,c)= vtr(((c-1)*(dp*wd)+(a-1)*...
dp+1+os):((c-1)*(dp*wd)+a*dp+os));
    end;
     end;
```

B.2 “zeroear”

```
%% converts the voxels from dose to fluence
%% zeroes the values set to air for the MC model
%% zeroear

nam = 'm6a'; %%'tca'; %%
nami = 'm6';%%'tc1'; %%
th2=th(2:9)-th(1:8);
for nm= 1:size(th2,2);
    eval([nam,'(:,:,nm)=',nami,'(:,:,nm)*th2(nm);']);
end

for nm= 1:size(th2,2);
    eval([nam,'_wer(:,:,nm)=',nami,'(:,:,nm+8)*th2(nm);']);
end
%%cu
eval([nam,'(1:21,1:6,1)=0;']);
eval([nam,'(1:21,10:15,1)=0;']);
eval([nam,'(1:21,10:12,2)=0;']);
eval([nam,'(1:21,1:3,7:8)=0;']);
eval([nam,'(1:21,13:15,7:8)=0;']);
eval([nam,'(19:21,4:12,7:8)=0;']);
eval([nam,'(1:15,4:12,8)=0;']);
eval([nam,'(4:12,4:12,7)=0;']);
eval([nam,'(4:9,4:12,6)=0;']);
eval([nam,'(4:6,4:12,5)=0;']);

eval(['cu',nam,'=sum(',nam,'(:,:,1:3),3);']);
     eval(['gd',nam,'=sum(',nam,'(:,:,4:8),3);']);


%% displays image of fluence
figure1 = figure;

     imagesc(eval(['gd',nam]));
title(,nam);
xlabel('Copper');
ylabel('Gadiolinium');
colorbar('EastOutside','Box','on');
set(gca,'YTick',[2 5 8 11 14 17 20],'YTickLabel',{'border 0.5mm',...
    '0,4mm ','0.49mm','0.50mm','0.51mm','0.60mm','border 0.5mm'},...
    'XTick',[2 5 8 11 14],'XTickLabel',...
```

```
    {'border 1mm','1mm ','1.01mm ','0.99mm','border 1mm'})

%% takes data from zeroair and converts it to ratios. rato
     nam='m6a';


for a=1:3;
    for b=1:5;
      el(a+3*(b-1)) = sum(sum(eval ...
(['gd',nam,'(3*b+1:3*(b+1),3*a+1:3*(a+1));'])));
    end
end
eval(['ratos',nam,' = (1./el)''*el']);
```

C Monte Carlo code

C.1 141KeV

C.1.1 141KeV 3ddose

Sample of 3ddose

```
21 15 8
 -10.5 -9.5 -8.5 -7.5 -6.5 -5.5 -4.5 -3.5 -2.5 -1.5 -0.5 0.5 1.5 2.5 3.5
 4.5 5.5 6.5 7.5 8.5 9.5 10.5
 -7.5 -6.5 -5.5 -4.5 -3.5 -2.5 -1.5 -0.5 0.5 1.5 2.5 3.5 4.5 5.5 6.5
 7.5
 0. 0.00100000005 0.00200000009 0.100999996 0.141000003 0.150000006
 0.151000008 0.15200001 0.161000013
 0. 0. 0. 0. 0. 0. 0. 0. 0. 0. 0. 0. 0. 0. 0. 0. 0. 0. 0.
 0. 0. 0. 4.22249424E-013 3.41696466E-013 3.35962626E-013 0.
 3.97642913E-013 3.1324628E-013 3.31366614E-013 3.71003937E-013
 2.89403774E-013 4.04917773E-013 2.57979269E-013 4.05820685E-013
 3.63092659E-013 2.72278306E-013 2.78883902E-013 3.13129569E-013
 2.99582532E-013 3.09666142E-013 4.21092394E-013 0. 0. 3.34610779E-013
 3.26122423E-013 4.05670916E-013 0. 3.47223466E-013 3.59466881E-013 0.
 3.50996507E-013 2.72629462E-013 3.67086053E-013 0. 4.02510171E-013
 2.58832721E-013 3.34910755E-013 5.2431442E-013 3.7364465E-013
 3.92911783E-013 3.37895749E-013 2.92694948E-013 0. 0. 2.62512697E-013
 2.67093571E-013 3.56852535E-013 3.38883654E-013 2.58644672E-013
 4.13866508E-013 2.81390107E-013 3.49864739E-013 3.52715019E-013
 2.74963891E-013 4.07586716E-013 4.32708446E-013 5.12598582E-013
 2.51943289E-013 3.42688215E-013 3.40374996E-013 4.04106874E-013
 2.56503748E-013 4.18931102E-013 0. 0. 3.64849975E-013 3.1516707E-013
 3.26897623E-013 2.94700047E-013 0. 3.65363387E-013 3.18188544E-013
 3.40553122E-013 3.60196832E-013 4.09572547E-013 5.22107152E-013
 2.72735812E-013 3.46698533E-013 0. 4.02360207E-013 2.58387088E-013
 3.44994991E-013 4.07230027E-013 2.56783411E-013 0. 0. 3.10899791E-013
 5.62086685E-013 3.71458264E-013 4.43802532E-013 4.65545234E-013
 4.80045639E-013 4.03826645E-013 6.72229231E-013 4.76498152E-013

..... truncated for brevity ....

 0.0576674971 0.0318446147 0.0343507753 0.0315509328 0.0585553765
 0.0393009599 0.0304050013 0.0605719901 0.0331426852 0.0334333761
 0.0108972948 0.0109575843 0.0110064581 0.0361311921 0.0353983183
 0.226678687 0.306595478 0.0469715513 0.0610770895 0.0279669634
 0.0270710933 0.0273120816 0.0335828088 0.0315187887 0.0631496331
 0.0299487499 0.032631207 0.073960634 0.0655265792 0.0341724002
 0.057936023 0.0109827607 0.0109505485 0.0109839513 0.0597237451
 0.0306761036 0.221563093 0.197051447 0.0589184064 0.0804141279
 0.0375885069 0.0654471395 0.0367216471 0.0354033019 0.075533346
 0.032635766 0.0650750336 0.0309943678 0.0313855154 0.0544946082
 0.0593352068 0.0323937118 0.0316417944 0.036618138 0.0760673412
 0.070227221 0.0728370341 0.195807557 0.212867337 0.0326309392
 0.0285284963 0.0309098308 0.0580148452 0.0425062822 0.0486958267
 0.0422388553 0.0597494973 0.0323693694 0.0508403646 0.0610879609
 0.074812804 0.0493388291 0.03210953 0.07600817 0.0493413817 0.0316885717
 0.0473099865 0.0377985271 0.226078569 0.999999881 0.212306561
 0.286821734 0.179327503 0.216992138 0.286565964 0.2357804 0.180384407
 0.999999881 0.273910725 0.317068836 0.320877839 0.192332413 0.286136098
 0.199783018 0.197279978 0.214856367 0.235989479 0.316319669 0.298613582
```

```
 0.999999881
```

C.1.2 141 KeV egslst

```
*******************************************************************************
 NRCC/UW EGSnrc user-code DOSXYZnrc ($Revision: 1.34 $ last edited $Date:
2006/09/22 20:56:11 $)
 ON i1586_pc_Windows_NT (gnu_win32)                          19:48:17 Feb 22
2008
*******************************************************************************
**                                                                           **
**                                  DOSXYZnrc                                **
**                               Z pronounced zed                            **
**                                                                           **
**     Code developed at the National Research Council of Canada and         **
**         University of Wisconsin as part of the OMEGA project              **
**                                                                           **
**       This is $Revision: 1.34 $ last edited$Date: 2006/09/22 20:56:11     **
**                                                                           **
*******************************************************************************

     The following parameters may be adjusted in dosxyz_user_macros.mortran
 $MXMED:    Max number of media:  7
 $MXSTACK:  Max stack size:        15
 $IMAX,etc: Max dose scoring regions in x,y,z directions:  128  128   56
 $MAXDOSE:  Max dose scoring regions consistent with above: 917505
 $DOSEZERO(=1) 1=> all doses with uncert > 50% are zeroed in .3ddose file

 The following parameters may be adjusted in srcxyz.macros
 $INVDIM:   number of elements in inverse CPD for input energy spectra = 1000
 $NENSRC:   number of bins in input energy spectrum =  200

===============================================================================
 -------------------------------------------------------------------------------

 Title:  all thick 141"allthick_aray _gv _tc.egsinp"
 -------------------------------------------------------------------------------

===============================================================================

 Number of media (min = 1, max =   7, 0 => CT data):                3
 Medium  1:                     air
 Medium  2:                     cu
 Medium  3:                     gdv

 ECUTIN,PCUTIN,(ESTEPE,SMAX--DUMMY INPUTS):
              0.001     0.001     0.000     0.000     0.000     0.000

 # regions in x (max= 128),y (max= 128),z (max=  56) directions
 (if<0,implies # groups of reg), IPHANT (1 to output a .egsphant
 file for dosxyz_show, 0[default] to not output this file)
     :      -1    -1    -8     1

 Input boundaries in the x-direction
 ----------------------------------
 Initial boundary:       -10.500
 Width in this group, number of regions in group:         1.000   21
 Boundaries
     -10.500      -9.500      -8.500      -7.500      -6.500      -5.500
      -4.500      -3.500      -2.500      -1.500      -0.500       0.500
```

```
      1.500       2.500       3.500       4.500       5.500
6.500
      7.500       8.500       9.500      10.500

 Input boundaries in the y-direction
 ----------------------------------
 Initial boundary:        -7.500
 Width in this group, number of regions in group:         1.000   15
 Boundaries
     -7.500      -6.500      -5.500      -4.500      -3.500      -2.500
     -1.500      -0.500       0.500       1.500       2.500       3.500
      4.500       5.500       6.500       7.500

 Input boundaries in the z-direction
 ----------------------------------
 Initial boundary:         0.000
 Width in this group, number of regions in group:         0.001    1
 Width in this group, number of regions in group:         0.001    1
 Width in this group, number of regions in group:         0.099    1
 Width in this group, number of regions in group:         0.040    1
 Width in this group, number of regions in group:         0.009    1
 Width in this group, number of regions in group:         0.001    1
 Width in this group, number of regions in group:         0.001    1
 Width in this group, number of regions in group:         0.009    1
 Boundaries
      0.000       0.001       0.002       0.101       0.141       0.150
      0.151       0.152       0.161

 Total # regions including exterior =      2521

 Input groups of regions for which density and medium are not defaults
 Lower,upper i, j, k,  MEDIUM, DENSITY (  1  21)(  1   6)(  2   3)   2
0.000
 Lower,upper i, j, k,  MEDIUM, DENSITY ( 1  21)( 13  15)(  2   3)   2   0.000
 Lower,upper i, j, k,  MEDIUM, DENSITY (  1  21)(  7  9)(  1   3) 2     0.000
 Lower,upper i, j, k,  MEDIUM, DENSITY (  1  21)( 10 12)(  3   3) 2     0.000
 Lower,upper i, j, k,  MEDIUM, DENSITY (  1  21)(  1  3)(  4   6) 3     0.000
 Lower,upper i, j, k,  MEDIUM, DENSITY (  1   3)(  4 12)(  4   6) 3     0.000
 Lower,upper i, j, k,  MEDIUM, DENSITY ( 19  21)(  4 12)(  4   6) 3     0.000
 Lower,upper i, j, k,  MEDIUM, DENSITY (  1  21)( 13 15)(  4   6) 3     0.000
 Lower,upper i, j, k,  MEDIUM, DENSITY (  4  18)(  4 12)(  4   4) 3     0.000
 Lower,upper i, j, k,  MEDIUM, DENSITY (  7  18)(  4 12)(  5   5) 3     0.000
 Lower,upper i, j, k,  MEDIUM, DENSITY ( 10  18)(  4 12)(  6   6) 3     0.000
 Lower,upper i, j, k,  MEDIUM, DENSITY ( 13  18)(  4 12)(  7   7) 3     0.000
 Lower,upper i, j, k,  MEDIUM, DENSITY ( 16  18)(  4 12)(  8   8) 3     0.000
 Lower,upper i, j, k,  MEDIUM, DENSITY
    Found blank line => end of this input

 Input groups of regions for which ECUT and PCUT are not defaults
 NB This option is disabled, just input 8 zeros.
 Dummy values of lower,upper i, j, k,  ECUT, PCUT
    Found blank line => end of this input

 Enter 8 numbers on one line
   3 pairs defininglower,upper x,y,z indicies of dose regions
                 for which results are to be output
   IZSCAN:       non-zero for z-scan/page
   MAX20:        if any one = 1, output summary of max 20 doses.
   end signaled by first pair both zero
   forno dose printed, MAX20 is still read from first line

         1  21     1  15     1   6     1     0
    Found blank line => end of this input
```

```
 NCASE,IWATCH,TIMMAX,INSEED1,INSEED2,BEAM_SIZE,ISMOOTH,IRESTART,IDAT,
 IREJECT,ESAVE_GLOBAL,NRCYCL,IPARALLEL,PARNUM,n_split,ihowfarless
 :
   100000000   0   0.99     33      97 100.00    0   0  0  0  0.00  0 0 0 1 0


 Index ranges of beam field
 --------------------------

     -9.500     9.500   i index ranges over i=  2 to  20
     -6.500     6.500   j index ranges over j=  2 to  14

*******************************************************************************

         Summary of source parameters (srcxyznrc Rev 1.6)

*******************************************************************************

                    Point source incident from the front(+ve z-axis)
                         Electric charge of the source:            0
                         x-boundaries:       -9.5000 cm-    9.5000 cm
                         y-boundaries:       -6.5000 cm-    6.5000 cm
                         SSD                           130.0000 cm

===============================================================================

                   Electron/Photon transport parameter

===============================================================================

 Photon cross sections                                        PEGS4
 Photon transport cutoff(MeV)                                     0.1000E-01
 Pair angular sampling                                         SIM
 Pair cross sections                                           BH
 Triplet production                                            Off
 Bound Compton scattering                                      OFF
 Radiative Compton corrections                                 Off
 Rayleigh scattering                                           OFF
 Atomic relaxations                                            OFF
 Photoelectron angular sampling                                OFF

 Electron transport cutoff(MeV)                                 0.5210
 Bremsstrahlung cross sections                                BH
 Bremsstrahlung angular sampling                               SIM
 Spin effects                                                  On
 Electron Impact Ionization                                    OFF
 Maxium electron step in cm (SMAX)                                 5.000
 Maximum fractional energy loss/step (ESTEPE)                  0.2500
 Maximum 1st elastic moment/step (XIMAX)                       0.5000
 Boundary crossing algorithm                                   PRESTA-I
 Skin-depth for boundary crossing (MFP)                        5.803
 Electron-step algorithm                                       PRESTA-II
===============================================================================
 Medium               AE        AP
 air                0.521     0.010
 cu                 0.521     0.010
 gdv                0.521     0.010
 No range rejection.
 ************************************************************
  Histories to be simulated for this run    100000000
```

```
 Histories to be analyzed after this run   100000000

 ************************************************************
  Elapsed wall clock time to this point=       1.664 s

  CPU time so far for this run =       0.751 s

 BATCH #  TIME-ELAPSED  TOTAL CPUTIME  RATIO  TIME OF DAY  RNG    pointers

   1          0.0            0.0      0.00    19:48:18   ixx jxx =   97  33
   2       1645.1         1540.5      1.07    20:15:43   ixx jxx =   40  73
   3       3476.9         3280.0      1.06    20:46:15   ixx jxx =   77  13
   4       5308.8         5027.6      1.06    21:16:47   ixx jxx =   54  87
   5       7146.9         6791.2      1.05    21:47:25   ixx jxx =   81  17
   6       8971.5         8548.1      1.05    22:17:50   ixx jxx =   93  29
   7      10810.3        10317.9      1.05    22:48:29   ixx jxx =   91  27
   8      12664.6        12089.2      1.05    23:19:23   ixx jxx =   96  32
   9      14503.1        13848.6      1.05    23:50:01   ixx jxx =   58  91
Wall clock has gone past 24:00 hrs.
 Elapsed time adjusted assuming batches took < 1 day to complete.
    10      16398.8        15619.3      1.05    00:21:37   ixx jxx =   96  32

 Total CPU time for run = 17387.0 s =   4.830 hr =>   20705075. hist/hr
   On  i1586_pc_Windows_NT (gnu_win32)

 Fraction of incident energy deposited in the phantom =      0.2384

 Number of charged particle steps simulated,   N_step   =     1922617435
 Number of charged particle steps/incident fluence      =    4.74886E+03
 No. of PRESTA-II steps/total no. of charged particle steps =        0.98586
```

```
1all thick 141"allthick_aray _gv _tc.egsinp"

    Elec/positron planar energy fluence scored in a 1cm**2 circle
    centered at z-axison the phantom surface =  0.000E+00(1/cm**2)

    Photon planarenergy fluence scored in a 1cm**2 circle
    centered at z-axis on the phantom surface =  5.715E+04(1/cm**2)

    Elec/positron planar fluence scored in a 1cm**2 circle
    centered at z-axis on the phantom surface =  0.000E+00(1/cm**2)

    Photon planar fluence scored in a 1cm**2 circle
    centered at z-axis on the phantom surface =  4.062E+05(1/cm**2)

    Average planar fluence (number/beam area), F =  4.049E+05(1/cm**2)

         DOSXYZnrc ($Revision: 1.34 $) Dose outputs (dose/F, Gy.cm**2)

              for x=   -10.500 to    -9.500     i=  1
 ybounds: -7.500      -6.500          -5.500          -4.500           -3.500
         j=        1               2               3               4
 zbounds (     0.000)
0.001   1  0.000E+00-99.9%  1.084E-14-66.6%  0.000E+00-99.9%  1.487E-15-99.9%
0.002   2  0.000E+00-99.9%  2.636E-14-36.9%  1.572E-14-52.9%  1.887E-14-42.3%
0.101   3  1.881E-15-16.1%  2.878E-14- 4.1%  3.225E-14- 3.9%  3.097E-14- 4.0%
0.141   4  1.226E-14-18.4%  2.849E-13- 4.0%  3.211E-13- 3.8%  3.079E-13- 3.8%
0.150   5  6.238E-15-51.4%  2.592E-13- 8.5%  2.615E-13- 8.4%  2.525E-13- 8.5%
0.151   6  2.191E-15-99.9%  1.312E-13-19.9%  1.901E-13-17.2%  1.070E-13-17.4%

              for x=   -10.500 to    -9.500     i=  1
 ybounds: -3.500      -2.500          -1.500          -0.500           0.500
         j=        5               6               7               8
 zbounds (     0.000)
0.001   1  1.607E-15-99.9%  1.353E-14-87.1%  1.673E-14-46.0%  6.120E-16-72.8%
0.002   2  9.500E-15-56.4%  2.006E-14-40.7%  1.793E-14-43.7%  1.123E-14-53.9%
0.101   3  3.067E-14- 4.0%  2.931E-14- 4.1%  3.086E-14- 4.0%  2.905E-14- 4.1%
0.141   4  3.184E-13- 3.8%  2.967E-13- 3.9%  3.026E-13- 3.8%  2.906E-13- 3.9%
0.150   5  2.674E-13- 8.2%  2.511E-13- 8.7%  3.043E-13- 7.9%  2.972E-13- 7.9%
0.151   6  1.347E-13-18.6%  1.455E-13-19.7%  1.739E-13-19.2%  1.535E-13-17.9%

              for x=   -10.500 to    -9.500     i=  1
 ybounds:  0.500      1.500           2.500           3.500           4.500
         j=        9              10              11              12
 zbounds (     0.000)
0.001   1  1.560E-14-47.9%  0.000E+00-99.9%  6.448E-15-59.8%  0.000E+00-99.9%
0.002   2  4.960E-15-56.9%  1.552E-14-99.9%  6.428E-15-59.9%  0.000E+00-99.9%
0.101   3  2.822E-14- 4.1%  3.048E-14- 4.0%  2.887E-14- 4.1%  2.982E-14- 4.0%
0.141   4  2.944E-13- 3.9%  2.971E-13- 3.9%  2.930E-13- 3.9%  3.097E-13- 3.8%
0.150   5  2.503E-13- 8.6%  3.065E-13- 7.8%  2.889E-13- 8.0%  2.990E-13- 7.9%
0.151   6  9.842E-14-18.6%  1.321E-13-18.8%  1.234E-13-18.0%  1.007E-13-17.7%
              for x=   -10.500 to    -9.500     i=  1
 ybounds:  4.500       5.500           6.500           7.500
         j=       13              14              15
 zbounds (     0.000)
  0.001   1  4.276E-15-70.8%  2.650E-15-99.9%  0.000E+00-99.9%
  0.002   2  1.719E-14-46.1%  1.531E-14-45.8%  0.000E+00-99.9%
  0.101   3  3.075E-14- 4.0%  2.919E-14- 4.1%  1.604E-15-16.5%
  0.141   4  2.886E-13- 3.9%  2.901E-13- 3.9%  1.249E-14-18.1%
  0.150   5  2.859E-13- 8.0%  2.845E-13- 8.1%  4.868E-15-55.2%
  0.151   6  1.106E-13-18.6%  1.350E-13-17.3%  3.251E-15-76.4%
```

```
1all thick 141"allthick_aray _gv _tc.egsinp"

    Elec/positron planar energy fluence scored in a 1cm**2 circle
    centered at z-axis on the phantom surface =  0.000E+00(1/cm**2)

    Photon planar energy fluence scored in a 1cm**2 circle
    centered at z-axis on the phantom surface =  5.715E+04(1/cm**2)

    Elec/positron planar fluence scored in a 1cm**2 circle
    centered at z-axis on the phantom surface =  0.000E+00(1/cm**2)

    Photon planar fluence scored in a 1cm**2 circle
    centered at z-axis on the phantom surface =  4.062E+05(1/cm**2)

    Average planar fluence (number/beam area), F =  4.049E+05(1/cm**2)

         DOSXYZnrc ($Revision: 1.34 $) Dose outputs (dose/F, Gy.cm**2)

              for x=    -9.500 to    -8.500     i=  2
 ybounds: -7.500      -6.500          -5.500          -4.500          -3.500
         j=        1               2               3               4
 zbounds (     0.000)
0.001   1  1.562E-14-81.9%  4.222E-13-15.6%  3.346E-13-14.1%  2.625E-13-12.7%
0.002   2  1.296E-14-53.6%  1.751E-12- 4.3%  1.600E-12- 4.3%  1.648E-12- 4.3%
0.101   3  2.834E-14- 4.1%  2.952E-12- 0.4%  2.955E-12- 0.4%  2.963E-12- 0.4%
0.141   4  2.327E-13- 4.3%  2.049E-11- 0.5%  2.062E-11- 0.5%  2.066E-11- 0.5%
0.150   5  2.103E-13- 9.3%  1.778E-11- 1.1%  1.817E-11- 1.0%  1.806E-11- 1.0%
0.151   6  7.527E-14-23.8%  8.468E-12- 2.4%  8.437E-12- 2.4%  8.376E-12- 2.5%

              for x=    -9.500 to    -8.500     i=  2
 ybounds: -3.500      -2.500          -1.500          -0.500           0.500
         j=        5               6               7               8
 zbounds (     0.000)
0.001   1  3.648E-13-12.3%  3.109E-13-12.7%  1.537E-12- 4.6%  1.526E-12- 4.5%
0.002   2  1.611E-12- 4.3%  1.720E-12- 4.3%  2.696E-12- 3.7%  2.659E-12- 3.6%
0.101   3  2.990E-12- 0.4%  2.968E-12- 0.4%  2.960E-12- 0.4%  2.983E-12- 0.4%
0.141   4  2.080E-11- 0.5%  2.069E-11- 0.5%  2.069E-11- 0.5%  2.069E-11- 0.5%
0.150   5  1.859E-11- 1.0%  1.844E-11- 1.0%  1.832E-11- 1.0%  1.835E-11- 1.0%
0.151   6  8.323E-12- 2.4%  8.394E-12- 2.5%  8.719E-12- 2.4%  8.795E-12- 2.4%

              for x=    -9.500 to    -8.500     i=  2
 ybounds:  0.500       1.500           2.500           3.500           4.500
         j=        9              10              11              12
 zbounds (     0.000)
0.001   1  1.572E-12- 4.3%  2.754E-13-12.2%  3.169E-13-13.9%  3.044E-13-25.6%
0.002   2  2.533E-12- 3.7%  2.691E-13-11.5%  3.435E-13-14.9%  2.584E-12-87.2%
0.101   3  2.973E-12- 0.4%  2.945E-12- 0.4%  2.962E-12- 0.4%  2.972E-12- 0.4%
0.141   4  2.067E-11- 0.5%  2.088E-11- 0.5%  2.076E-11- 0.5%  2.073E-11- 0.5%
0.150   5  1.835E-11- 1.0%  1.806E-11- 1.0%  1.862E-11- 1.0%  1.818E-11- 1.0%
0.151   6  8.526E-12- 2.4%  7.902E-12- 2.5%  8.682E-12- 2.4%  8.838E-12- 2.4%

              for x=    -9.500 to    -8.500     i=  2
 ybounds:  4.500       5.500           6.500           7.500
         j=       13              14              15
 zbounds (     0.000)
  0.001   1  4.074E-13-15.0%  3.646E-13-18.7%  1.230E-14-80.0%
  0.002   2  1.632E-12- 4.3%  1.553E-12- 4.3%  4.607E-15-80.4%
  0.101   3  2.989E-12- 0.4%  2.944E-12- 0.4%  2.486E-14- 4.4%
  0.141   4  2.077E-11- 0.5%  2.066E-11- 0.5%  2.167E-13- 4.5%
  0.150   5  1.798E-11- 1.1%  1.782E-11- 1.1%  1.967E-13- 9.5%
  0.151   6  8.074E-12- 2.5%  8.346E-12- 2.5%  1.193E-13-20.1%
```

```
1all thick 141"allthick_aray _gv _tc.egsinp"

    Elec/positron planar energy fluence scored in a 1cm**2 circle
    centered at z-axis on the phantom surface =  0.000E+00(1/cm**2)

    Photon planar energy fluence scored in a 1cm**2 circle
    centered at z-axis on the phantom surface =  5.715E+04(1/cm**2)

    Elec/positron planar fluence scored in a 1cm**2 circle
    centered at z-axis on the phantom surface =  0.000E+00(1/cm**2)

    Photon planar fluence scored in a 1cm**2 circle
    centered at z-axis on the phantom surface =  4.062E+05(1/cm**2)

    Average planar fluence (number/beam area), F =  4.049E+05(1/cm**2)

         DOSXYZnrc ($Revision: 1.34 $) Dose outputs (dose/F, Gy.cm**2)

              for x=    -8.500 to    -7.500     i=  3
 ybounds: -7.500     -6.500          -5.500           -4.500           -3.500
         j=        1               2                3                4
 zbounds (     0.000)
0.001   1  0.000E+00-99.9%  3.417E-13-12.1%  3.261E-13-13.6%  2.671E-13-12.5%
0.002   2  1.442E-14-49.8%  1.682E-12- 4.3%  1.597E-12- 4.3%  1.629E-12- 4.2%
0.101   3  2.712E-14- 4.2%  2.978E-12- 0.4%  2.976E-12- 0.4%  2.994E-12- 0.4%
0.141   4  2.351E-13- 4.3%  2.080E-11- 0.5%  2.078E-11- 0.5%  2.093E-11- 0.5%
0.150   5  2.384E-13- 8.7%  1.797E-11- 1.1%  1.845E-11- 1.0%  1.831E-11- 1.0%
0.151   6  1.298E-13-23.2%  8.471E-12- 2.4%  8.454E-12- 2.4%  8.868E-12- 2.4%

              for x=    -8.500 to    -7.500     i=  3
 ybounds: -3.500     -2.500          -1.500           -0.500            0.500
         j=        5               6                7                8
 zbounds (     0.000)
0.001   1  3.152E-13-11.6%  5.621E-13-44.9%  1.733E-12- 4.2%  1.629E-12- 4.2%
0.002   2  1.614E-12- 4.4%  1.641E-12- 4.3%  2.851E-12- 3.5%  2.682E-12- 3.6%
0.101   3  3.003E-12- 0.4%  2.984E-12- 0.4%  3.015E-12- 0.4%  3.002E-12- 0.4%
0.141   4  2.093E-11- 0.5%  2.080E-11- 0.5%  2.086E-11- 0.5%  2.078E-11- 0.5%
0.150   5  1.863E-11- 1.0%  1.800E-11- 1.1%  1.837E-11- 1.0%  1.844E-11- 1.0%
0.151   6  8.697E-12- 2.4%  8.341E-12- 2.4%  8.409E-12- 2.4%  8.350E-12- 2.4%

              for x=    -8.500 to    -7.500     i=  3
 ybounds:  0.500      1.500           2.500            3.500            4.500
         j=        9              10               11               12
 zbounds (     0.000)
0.001   1  1.548E-12- 4.4%  3.088E-13-15.3%  3.550E-13-24.7%  1.236E-12-63.7%
0.002   2  2.623E-12- 3.7%  4.387E-12-66.1%  2.252E-12-82.9%  3.522E-12-85.8%
0.101   3  2.996E-12- 0.4%  2.989E-12- 0.4%  2.977E-12- 0.4%  2.980E-12- 0.4%
0.141   4  2.090E-11- 0.5%  2.084E-11- 0.5%  2.087E-11- 0.5%  2.097E-11- 0.5%
0.150   5  1.826E-11- 1.0%  1.821E-11- 1.0%  1.825E-11- 1.0%  1.840E-11- 1.0%
0.151   6  8.539E-12- 2.4%  8.268E-12- 2.4%  8.763E-12- 2.4%  8.476E-12- 2.4%

              for x=    -8.500 to    -7.500     i=  3
 ybounds:  4.500      5.500           6.500            7.500
         j=       13              14               15
 zbounds (     0.000)
  0.001   1  1.514E-12-77.5%  3.116E-13-14.7%  1.828E-15-99.9%
  0.002   2  1.582E-12- 4.4%  1.457E-12- 4.5%  9.903E-15-58.7%
  0.101   3  2.969E-12- 0.4%  2.968E-12- 0.4%  2.682E-14- 4.2%
  0.141   4  2.076E-11- 0.5%  2.076E-11- 0.5%  2.403E-13- 4.3%
  0.150   5  1.835E-11- 1.0%  1.827E-11- 1.0%  1.867E-13- 9.9%
  0.151   6  8.650E-12- 2.4%  8.650E-12- 2.4%  1.121E-13-22.5%
```

```
1all thick 141"allthick_aray _gv _tc.egsinp"

    Elec/positron planar energy fluence scored in a 1cm**2 circle
    centered at z-axis on the phantom surface =  0.000E+00(1/cm**2)

    Photon planar energy fluence scored in a 1cm**2 circle
    centered at z-axis on the phantom surface =  5.715E+04(1/cm**2)

    Elec/positron planar fluence scored in a 1cm**2 circle
    centered at z-axis on the phantom surface =  0.000E+00(1/cm**2)

    Photon planar fluence scored in a 1cm**2 circle
    centered at z-axis on the phantom surface =  4.062E+05(1/cm**2)

    Average planar fluence (number/beam area), F =  4.049E+05(1/cm**2)

         DOSXYZnrc ($Revision: 1.34 $) Dose outputs (dose/F, Gy.cm**2)

              for x=    -7.500 to    -6.500     i=  4
 ybounds: -7.500     -6.500          -5.500           -4.500           -3.500
         j=        1               2                3                4
 zbounds (     0.000)
0.001   1  6.911E-15-76.4%  3.360E-13-11.4%  4.057E-13-20.7%  3.569E-13-16.4%
0.002   2  1.459E-14-46.7%  1.624E-12- 4.4%  1.713E-12- 4.2%  1.682E-12- 4.4%
0.101   3  2.793E-14- 4.1%  2.966E-12- 0.4%  2.994E-12- 0.4%  2.998E-12- 0.4%
0.141   4  2.283E-13- 4.4%  2.078E-11- 0.5%  2.102E-11- 0.5%  2.011E-11- 0.5%
0.150   5  2.081E-13- 9.3%  1.807E-11- 1.0%  1.837E-11- 1.0%  7.713E-12- 3.6%
0.151   6  7.002E-14-29.1%  8.749E-12- 2.4%  8.848E-12- 2.4%  7.645E-12- 5.3%

              for x=    -7.500 to    -6.500     i=  4
 ybounds: -3.500     -2.500          -1.500           -0.500            0.500
         j=        5               6                7                8
 zbounds (     0.000)
0.001   1  3.269E-13-14.5%  3.715E-13-12.6%  1.743E-12- 4.2%  1.630E-12- 4.2%
0.002   2  1.809E-12- 4.2%  1.551E-12- 4.3%  2.813E-12- 3.6%  2.626E-12- 3.6%
0.101   3  3.001E-12- 0.4%  3.000E-12- 0.4%  2.989E-12- 0.4%  2.989E-12- 0.4%
0.141   4  2.029E-11- 0.5%  2.015E-11- 0.5%  2.008E-11- 0.5%  2.001E-11- 0.5%
0.150   5  8.706E-12- 6.2%  7.659E-12- 3.6%  7.576E-12- 3.9%  8.468E-12- 6.5%
0.151   6  1.322E-11-28.8%  1.370E-11-33.4%  7.668E-12- 8.6%  1.109E-11-21.9%

              for x=    -7.500 to    -6.500     i=  4
 ybounds:  0.500       1.500           2.500           3.500            4.500
         j=        9              10               11               12
 zbounds (     0.000)
0.001   1  1.627E-12- 4.3%  1.090E-12-63.4%  3.380E-13-14.5%  3.670E-13-14.5%
0.002   2  2.785E-12- 3.5%  2.258E-12-81.1%  3.387E-12-64.8%  3.857E-13-14.3%
0.101   3  2.994E-12- 0.4%  2.983E-12- 0.4%  2.966E-12- 0.4%  2.993E-12- 0.4%
0.141   4  2.030E-11- 0.5%  2.031E-11- 0.5%  2.027E-11- 0.5%  2.027E-11- 0.5%
0.150   5  7.908E-12- 3.7%  8.111E-12- 5.5%  8.225E-12- 7.4%  8.532E-12- 4.4%
0.151   6  1.140E-11-28.4%  9.096E-12-12.8%  1.049E-11-31.2%  1.111E-11-29.7%

              for x=    -7.500 to    -6.500     i=  4
 ybounds:  4.500       5.500           6.500            7.500
         j=       13              14               15
 zbounds (     0.000)
  0.001   1  3.681E-13-12.2%  3.244E-13-14.1%  1.238E-14-53.5%
  0.002   2  1.506E-12- 4.4%  1.587E-12- 4.4%  1.336E-14-50.5%
  0.101   3  2.999E-12- 0.4%  2.965E-12- 0.4%  2.811E-14- 4.2%
  0.141   4  2.064E-11- 0.5%  2.061E-11- 0.5%  2.422E-13- 4.2%
  0.150   5  1.825E-11- 1.0%  1.840E-11- 1.0%  1.977E-13- 9.6%
  0.151   6  8.633E-12- 2.4%  8.472E-12- 2.5%  1.004E-13-22.3%
```

```
1all thick 141"allthick_aray _gv _tc.egsinp"

    Elec/positron planar energy fluence scored in a 1cm**2 circle
    centered at z-axis on the phantom surface =  0.000E+00(1/cm**2)

    Photon planar energy fluence scored in a 1cm**2 circle
    centered at z-axis on the phantom surface =  5.715E+04(1/cm**2)

    Elec/positron planar fluence scored in a 1cm**2 circle
    centered at z-axis on the phantom surface =  0.000E+00(1/cm**2)

    Photon planar fluence scored in a 1cm**2 circle
    centered at z-axis on the phantom surface =  4.062E+05(1/cm**2)

    Average planar fluence (number/beam area), F =  4.049E+05(1/cm**2)

         DOSXYZnrc ($Revision: 1.34 $) Dose outputs (dose/F, Gy.cm**2)

              for x=    -6.500 to    -5.500     i=  5
 ybounds: -7.500      -6.500          -5.500          -4.500          -3.500
         j=        1               2               3               4
 zbounds (     0.000)
0.001   1  1.784E-15-99.9%  3.566E-12-91.2%  3.541E-12-91.7%  3.389E-13-14.8%
0.002   2  2.061E-15-71.5%  1.577E-12- 4.3%  1.687E-12- 4.3%  1.726E-12- 4.3%
0.101   3  2.673E-14- 4.2%  2.984E-12- 0.4%  3.008E-12- 0.4%  3.011E-12- 0.4%
0.141   4  2.386E-13- 4.3%  2.067E-11- 0.5%  2.081E-11- 0.5%  2.023E-11- 0.5%
0.150   5  2.397E-13- 8.8%  1.846E-11- 1.0%  1.803E-11- 1.0%  8.799E-12- 5.7%
0.151   6  1.412E-13-20.0%  8.367E-12- 2.4%  8.410E-12- 2.5%  1.092E-11-29.5%

              for x=    -6.500 to    -5.500     i=  5
 ybounds: -3.500     -2.500          -1.500          -0.500           0.500
         j=        5               6               7               8
 zbounds (     0.000)
0.001   1  2.947E-13-11.6%  4.438E-13-33.7%  1.726E-12- 4.2%  1.507E-12- 4.4%
0.002   2  1.640E-12- 4.3%  1.739E-12- 4.3%  2.948E-12- 3.5%  2.726E-12- 3.6%
0.101   3  3.010E-12- 0.4%  3.004E-12- 0.4%  2.983E-12- 0.4%  2.994E-12- 0.4%
0.141   4  2.028E-11- 0.5%  2.018E-11- 0.5%  2.022E-11- 0.5%  2.024E-11- 0.5%
0.150   5  8.161E-12- 6.4%  8.638E-12- 6.9%  7.628E-12- 3.2%  7.956E-12- 5.7%
0.151   6  1.500E-11-27.6%  9.232E-12- 9.2%  1.038E-11-29.9%  1.093E-11-30.1%

              for x=    -6.500 to    -5.500     i=  5
 ybounds:  0.500       1.500           2.500           3.500           4.500
         j=        9              10              11              12
 zbounds (     0.000)
0.001   1  1.628E-12- 4.3%  4.040E-13-13.2%  3.630E-13-14.3%  2.826E-13-13.2%
0.002   2  2.785E-12- 3.5%  1.767E-12-74.7%  1.894E-12-81.5%  3.628E-13-21.0%
0.101   3  2.988E-12- 0.4%  2.982E-12- 0.4%  2.981E-12- 0.4%  2.991E-12- 0.4%
0.141   4  2.032E-11- 0.5%  2.035E-11- 0.5%  2.023E-11- 0.5%  2.034E-11- 0.5%
0.150   5  8.528E-12- 8.1%  7.823E-12- 5.8%  7.767E-12- 3.7%  7.922E-12- 5.8%
0.151   6  8.055E-12- 8.6%  7.339E-12- 5.3%  7.284E-12- 3.7%  7.662E-12- 7.1%

              for x=    -6.500 to    -5.500     i=  5
 ybounds:  4.500       5.500           6.500           7.500
         j=       13              14              15
 zbounds (     0.000)
  0.001   1  3.849E-13-13.8%  3.603E-13-14.2%  3.838E-14-99.9%
  0.002   2  1.716E-12- 4.2%  1.672E-12- 4.3%  1.275E-14-53.5%
  0.101   3  2.985E-12- 0.4%  2.972E-12- 0.4%  2.635E-14- 4.3%
  0.141   4  2.094E-11- 0.5%  2.058E-11- 0.5%  2.188E-13- 4.5%
  0.150   5  1.835E-11- 1.0%  1.782E-11- 1.1%  2.400E-13- 9.0%
  0.151   6  8.882E-12- 2.4%  8.562E-12- 2.4%  7.556E-14-21.3%
```

```
1all thick 141"allthick_aray _gv _tc.egsinp"

    Elec/positron planar energy fluence scored in a 1cm**2 circle
    centered at z-axis on the phantom surface =  0.000E+00(1/cm**2)

    Photon planar energy fluence scored in a 1cm**2 circle
    centered at z-axis on the phantom surface =  5.715E+04(1/cm**2)

    Elec/positron planar fluence scored in a 1cm**2 circle
    centered at z-axis on the phantom surface =  0.000E+00(1/cm**2)

    Photon planar fluence scored in a 1cm**2 circle
    centered at z-axis on the phantom surface =  4.062E+05(1/cm**2)

    Average planar fluence (number/beam area), F =  4.049E+05(1/cm**2)

         DOSXYZnrc ($Revision: 1.34 $) Dose outputs (dose/F, Gy.cm**2)

              for x=    -5.500 to    -4.500     i=  6
 ybounds: -7.500      -6.500         -5.500           -4.500           -3.500
         j=        1               2                3                4
 zbounds (     0.000)
0.001   1  5.020E-15-73.3%  3.976E-13-23.5%  3.472E-13-16.2%  2.586E-13-11.9%
0.002   2  9.932E-15-45.9%  1.631E-12- 4.3%  1.647E-12- 4.3%  1.568E-12- 4.4%
0.101   3  2.715E-14- 4.2%  2.979E-12- 0.4%  2.987E-12- 0.4%  3.006E-12- 0.4%
0.141   4  2.582E-13- 4.1%  2.062E-11- 0.5%  2.074E-11- 0.5%  2.014E-11- 0.5%
0.150   5  2.112E-13- 9.1%  1.831E-11- 1.0%  1.849E-11- 1.0%  8.108E-12- 3.9%
0.151   6  1.412E-13-22.3%  8.521E-12- 2.4%  8.459E-12- 2.4%  7.983E-12- 5.9%

              for x=    -5.500 to    -4.500     i=  6
 ybounds: -3.500      -2.500           -1.500           -0.500           0.500
         j=        5               6                7                8
 zbounds (     0.000)
0.001   1  3.629E-12-89.9%  4.655E-13-17.6%  1.592E-12- 4.5%  1.603E-12- 4.3%
0.002   2  1.646E-12- 4.2%  1.781E-12- 4.2%  2.713E-12- 3.6%  2.892E-12- 3.5%
0.101   3  3.013E-12- 0.4%  2.988E-12- 0.4%  3.000E-12- 0.4%  2.988E-12- 0.4%
0.141   4  2.025E-11- 0.5%  2.016E-11- 0.5%  2.027E-11- 0.5%  2.035E-11- 0.5%
0.150   5  7.553E-12- 3.8%  8.021E-12- 4.7%  7.483E-12- 3.8%  7.703E-12- 6.4%
0.151   6  7.350E-12- 5.2%  7.275E-12- 5.0%  7.778E-12- 5.7%  1.015E-11-31.7%

              for x=    -5.500 to    -4.500     i=  6
 ybounds:  0.500       1.500          2.500            3.500            4.500
         j=        9              10               11               12
 zbounds (     0.000)
0.001   1  1.628E-12- 4.2%  3.409E-13-21.0%  3.262E-13-23.4%  2.199E-13-13.8%
0.002   2  2.760E-12- 3.6%  3.836E-13-21.3%  1.844E-12-60.9%  3.753E-13-41.4%
0.101   3  2.993E-12- 0.4%  2.974E-12- 0.4%  2.989E-12- 0.4%  2.969E-12- 0.4%
0.141   4  2.033E-11- 0.5%  2.029E-11- 0.5%  2.015E-11- 0.5%  2.044E-11- 0.5%
0.150   5  7.700E-12- 3.3%  8.109E-12- 4.1%  7.929E-12- 3.7%  8.075E-12- 4.0%
0.151   6  8.363E-12- 6.5%  8.525E-12- 6.6%  1.312E-11-29.9%  1.068E-11-31.6%

              for x=    -5.500 to    -4.500     i=  6
 ybounds:  4.500       5.500            6.500            7.500
         j=       13              14               15
 zbounds (     0.000)
0.001   1  3.770E-13-16.7%  4.828E-13-19.4%  7.655E-15-71.1%
0.002   2  1.615E-12- 4.4%  1.576E-12- 4.3%  2.490E-14-39.1%
0.101   3  2.980E-12- 0.4%  2.979E-12- 0.4%  2.714E-14- 4.2%
0.141   4  2.090E-11- 0.5%  2.083E-11- 0.5%  2.415E-13- 4.2%
0.150   5  1.857E-11- 1.0%  1.792E-11- 1.1%  2.229E-13- 9.2%
0.151   6  8.818E-12- 2.4%  8.270E-12- 2.5%  9.826E-14-22.0%
```

```
1all thick 141"allthick_aray _gv _tc.egsinp"

    Elec/positron planar energy fluence scored in a 1cm**2 circle
    centered at z-axis on the phantom surface =  0.000E+00(1/cm**2)

    Photon planar energy fluence scored in a 1cm**2 circle
    centered at z-axis on the phantom surface =  5.715E+04(1/cm**2)

    Elec/positron planar fluence scored in a 1cm**2 circle
    centered at z-axis on the phantom surface =  0.000E+00(1/cm**2)

    Photon planar fluence scored in a 1cm**2 circle
    centered at z-axis on the phantom surface =  4.062E+05(1/cm**2)

    Average planar fluence (number/beam area), F =  4.049E+05(1/cm**2)

         DOSXYZnrc ($Revision: 1.34 $) Dose outputs (dose/F, Gy.cm**2)

              for x=    -4.500 to    -3.500     i=  7
 ybounds: -7.500      -6.500           -5.500           -4.500           -
3.500
         j=        1               2             3              4
 zbounds (     0.000)
0.001   1  6.119E-15-76.0%  3.132E-13-11.9%  3.595E-13-18.1%  4.139E-13-14.9%
0.002   2  9.452E-15-61.6%  1.599E-12- 4.3%  1.588E-12- 4.4%  1.616E-12- 4.3%
0.101   3  2.599E-14- 4.3%  2.978E-12- 0.4%  3.022E-12- 0.4%  2.994E-12- 0.4%
0.141   4  2.386E-13- 4.2%  2.074E-11- 0.5%  2.091E-11- 0.5%  2.095E-11- 0.5%
0.150   5  2.315E-13- 8.7%  1.820E-11- 1.0%  1.847E-11- 1.0%  1.715E-11- 1.1%
0.151   6  1.021E-13-22.4%  8.301E-12- 2.5%  8.475E-12- 2.4%  7.202E-12- 4.9%

              for x=    -4.500 to    -3.500     i=  7
 ybounds: -3.500      -2.500           -1.500           -0.500          0.500
         j=        5               6              7               8
 zbounds (     0.000)
0.001   1  3.654E-13-15.6%  4.800E-13-22.0%  1.555E-12- 4.4%  1.668E-12- 4.2%
0.002   2  1.654E-12- 4.3%  1.616E-12- 4.3%  2.701E-12- 3.6%  2.726E-12- 3.6%
0.101   3  2.992E-12- 0.4%  2.990E-12- 0.4%  3.009E-12- 0.4%  3.029E-12- 0.4%
0.141   4  2.119E-11- 0.5%  2.105E-11- 0.5%  2.084E-11- 0.5%  2.100E-11- 0.5%
0.150   5  1.716E-11- 1.1%  1.717E-11- 1.1%  1.750E-11- 1.1%  1.703E-11- 1.1%
0.151   6  9.239E-12- 8.5%  1.464E-11-32.1%  8.060E-12- 4.9%  8.409E-12- 6.2%

              for x=    -4.500 to    -3.500     i=  7
 ybounds:  0.500       1.500          2.500            3.500            4.500
         j=        9              10              11              12
 zbounds (     0.000)
0.001   1  1.562E-12- 4.4%  3.075E-13-12.1%  3.169E-13-13.8%  2.566E-13-12.4%
0.002   2  2.667E-12- 3.6%  6.049E-12-60.3%  4.046E-13-22.4%  4.395E-12-66.9%
0.101   3  3.008E-12- 0.4%  2.988E-12- 0.4%  2.987E-12- 0.4%  3.002E-12- 0.4%
0.141   4  2.087E-11- 0.5%  2.085E-11- 0.5%  2.081E-11- 0.5%  2.092E-11- 0.5%
0.150   5  1.707E-11- 1.1%  1.716E-11- 1.1%  1.689E-11- 1.1%  1.701E-11- 1.1%
0.151   6  1.034E-11-31.7%  7.572E-12- 4.1%  8.846E-12-10.5%  1.517E-11-30.8%
              for x=    -4.500 to    -3.500     i=  7
 ybounds:  4.500       5.500           6.500            7.500
         j=       13              14              15
 zbounds (     0.000)
  0.001   1  3.440E-13-17.1%  6.432E-13-41.2%  2.669E-15-99.9%
  0.002   2  1.786E-12- 4.2%  1.566E-12- 4.4%  8.733E-15-65.9%
  0.101   3  3.011E-12- 0.4%  2.956E-12- 0.4%  2.716E-14- 4.2%
  0.141   4  2.073E-11- 0.5%  2.078E-11- 0.5%  2.616E-13- 4.1%
  0.150   5  1.831E-11- 1.0%  1.825E-11- 1.0%  2.614E-13- 8.4%
  0.151   6  8.485E-12- 2.5%  8.076E-12- 2.5%  1.515E-13-20.5%
```

```
1all thick 141"allthick_aray _gv _tc.egsinp"

    Elec/positron planar energy fluence scored in a 1cm**2 circle
    centered at z-axis on the phantom surface =  0.000E+00(1/cm**2)

    Photon planar energy fluence scored in a 1cm**2 circle
    centered at z-axis on the phantom surface =  5.715E+04(1/cm**2)

    Elec/positron planar fluence scored in a 1cm**2 circle
    centered at z-axis on the phantom surface =  0.000E+00(1/cm**2)

    Photon planar fluence scored in a 1cm**2 circle
    centered at z-axis on the phantom surface =  4.062E+05(1/cm**2)

    Average planar fluence (number/beam area), F =  4.049E+05(1/cm**2)

         DOSXYZnrc ($Revision: 1.34 $) Dose outputs (dose/F, Gy.cm**2)

              for x=    -3.500 to    -2.500     i=  8
 ybounds: -7.500      -6.500          -5.500          -4.500          -
3.500
         j=        1               2               3               4
 zbounds (     0.000)
0.001   1  6.603E-15-60.8%  3.314E-13-14.3%  4.701E-12-72.5%  2.814E-13-12.3%
0.002   2  1.042E-14-39.9%  1.707E-12- 4.3%  1.680E-12- 4.2%  1.639E-12- 4.3%
0.101   3  2.610E-14- 4.3%  2.997E-12- 0.4%  2.993E-12- 0.4%  2.984E-12- 0.4%
0.141   4  2.385E-13- 4.3%  2.082E-11- 0.5%  2.094E-11- 0.5%  2.085E-11- 0.5%
0.150   5  2.188E-13- 9.1%  1.818E-11- 1.0%  1.827E-11- 1.0%  1.718E-11- 1.1%
0.151   6  1.010E-13-20.8%  8.151E-12- 2.4%  8.246E-12- 2.4%  9.770E-12- 8.8%

              for x=    -3.500 to    -2.500     i=  8
 ybounds: -3.500      -2.500          -1.500          -0.500          0.500
         j=        5               6               7               8
 zbounds (     0.000)
0.001   1  3.182E-13-12.1%  4.038E-13-22.2%  1.553E-12- 4.4%  1.610E-12- 4.3%
0.002   2  1.532E-12- 4.4%  1.566E-12- 4.4%  2.672E-12- 3.6%  2.781E-12- 3.6%
0.101   3  2.982E-12- 0.4%  2.999E-12- 0.4%  3.001E-12- 0.4%  3.024E-12- 0.4%
0.141   4  2.100E-11- 0.5%  2.100E-11- 0.5%  2.087E-11- 0.5%  2.088E-11- 0.5%
0.150   5  1.743E-11- 1.1%  1.748E-11- 1.1%  1.721E-11- 1.1%  1.699E-11- 1.1%
0.151   6  8.733E-12-12.6%  7.847E-12- 6.0%  7.351E-12- 4.8%  8.958E-12- 8.1%
              for x=    -3.500 to    -2.500     i=  8
 ybounds:  0.500       1.500          2.500          3.500          4.500
         j=        9              10              11              12
 zbounds (     0.000)
0.001   1  1.683E-12- 4.3%  3.729E-13-12.3%  4.108E-13-12.5%  2.554E-13-12.4%
0.002   2  2.690E-12- 3.6%  3.648E-12-89.5%  1.324E-12-66.1%  2.874E-13-12.7%
0.101   3  2.990E-12- 0.4%  3.015E-12- 0.4%  2.981E-12- 0.4%  2.998E-12- 0.4%
0.141   4  2.102E-11- 0.5%  2.090E-11- 0.5%  2.090E-11- 0.5%  2.095E-11- 0.5%
0.150   5  1.724E-11- 1.1%  1.672E-11- 1.1%  1.697E-11- 1.1%  1.698E-11- 1.1%
0.151   6  9.350E-12- 8.9%  8.237E-12- 6.8%  7.333E-12- 5.2%  8.113E-12- 7.4%

              for x=    -3.500 to    -2.500     i=  8
 ybounds:  4.500       5.500          6.500          7.500
         j=       13              14              15
 zbounds (     0.000)
  0.001   1  3.586E-12-90.4%  3.290E-13-14.0%  2.395E-15-99.9%
  0.002   2  1.739E-12- 4.2%  1.540E-12- 4.4%  9.159E-15-51.9%
  0.101   3  3.014E-12- 0.4%  2.997E-12- 0.4%  2.760E-14- 4.2%
  0.141   4  2.082E-11- 0.5%  2.094E-11- 0.5%  2.416E-13- 4.2%
  0.150   5  1.838E-11- 1.0%  1.794E-11- 1.1%  2.138E-13- 9.3%
  0.151   6  8.590E-12- 2.4%  8.448E-12- 2.4%  1.209E-13-20.8%
```

```
1all thick 141"allthick_aray _gv _tc.egsinp"

    Elec/positron planar energy fluence scored in a 1cm**2 circle
    centered at z-axis on the phantom surface =  0.000E+00(1/cm**2)

    Photon planar energy fluence scored in a 1cm**2 circle
    centered at z-axis on the phantom surface =  5.715E+04(1/cm**2)

    Elec/positron planar fluence scored in a 1cm**2 circle
    centered at z-axis on the phantom surface =  0.000E+00(1/cm**2)

    Photon planar fluence scored in a 1cm**2 circle
    centered at z-axis on the phantom surface =  4.062E+05(1/cm**2)

    Average planar fluence (number/beam area), F =  4.049E+05(1/cm**2)

         DOSXYZnrc ($Revision: 1.34 $) Dose outputs (dose/F, Gy.cm**2)

              for x=    -2.500 to    -1.500     i=  9
 ybounds: -7.500      -6.500          -5.500          -4.500          -
3.500
         j=        1               2               3               4
 zbounds (     0.000)
0.001   1  3.370E-15-99.9%  3.710E-13-12.9%  3.510E-13-16.8%  3.499E-13-12.8%
0.002   2  4.081E-15-58.9%  1.673E-12- 4.3%  1.538E-12- 4.4%  1.747E-12- 4.2%
0.101   3  2.627E-14- 4.3%  2.984E-12- 0.4%  2.980E-12- 0.4%  3.014E-12- 0.4%
0.141   4  2.585E-13- 4.1%  2.073E-11- 0.5%  2.101E-11- 0.5%  2.079E-11- 0.5%
0.150   5  2.136E-13- 9.3%  1.837E-11- 1.0%  1.848E-11- 1.0%  1.713E-11- 1.1%
0.151   6  5.642E-14-23.6%  8.150E-12- 2.4%  8.540E-12- 2.4%  8.732E-12- 7.6%
              for x=    -2.500 to    -1.500     i=  9
 ybounds: -3.500      -2.500          -1.500          -0.500          0.500
         j=        5               6               7               8
 zbounds (     0.000)
0.001   1  3.406E-13-12.0%  6.722E-13-40.7%  1.507E-12- 4.3%  1.653E-12- 4.4%
0.002   2  1.680E-12- 4.3%  1.641E-12- 4.3%  2.791E-12- 3.6%  2.590E-12- 3.6%
0.101   3  2.979E-12- 0.4%  3.006E-12- 0.4%  2.983E-12- 0.4%  3.020E-12- 0.4%
0.141   4  2.102E-11- 0.5%  2.076E-11- 0.5%  2.085E-11- 0.5%  2.088E-11- 0.5%
0.150   5  1.747E-11- 1.1%  1.710E-11- 1.1%  1.691E-11- 1.1%  1.709E-11- 1.1%
0.151   6  7.259E-12- 4.6%  8.302E-12- 6.6%  7.702E-12- 6.6%  7.121E-12- 5.2%

              for x=    -2.500 to    -1.500     i=  9
 ybounds:  0.500       1.500           2.500           3.500          4.500
         j=        9              10              11              12
 zbounds (     0.000)
0.001   1  1.507E-12- 4.4%  3.647E-12-89.6%  3.438E-13-17.3%  7.577E-13-54.6%
0.002   2  2.578E-12- 3.6%  4.705E-12-67.0%  1.894E-12-82.7%  6.856E-13-45.0%
0.101   3  3.031E-12- 0.4%  3.007E-12- 0.4%  2.981E-12- 0.4%  3.001E-12- 0.4%
0.141   4  2.076E-11- 0.5%  2.099E-11- 0.5%  2.103E-11- 0.5%  2.092E-11- 0.5%
0.150   5  1.702E-11- 1.1%  1.745E-11- 1.1%  1.728E-11- 1.1%  1.695E-11- 1.1%
0.151   6  9.064E-12- 7.6%  1.180E-11-28.6%  7.771E-12- 6.5%  7.262E-12- 5.3%

              for x=    -2.500 to    -1.500     i=  9
 ybounds:  4.500       5.500           6.500           7.500
         j=       13              14              15
 zbounds (     0.000)
  0.001   1  3.416E-13-11.7%  3.641E-12-89.4%  2.357E-15-99.9%
  0.002   2  1.730E-12- 4.2%  1.598E-12- 4.4%  8.871E-15-55.5%
  0.101   3  2.992E-12- 0.4%  2.996E-12- 0.4%  2.810E-14- 4.1%
  0.141   4  2.094E-11- 0.5%  2.085E-11- 0.5%  2.325E-13- 4.3%
  0.150   5  1.839E-11- 1.0%  1.816E-11- 1.0%  2.107E-13- 9.4%
  0.151   6  8.070E-12- 2.4%  8.219E-12- 2.5%  6.145E-14-21.6%
```

```
1all thick 141"allthick_aray _gv _tc.egsinp"

    Elec/positron planar energy fluence scored in a 1cm**2 circle
    centered at z-axis on the phantom surface =  0.000E+00(1/cm**2)

    Photon planar energy fluence scored in a 1cm**2 circle
    centered at z-axis on the phantom surface =  5.715E+04(1/cm**2)

    Elec/positron planar fluence scored in a 1cm**2 circle
    centered at z-axis on the phantom surface =  0.000E+00(1/cm**2)

    Photon planar fluence scored in a 1cm**2 circle
    centered at z-axis on the phantom surface =  4.062E+05(1/cm**2)

    Average planar fluence (number/beam area), F =  4.049E+05(1/cm**2)

         DOSXYZnrc ($Revision: 1.34 $) Dose outputs (dose/F, Gy.cm**2)

              for x=    -1.500 to    -0.500     i= 10
 ybounds: -7.500      -6.500           -5.500           -4.500           -
3.500
         j=        1                2                3                4
 zbounds (     0.000)
0.001   1  6.419E-15-99.9%  2.894E-13-13.8%  2.726E-13-14.4%  3.527E-13-21.5%
0.002   2  1.077E-14-46.9%  1.629E-12- 4.4%  1.572E-12- 4.4%  1.656E-12- 4.4%
0.101   3  2.606E-14- 4.3%  2.960E-12- 0.4%  2.993E-12- 0.4%  2.988E-12- 0.4%
0.141   4  2.635E-13- 4.0%  2.078E-11- 0.5%  2.102E-11- 0.5%  2.102E-11- 0.5%
0.150   5  2.262E-13- 9.0%  1.814E-11- 1.0%  1.837E-11- 1.0%  1.842E-11- 1.0%
0.151   6  1.122E-13-21.0%  8.153E-12- 2.5%  8.460E-12- 2.5%  8.647E-12- 2.5%
              for x=    -1.500 to    -0.500     i= 10
 ybounds: -3.500      -2.500           -1.500           -0.500          0.500
         j=        5                6                7                8
 zbounds (     0.000)
0.001   1  3.602E-13-13.9%  4.765E-13-18.7%  1.633E-12- 4.4%  1.792E-12- 4.2%
0.002   2  1.764E-12- 4.2%  1.518E-12- 4.4%  2.635E-12- 3.6%  2.839E-12- 3.6%
0.101   3  2.999E-12- 0.4%  3.002E-12- 0.4%  3.017E-12- 0.4%  3.020E-12- 0.4%
0.141   4  2.093E-11- 0.5%  2.101E-11- 0.5%  2.106E-11- 0.5%  2.094E-11- 0.5%
0.150   5  1.845E-11- 1.0%  1.877E-11- 1.0%  1.824E-11- 1.0%  1.830E-11- 1.0%
0.151   6  8.620E-12- 2.4%  8.798E-12- 2.4%  8.418E-12- 2.5%  8.714E-12- 2.4%

              for x=    -1.500 to    -0.500     i= 10
 ybounds:  0.500       1.500          2.500          3.500          4.500
         j=        9               10               11               12
 zbounds (     0.000)
0.001   1  1.633E-12- 4.3%  3.536E-13-12.7%  2.631E-13-13.1%  3.466E-13-22.7%
0.002   2  2.859E-12- 3.5%  6.461E-13-42.2%  1.763E-12-84.9%  3.669E-13-21.7%
0.101   3  3.009E-12- 0.4%  2.998E-12- 0.4%  2.980E-12- 0.4%  2.995E-12- 0.4%
0.141   4  2.098E-11- 0.5%  2.098E-11- 0.5%  2.116E-11- 0.5%  2.115E-11- 0.5%
0.150   5  1.838E-11- 1.0%  1.840E-11- 1.0%  1.798E-11- 1.0%  1.830E-11- 1.0%
0.151   6  8.195E-12- 2.4%  8.743E-12- 2.4%  8.169E-12- 2.4%  8.244E-12- 2.5%

              for x=    -1.500 to    -0.500     i= 10
 ybounds:  4.500       5.500            6.500            7.500
         j=       13               14               15
 zbounds (     0.000)
  0.001   1  3.675E-13-12.0%  2.952E-13-13.5%  3.254E-15-71.1%
  0.002   2  1.835E-12- 4.2%  1.480E-12- 4.5%  2.327E-14-37.8%
  0.101   3  3.033E-12- 0.4%  2.961E-12- 0.4%  2.657E-14- 4.2%
  0.141   4  2.092E-11- 0.5%  2.070E-11- 0.5%  2.439E-13- 4.2%
  0.150   5  1.820E-11- 1.0%  1.833E-11- 1.0%  2.379E-13- 8.7%
  0.151   6  8.409E-12- 2.4%  8.374E-12- 2.4%  1.519E-13-20.3%
```

```
1all thick 141"allthick_aray _gv _tc.egsinp"

    Elec/positron planar energy fluence scored in a 1cm**2 circle
    centered at z-axis on the phantom surface =  0.000E+00(1/cm**2)

    Photon planar energy fluence scored in a 1cm**2 circle
    centered at z-axis on the phantom surface =  5.715E+04(1/cm**2)

    Elec/positron planar fluence scored in a 1cm**2 circle
    centered at z-axis on the phantom surface =  0.000E+00(1/cm**2)

    Photon planar fluence scored in a 1cm**2 circle
    centered at z-axis on the phantom surface =  4.062E+05(1/cm**2)

    Average planar fluence (number/beam area), F =  4.049E+05(1/cm**2)
         DOSXYZnrc ($Revision: 1.34 $) Dose outputs (dose/F, Gy.cm**2)

              for x=    -0.500 to     0.500     i= 11
 ybounds: -7.500      -6.500           -5.500           -4.500           -
3.500
         j=        1                2                3                4
 zbounds (     0.000)
0.001   1  4.617E-14-99.9%  4.049E-13-31.7%  3.671E-13-15.3%  2.750E-13-14.5%
0.002   2  1.068E-14-48.2%  1.607E-12- 4.4%  1.517E-12- 4.4%  1.646E-12- 4.3%
0.101   3  2.785E-14- 4.1%  2.996E-12- 0.4%  2.985E-12- 0.4%  3.003E-12- 0.4%
0.141   4  2.559E-13- 4.2%  2.067E-11- 0.5%  2.083E-11- 0.5%  2.081E-11- 0.5%
0.150   5  2.208E-13- 9.0%  1.803E-11- 1.0%  1.829E-11- 1.0%  1.851E-11- 1.0%
0.151   6  1.049E-13-20.5%  8.292E-12- 2.4%  8.603E-12- 2.4%  8.140E-12- 2.5%

              for x=    -0.500 to     0.500     i= 11
 ybounds: -3.500      -2.500           -1.500           -0.500          0.500
         j=        5                6                7                8
 zbounds (     0.000)
0.001   1  4.096E-13-17.9%  5.011E-13-39.6%  1.527E-12- 4.5%  1.734E-12- 4.3%
0.002   2  1.700E-12- 4.2%  1.697E-12- 4.3%  2.675E-12- 3.6%  2.904E-12- 3.5%
0.101   3  3.018E-12- 0.4%  3.010E-12- 0.4%  2.994E-12- 0.4%  2.994E-12- 0.4%
0.141   4  2.078E-11- 0.5%  2.116E-11- 0.5%  2.092E-11- 0.5%  2.106E-11- 0.5%
0.150   5  1.854E-11- 1.0%  1.854E-11- 1.0%  1.838E-11- 1.0%  1.814E-11- 1.0%
0.151   6  8.380E-12- 2.4%  8.373E-12- 2.4%  8.652E-12- 2.4%  8.448E-12- 2.4%

              for x=    -0.500 to     0.500     i= 11
 ybounds:  0.500       1.500          2.500          3.500          4.500
         j=        9               10               11               12
 zbounds (     0.000)
0.001   1  1.611E-12- 4.4%  2.713E-13-17.3%  4.261E-13-19.3%  2.248E-12-77.4%
0.002   2  2.640E-12- 3.7%  1.037E-12-64.9%  3.752E-12-87.5%  3.722E-13-14.9%
0.101   3  3.007E-12- 0.4%  2.983E-12- 0.4%  2.985E-12- 0.4%  2.975E-12- 0.4%
0.141   4  2.109E-11- 0.5%  2.094E-11- 0.5%  2.107E-11- 0.5%  2.103E-11- 0.5%
0.150   5  1.848E-11- 1.0%  1.814E-11- 1.0%  1.839E-11- 1.0%  1.869E-11- 1.0%
0.151   6  8.635E-12- 2.4%  8.268E-12- 2.5%  8.504E-12- 2.5%  8.553E-12- 2.4%
              for x=    -0.500 to     0.500     i= 11
 ybounds:  4.500       5.500            6.500            7.500
         j=       13               14               15
 zbounds (     0.000)
  0.001   1  2.946E-13-12.5%  3.618E-12-90.1%  3.799E-15-71.2%
  0.002   2  1.582E-12- 4.3%  1.510E-12- 4.5%  1.204E-14-46.8%
  0.101   3  3.021E-12- 0.4%  2.982E-12- 0.4%  2.858E-14- 4.1%
  0.141   4  2.083E-11- 0.5%  2.057E-11- 0.5%  2.372E-13- 4.3%
  0.150   5  1.851E-11- 1.0%  1.798E-11- 1.1%  2.341E-13- 8.8%
  0.151   6  8.385E-12- 2.5%  8.444E-12- 2.4%  8.144E-14-27.2%

 Truncated at middle x voxel for brevity
```

C.2 6Mv

C.2.1 6mv 3ddose

```
21 15 8
 -10.5 -9.5 -8.5 -7.5 -6.5 -5.5 -4.5 -3.5 -2.5 -1.5 -0.5  0.5  1.5  2.5  3.5
  4.5  5.5  6.5  7.5  8.5  9.5  10.5
 -7.5 -6.5 -5.5 -4.5 -3.5 -2.5 -1.5 -0.5  0.5  1.5  2.5  3.5  4.5  5.5  6.5
  7.5
  0.  0.00100000005  0.00200000009  0.100999996  0.141000003  0.150000006
  0.151000008  0.15200001  0.161000013
```

C.2.2 6mv egslst

```
**********************************************************************
 NRCC/UW EGSnrc user-code DOSXYZnrc ($Revision: 1.34 $ last edited $Date:
2006/09/22 20:56:11 $)
 ON i1586_pc_Windows_NT (gnu_win32)                        08:27:36 Feb 23
2008
**********************************************************************
**                                                                  **
**                                DOSXYZnrc                         **
**                             Z pronounced zed                     **
**                                                                  **
**     Code developed at the National Research Council of Canada and **
**          University of Wisconsin as part of the OMEGA project    **
**                                                                  **
**        This is $Revision: 1.34 $ last edited$Date: 2006/09/22 20:56:11 **
**                                                                  **
**********************************************************************

     The following parameters may be adjusted in dosxyz_user_macros.mortran
 $MXMED:    Max number of media:  7
 $MXSTACK:  Max stack size:        15
 $IMAX,etc: Max dose scoring regions in x,y,z directions:  128  128   56
 $MAXDOSE:  Max dose scoring regions consistent with above: 917505
 $DOSEZERO(=1) 1=> all doses with uncert > 50% are zeroed in .3ddose file


 The following parameters may be adjusted in srcxyz.macros
 $INVDIM:   number of elements in inverse CPD for input energy spectra = 1000
 $NENSRC:   number of bins in input energy spectrum =  200

======================================================================
 ----------------------------------------------------------------------

 Title:  all thick mohan 6 "allthick_aray_gv.egsinp"
 ----------------------------------------------------------------------

======================================================================


 Number of media (min = 1, max =   7, 0 => CT data):                3
 Medium  1:                    air
 Medium  2:                    cu
 Medium  3:                    gdv

 ECUTIN,PCUTIN,(ESTEPE,SMAX--DUMMY INPUTS):
              0.001     0.001     0.000     0.000     0.000     0.000
```

```
# regions in x (max= 128),y (max= 128),z (max=  56) directions
(if<0,implies # groups of reg), IPHANT (1 to output a .egsphant
file for dosxyz_show, 0[default] to not output this file)
    :      -1    -1    -8     1

Input boundaries in the x-direction
-----------------------------------
Initial boundary:       -10.500
Width in this group, number of regions in group:         1.000   21
Boundaries
    -10.500      -9.500      -8.500      -7.500      -6.500      -5.500
     -4.500      -3.500      -2.500      -1.500      -0.500       0.500
      1.500       2.500       3.500       4.500       5.500       6.500
      7.500       8.500       9.500      10.500

Input boundaries in the y-direction
-----------------------------------
Initial boundary:        -7.500
Width in this group, number of regions in group:         1.000   15
Boundaries
     -7.500      -6.500      -5.500      -4.500      -3.500      -2.500
     -1.500      -0.500       0.500       1.500       2.500       3.500
      4.500       5.500       6.500       7.500

Input boundaries in the z-direction
-----------------------------------
Initial boundary:         0.000
Width in this group, number of regions in group:         0.001    1
Width in this group, number of regions in group:         0.001    1
Width in this group, number of regions in group:         0.099    1
Width in this group, number of regions in group:         0.040    1
Width in this group, number of regions in group:         0.009    1
Width in this group, number of regions in group:         0.001    1
Width in this group, number of regions in group:         0.001    1
Width in this group, number of regions in group:         0.009    1
Boundaries
      0.000       0.001       0.002       0.101       0.141       0.150
      0.151       0.152       0.161

Total # regions including exterior =      2521

Input groups of regions for which density and medium are not defaults
Lower,upper i, j, k,  MEDIUM, DENSITY (  1  21)(  1   6)(  2   3)   2  0.000
Lower,upper i, j, k,  MEDIUM, DENSITY (  1  21)( 13  15)(  2   3)   2  0.000
Lower,upper i, j, k,  MEDIUM, DENSITY (  1  21)(  7   9)(  1   3)   2  0.000
Lower,upper i, j, k,  MEDIUM, DENSITY (  1  21)( 10  12)(  3   3)   2  0.000
Lower,upper i, j, k,  MEDIUM, DENSITY (  1  21)(  1   3)(  4   6)   3  0.000
Lower,upper i, j, k,  MEDIUM, DENSITY (  1   3)(  4  12)(  4   6)   3  0.000
Lower,upper i, j, k,  MEDIUM, DENSITY ( 19  21)(  4  12)(  4   6)   3  0.000
Lower,upper i, j, k,  MEDIUM, DENSITY (  1  21)( 13  15)(  4   6)   3  0.000
Lower,upper i, j, k,  MEDIUM, DENSITY (  4  18)(  4  12)(  4   4)   3  0.000
Lower,upper i, j, k,  MEDIUM, DENSITY (  7  18)(  4  12)(  5   5)   3  0.000
Lower,upper i, j, k,  MEDIUM, DENSITY ( 10  18)(  4  12)(  6   6)   3  0.000
Lower,upper i, j, k,  MEDIUM, DENSITY ( 13  18)(  4  12)(  7   7)   3  0.000
Lower,upper i, j, k,  MEDIUM, DENSITY ( 16  18)(  4  12)(  8   8)   3  0.000
Lower,upper i, j, k,  MEDIUM, DENSITY
   Found blank line => end of this input


Input groups of regions for which ECUT and PCUT are not defaults
NB This option is disabled, just input 8 zeros.
Dummy values of lower,upper i, j, k,  ECUT, PCUT
   Found blank line => end of this input
```

```
 Enter 8 numbers on one line
   3 pairs defininglower,upper x,y,z indicies of dose regions
                 for which results are to be output
   IZSCAN:       non-zero for z-scan/page
   MAX20:        if any one = 1, output summary of max 20 doses.
   end signaled by first pair both zero
   forno dose printed, MAX20 is still read from first line

         1  21     1  15     1   6     1     0
    Found blank line => end of this input

   Read input energy spectrum from:
C:/HEN_HOUSE/spectra/mohan6.spectrum
  Have read   24 input energy bins from file
      Counts/MeV assumed
    Energy ranges from     0.000 MeV to       6.000 MeV



 *******WARNING******
                  SOME OF NORMALISED BIN PROBABILITIES SO SMALL BINS MAY BE
MISSED



 NCASE,IWATCH,TIMMAX,INSEED1,INSEED2,BEAM_SIZE,ISMOOTH,IRESTART,IDAT,
 IREJECT,ESAVE_GLOBAL,NRCYCL,IPARALLEL,PARNUM,n_split,ihowfarless
 :
100000000   0   6.00    33    97 100.00    0   0  0  0   0.00  0   0  0  1  0



 Index ranges of beam field
 --------------------------

     -9.500     9.500   i index ranges over i=  2 to  20
     -6.500     6.500   j index ranges over j=  2 to  14

 ******************************************************************************

         Summary of source parameters (srcxyznrc Rev 1.6)
 ******************************************************************************

                    Point source incident from the front(+ve z-axis)
                         Electric charge of the source:            0
                         x-boundaries:       -9.5000 cm-    9.5000 cm
                         y-boundaries:       -6.5000 cm-    6.5000 cm
                         SSD                             130.0000 cm


================================================================================

                   Electron/Photon transport parameter

================================================================================

 Photon cross sections                                        PEGS4
 Photon transport cutoff(MeV)                                      0.1000E-01
 Pair angular sampling                                         SIM
 Pair cross sections                                           BH
 Triplet production                                            Off
```

```
 Bound Compton scattering                                    OFF
 Radiative Compton corrections                               Off
 Rayleigh scattering                                         OFF
 Atomic relaxations                                          OFF
 Photoelectron angular sampling                              OFF

 Electron transport cutoff(MeV)                               0.5210
 Bremsstrahlung cross sections                               BH
 Bremsstrahlung angular sampling                             SIM
 Spin effects                                                On
 Electron Impact Ionization                                  OFF
 Maxium electron step in cm (SMAX)                                 5.000
 Maximum fractional energy loss/step (ESTEPE)                0.2500
 Maximum 1st elastic moment/step (XIMAX)                     0.5000
 Boundary crossing algorithm                                 PRESTA-I
 Skin-depth for boundary crossing (MFP)                      5.803
 Electron-step algorithm                                     PRESTA-II

================================================================================


 Medium               AE        AP
 air                0.521     0.010
 cu                 0.521     0.010
 gdv                0.521     0.010

 No range rejection.


 ***************************************************************

  Histories to be simulated for this run    100000000

  Histories to be analyzed after this run   100000000

 ***************************************************************
   Elapsed wall clock time to this point=       3.604 s


   CPU time so far for this run =       1.041 s


 BATCH #  TIME-ELAPSED  TOTAL CPUTIME  RATIO  TIME OF DAY  RNG pointers

     1          0.0            0.0      0.00    08:27:39   ixx jxx =   97  33
     2       1740.4          820.0      2.12    08:56:41   ixx jxx =   38  71
     3       3416.0         1677.0      2.04    09:24:36   ixx jxx =   48  81
     4       4361.6         2512.5      1.74    09:40:22   ixx jxx =   65   1
     5       5320.6         3357.5      1.58    09:56:21   ixx jxx =   56  89
     6       6218.6         4162.1      1.49    10:11:19   ixx jxx =   61  94
     7       6928.0         4844.1      1.43    10:23:08   ixx jxx =    6  39
     8       7648.3         5535.9      1.38    10:35:08   ixx jxx =   92  28
     9       8360.0         6221.5      1.34    10:47:00   ixx jxx =    3  36
    10       9078.1         6912.0      1.31    10:58:58   ixx jxx =   72   8

 Total CPU time for run =  7611.9 s =   2.114 hr =>   47294210. hist/hr
   On  i1586_pc_Windows_NT (gnu_win32)

 Fraction of incident energy deposited in the phantom =      0.0174


 Number of charged particle steps simulated,   N_step   =      712153270
 Number of charged particle steps/incident fluence      =    1.75902E+03
```

```
 No. of PRESTA-II steps/total no. of charged particle steps =
0.96877

1all thick mohan 6 "allthick_aray_gv.egsinp"

    Elec/positron planar energy fluence scored in a 1cm**2 circle
    centered at z-axison the phantom surface =  0.000E+00(1/cm**2)

    Photon planarenergy fluence scored in a 1cm**2 circle
    centered at z-axis on the phantom surface =  7.677E+05(1/cm**2)

    Elec/positron planar fluence scored in a 1cm**2 circle
    centered at z-axis on the phantom surface =  0.000E+00(1/cm**2)

    Photon planar fluence scored in a 1cm**2 circle
    centered at z-axis on the phantom surface =  4.048E+05(1/cm**2)

    Average planar fluence (number/beam area), F =  4.049E+05(1/cm**2)

         DOSXYZnrc ($Revision: 1.34 $) Dose outputs (dose/F, Gy.cm**2)

              for x=   -10.500 to    -9.500     i=  1

 ybounds: -7.500      -6.500          -5.500          -4.500           -3.500
         j=        1                2                3                4
 zbounds (     0.000)
0.001   1  0.000E+00-99.9%  1.745E-14-75.9%  5.700E-15-45.7%  1.001E-14-42.7%
0.002   2  0.000E+00-99.9%  9.495E-15-48.9%  1.898E-14-40.4%  1.479E-14-37.5%
0.101   3  2.827E-15-18.6%  5.328E-14- 8.5%  6.180E-14- 8.1%  6.825E-14- 8.1%
0.141   4  1.327E-14-27.3%  1.451E-13- 9.6%  1.563E-13- 9.5%  1.420E-13- 9.1%
0.150   5  1.272E-14-35.9%  9.549E-14-14.7%  1.230E-13-13.8%  9.883E-14-16.1%
0.151   6  4.824E-15-39.8%  4.739E-14-17.9%  6.821E-14-21.2%  6.274E-14-17.9%

              for x=   -10.500 to    -9.500     i=  1

 ybounds: -3.500      -2.500          -1.500          -0.500            0.500
         j=        5                6                7                8
 zbounds (     0.000)
0.001   1  2.272E-14-37.8%  3.112E-15-59.9%  1.238E-14-79.4%  3.249E-14-46.7%
0.002   2  1.309E-14-45.3%  1.776E-14-42.9%  3.264E-15-55.7%  1.959E-14-39.7%
0.101   3  7.619E-14- 7.8%  6.678E-14- 8.0%  6.866E-14- 7.3%  6.271E-14- 8.2%
0.141   4  1.360E-13- 9.2%  1.570E-13- 9.4%  1.489E-13- 9.1%  1.396E-13- 9.2%
0.150   5  9.595E-14-14.8%  1.305E-13-14.7%  9.974E-14-13.8%  8.967E-14-14.4%
0.151   6  5.221E-14-21.4%  7.373E-14-20.9%  5.741E-14-17.1%  5.392E-14-17.6%

           for x=   -10.500 to    -9.500     i=  1

 ybounds:  0.500       1.500           2.500           3.500            4.500
         j=        9               10               11               12
 zbounds (     0.000)
0.001   1  7.657E-15-34.2%  1.606E-14-61.9%  8.566E-15-54.1%  4.211E-15-73.0%
0.002   2  1.749E-14-39.9%  1.596E-14-61.7%  8.566E-15-54.1%  4.665E-15-66.6%
0.101   3  6.933E-14- 7.5%  6.876E-14- 7.2%  6.369E-14- 8.1%  6.174E-14- 7.8%
0.141   4  1.516E-13- 9.9%  1.622E-13- 8.7%  1.477E-13-10.1%  1.805E-13- 9.7%
0.150   5  9.465E-14-14.1%  1.100E-13-14.4%  7.766E-14-14.7%  9.260E-14-15.8%
0.151   6  6.867E-14-17.7%  7.091E-14-20.7%  5.571E-14-20.2%  5.444E-14-20.9%

              for x=   -10.500 to    -9.500     i=  1

 ybounds:  4.500       5.500            6.500            7.500
         j=       13               14               15
 zbounds (     0.000)
  0.001   1  1.137E-14-44.9%  9.705E-15-43.0%  0.000E+00-99.9%
```

```
0.002    2  3.103E-14-44.6%  9.016E-15-34.4%  4.657E-17-99.9%
0.101    3  7.120E-14- 7.2%  6.151E-14- 7.8%  4.753E-15-33.3%
0.141    4  1.518E-13- 8.9%  1.568E-13- 9.7%  1.500E-14-26.0%
0.150    5  1.013E-13-14.3%  1.136E-13-13.4%  6.732E-15-58.1%
0.151    6  5.141E-14-22.4%  7.021E-14-22.6%  2.060E-15-78.5%
```

D Vision manual

D.1 IAS2 settings

To change the settings on IAS2, the service monitor software is used, the settings that need to be changed are; “RTIS config>>Trigger Board TB2>>trigger synchronization mode” needs to be set to “immediate & internal freq” and “RTIS config>>image correction>>image correction type” need to be set to “no correction”. To reduce the noise the due to the metal cove being removed the IAS2 need to have the reset frames for each image increased from 1 to 2, by “Scanning Modes>> (dose rate) >> reset frames”

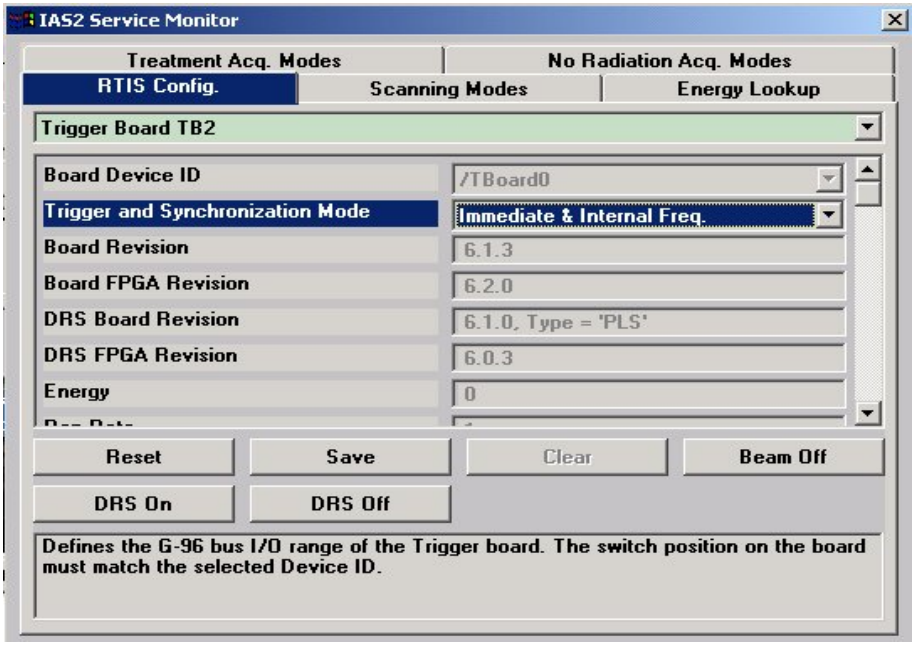

Figure D.6.1 Service monitor trigger settings

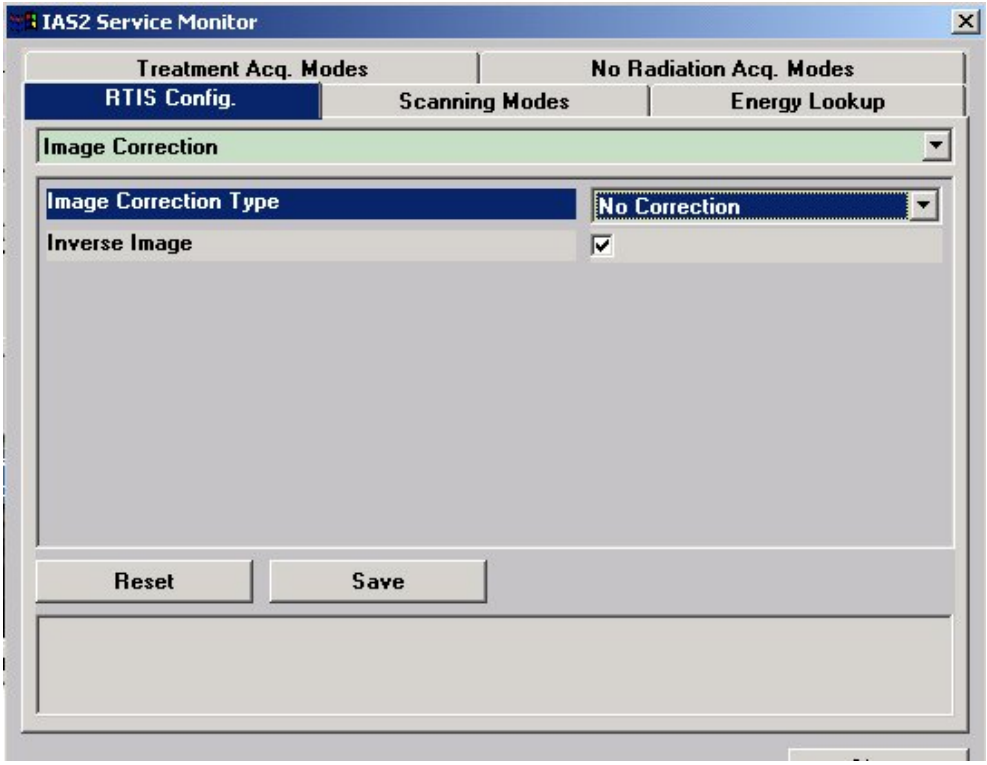

Figure D.6.2 Service monitor image correction

References

1. The New Zealand Health information Service, *Cancer: New Registrations and Deaths 2003*. 2007, The Ministry of Health: wellington.
2. The New Zealand Health information Service, *Improving Non-Surgical Cancer Treatment Services in New Zealand*. 2001, The Ministry of Health: wellington.
3. Greer, P. and M. Barnes, *Assessment of the aS500 amorphous silicon EPID for measurement of enhanced dynamic wedge.* Radiotherapy and Oncology, 2005. **76**: p. S193-S193.
4. Langmack, K.A., *Portal imaging.* Br J Radiol, 2001. **74**(885): p. 789-804.
5. J. E. Marks, A.G.H., H. G. Sutton, M. L. Griem,, *The value of frequent treatment verification films in reducing localization error in the irradiation of complex fields.* Cancer, 1976. **37**(6): p. 2755-2761.
6. Munro, P., J.A. Rawlinson, and A. Fenster, *Therapy imaging: a signal-to-noise analysis of a fluoroscopic imaging system for radiotherapy localization.* Medical Physics, 1990. **17**(5): p. 763-72.
7. Greer, P.B. and M.P. Barnes, *Investigation of an amorphous silicon EPID for measurement and quality assurance of enhanced dynamic wedge.* Physics in Medicine & Biology, 2007. **52**(4): p. 1075-87.
8. Van Esch, A., T. Depuydt, and D.P. Huyskens, *The use of an aSi-based EPID for routine absolute dosimetric pre-treatment verification of dynamic IMRT fields.* Radiotherapy & Oncology, 2004. **71**(2): p. 223-34.
9. Greer, P.B., et al., *Experimental investigation of the response of an amorphous silicon EPID to intensity modulated radiotherapy beams.* Medical Physics, 2007. **34**(11): p. 4389-98.
10. Grein, E.E., R. Lee, and K. Luchka, *An investigation of a new amorphous silicon electronic portal imaging device for transit dosimetry.* Medical Physics, 2002. **29**(10): p. 2262-8.
11. Varian Medical Systems, *Hardwear Configuration Portal dosimetry Version 8*. 2006.
12. Greer, P.B., *Correction of pixel sensitivity variation and off-axis response for amorphous silicon EPID dosimetry.* Medical Physics, 2005. **32**(12): p. 3558-68.
13. El-Mohri, Y., et al., *Relative dosimetry using active matrix flat-panel imager (AMFPI) technology.* Medical Physics, 1999. **26**(8): p. 1530-41.
14. Supertech, *Supertech websit*, http://www.supertechx-ray.com/a4720-r.htm.
15. McCurdy, B.M., K. Luchka, and S. Pistorius, *Dosimetric investigation and portal dose image prediction using an amorphous silicon electronic portal imaging device.* Medical Physics, 2001. **28**(6): p. 911-24.
16. Varian Medical Systems, ed. *PortailVision aS500 Rel.6 Referance manual*. 2000.
17. *Tutorial on Portal Imaging*, http://web.ucsf.edu/jpouliot/Tutorial/HU/Lesson2.htm: San Francisco.
18. Varian Medical Systems, *HE Clinac iX & Trilogy System Verification Summary*. 2005.
19. Kirkby, C. and R. Sloboda, *Consequences of the spectral response of an a-Si EPID and implications for dosimetric calibration.* Medical Physics, 2005. **32**(8): p. 2649-58.
20. Oberg, E. and F.D. Jones, *Machinery's handbook.* 1988: New York, Industrial Press, 1959-.
21. Kirby, M.C., *The consequences of fixed-pattern noise and image movement on electronic portal images.* Physics in Medicine and Biology, 1996. **41**(11): p. 2345.
22. Kawrakow, I. and D.W.O. Rogers, *The EGSnrc Code System*. 2003: National Research Council of Canada.
23. Chytyk, K. and B.M. McCurdy, *Investigation of tilted dose kernels for portal dose prediction in a-Si electronic portal imagers.* Medical Physics, 2006. **33**(9): p. 3333-9.

24. Spezi, E. and D.G. Lewis, *Full forward Monte Carlo calculation of portal dose from MLC collimated treatment beams.[erratum appears in Phys Med Biol. 2004 Jan 21;49(2):355].* Physics in Medicine & Biology, 2002. **47**(3): p. 377-90.
25. Chang, J. and C.C. Ling, *Using the frame averaging of aS500 EPID for IMRT verification.* Journal of Applied Clinical Medical Physics, 2003. **4**(4): p. 287-99.
26. Berger, L., et al., *Performance optimization of the Varian aS500 EPID system.* Journal of Applied Clinical Medical Physics, 2006. **7**(1): p. 105-14.
27. Leong, J., *Use of digital fluoroscopy as an on-line verification device in radiation therapy.* Physics in Medicine & Biology, 1986. **31**(9): p. 985-92.
28. Munro, P., *Portal imaging technology: Past, present, and future.* Seminars in Radiation Oncology, Innovations in Treatment Delivery, 1995. **5**(2): p. 115-133.
29. Symonds-Tayler, J.R., M. Partridge, and P.M. Evans, *An electronic portal imaging device for transit dosimetry.* Physics in Medicine & Biology, 1997. **42**(11): p. 2273-83.
30. Kroonwijk, M., et al., *In vivo dosimetry for prostate cancer patients using an electronic portal imaging device (EPID); demonstration of internal organ motion.* Radiotherapy & Oncology, 1998. **49**(2): p. 125-32.
31. Greer, P.B. and T. van Doorn, *A design for a dual assembly multileaf collimator.* Medical Physics, 2000. **27**(10): p. 2242-55.
32. Anton, H. and A. Herr, *Calculus with analytic geometry*. 5th ed. ed. Vol. 1. 1995: New York : Wiley, c1995. 1000.
33. Childress, N., *Doselab*, source forge.
34. Monnin, P., et al., *A comparison of the imaging characteristics of the new Kodak Hyper Speed G film with the current T-MAT G/RA film and the CR 9000 system.* Physics in Medicine & Biology, 2005. **50**(19): p. 4541-52.
35. Young, H.D., *Statistical Treatment of Experimental Data*. 1962, New York: McGraw-Hill Book Company Inc. 172.
36. Widrow, B., *Statistical analysis of amplitude quantized sampled data systems.* Transactions of the American Institute of Electrical Engineering, Part II: Applications and Industry, 1960. **79**: p. 555-568.
37. Talamonti, C., M. Casati, and M. Bucciolini, *Pretreatment verification of IMRT absolute dose distributions using a commercial a-Si EPID.* Medical Physics, 2006. **33**(11): p. 4367-78.